Exploring the molecular machinery of Armillaria ostoyae: Advancing insights into pathogenicity, bioremediation and self-defences

PhD dissertation

Simang Champramary

Supervisor:

Dr. Sipos György

Doctoral School of Biology

Department of Microbiology

Faculty of Science and Informatics

University of Szeged

SZTE TTIK

2024

Szeged

TABLE OF CONTENTS

ABBREVIATIONS..... 3
1. INTRODUCTION.....4
1.1. Identification and nomenclature of *Armillaria*.....4
1.1.1. *Armillaria* occurrence and lifestyle.....6
1.1.2. Infection strategies of *Armillaria*.....8
1.1.3. The life cycle of *Armillaria*..... 9
1.2. Molecular background of the plant-fungus interactions.....11
1.2.1. SSPs and other classically secreted proteins.....11
1.2.2. Leaderless secretory proteins (LSPs).....13
1.2.3. Secreted proteases as virulence factors.....13
1.2.4. Role of plant cell wall degrading enzymes during infection..... 14
1.2.5. Role of secondary metabolites in fungus-plant interaction.....15
1.2.6. Role of lncRNA (long non-coding RNAs) in fungal plant pathogenesis..... 16
1.3. Interaction of *Armillaria* with the microbiome..... 17
1.4. Biocontrol of *Armillaria*.....18
1.5. Prospects using armillarioids in mycoremediation.....18
1.6. Application of Machine Learning in modelling the white-rot infection strategy of *Armillaria*..... *19*
1.6.1. Supervised Machine Learning..... 19
1.6.2. Feature Engineering.....20
1.6.3. Unsupervised Machine Learning.....20
1.6.4. Performance assessment of Machine Learning models.....21
2. AIMS OF THE STUDY.....22
3. MATERIALS AND METHODS.....23
3.1. Inoculum preparation.....23
3.2. Preparation of host plants and *A. ostoyae* control..... 23
3.3. Inoculation of seedlings with fungi and incubation.....23
3.4. Assessment of fungus-inoculated seedlings..... 24
3.5. Sample collection and RNA-sequencing.....24
3.6. Bioinformatics analysis of virulence- and pathogenicity-related genes expressed in *A. ostoyae*.....*25*
3.6.1. Analysis of the fungal transcriptome for identifying pathogenicity- and virulence-related genes..... 25
3.6.2. Functional annotation and enrichment analysis.....25
3.6.3. Identification of secretory proteins and comparative secretome analysis.....26
3.6.4. Building a Machine Learning model and feature extraction 27
3.7. lncRNA analysis in *A. ostoyae*.....29
3.7.1. Differential expression analysis of lncRNA..... 29
3.7.2. Identification of lncRNAs.....29
3.7.3. lncRNA target gene prediction and functional enrichment analysis.....30
3.8. Analysis of the *A. ostoyae* microbiome and differential expression of metatranscriptome..... 30
3.9. Transcriptomic analysis of haploid *A. ostoyae* biocontrol using *Trichoderma atroviride*..... 31

3.10. Comparing biodegradation prospects of *Armillaria* 31
4. RESULTS 33
4.1. In vivo infection of spruce seedlings with *A. ostoyae* isolate 33
4.1.1. Differences in plant invasion tactics are shown by sample-specific gene expression 34
4.1.2. Investigation of potential virulence- and pathogenicity-related secretory proteins 36
4.1.3. Comparative study of putative *A. ostoyae* secretory genes expressed during in vivo and in vitro plant tissue invasions 39
4.1.4. Secondary metabolite genes upregulated in Rhizo, Symp and Necro stages 44
4.1.5 Pathogenicity model for *A. ostoya*e infection strategies as white rotting fungus 45
4.2. lncRNAs in the *A. ostoyae* genome 48
4.2.1. Differential expression analysis of transcripts 49
4.2.2. lncRNAs, co-regulators of infection? 49
4.3. Microbiome analysis of *A. ostoyae* 53
4.3.1. Bacterial community patterns 53
4.3.2. Differential abundance analysis 56
4.3.3. Differential metatranscriptome analysis 56
4.3.4. Functional analysis of the metatranscriptome 56
4.4. Interaction of *A. ostoyae* with *T. atroviride* 58
4.4.1. Identification and functional analysis of genes involved in the *A. ostoyae* and *T. atroviride* interaction 58
4.5. Identification of the biodegradation prospects of *Armillaria* species 59
4.5.1. Genome-level comparative analysis identifies specialization of armillarioid fungi 59
4.5.2. Checking the expression profiles of the mycoremediation-related genes 64
5. DISCUSSION 66
5.1. Comparative transcriptomic analyses of the *A. ostoyae* mycelia reveal specificities in the gene expression patterns 66
5.2. Unique sets of the Gsecretome were involved in the host-pathogen interactions 67
5.3. Functional characterization of secreted proteins in *A. ostoyae* during plant pathogenesis 68
5.4. Decoding fungal lifestyles through orthogroup repertoires 70
5.5. Unraveling the complex molecular mechanisms of gene regulation during *A. ostoyae* infection through lncRNA 71
5.6. Diverse microbial and gene expression patterns observed in Symp, Necro, and Rhizo 73
5.7. *A. ostoyae* and *T. atroviride* genes in action 75
5.8. The mycoremediation potentials of the armillarioids 76
SUMMARY 79
ÖSSZEFOGLALÓ 82
ACKNOWLEDGEMENTS 85
FINANCIAL SUPPORT 86
LIST OF REFERENCES 87
LIST OF PUBLICATIONS 115
SUPPLEMENTARY MATERIALS 117

ABBREVIATIONS

Armillaria ostoyae C18 (AO)
Armillaria ostoyae C18 mycelium collected from sudden dieback tree (Necro)
Armillaria ostoyae C18 mycelium collected from symptomatic tree (Symp)
Armillaria ostoyae C18 rhizomorphs collected from soil (Rhizo)
Auxiliary activities (AAs)
Biocontrol agents (BCAs)
Biological processes (BP)
Carbohydrate esterase (CE)
Carbohydrate-active enzymes (CAZymes)
Cell wall-degrading enzymes (CWDE)
Cellular components (CC)
Classically secreted proteins (CSP)
Counts per million (CPM)
Differentially expressed genes (DEGs)
Dimethylallyltryptophan synthase (DMATS)
Extreme gradient boosting (XGBoost)
Gene ontology (GO)
Glycosyl hydrolase (GH)
Hierarchical clustering based on principal components (HCPC)
Indoleamine 2,3-dioxygenase (IDO)
Internal Transcribed Spacer (ITS)
Leaderless secretory proteins (LSP)
Long Non-Coding RNA (lncRNA)
Mass spectrometry (MS)
Molecular function (MF)
Non-ribosomal peptide (NRP)
Non-ribosomal peptide synthetase (NRPS)
Nonsense mediated decay (NMD)
Plant cell-wall (PCW)
Polyketide (PK)
Polyketide synthase (PKS)
Principal component analysis (PCA)
Random forest (RF)
RNA polymerase II (*rpb2*)
Small secreted proteins (SSPs)
Szeged Microbiology Collection (SZMC)
Translation elongation factor 1-alpha (TEF1)
Trichoderma atroviride SZMC 24276 (TA)
Leaderless secretory proteins (LSP)

1. INTRODUCTION

Armillaria, occasionally referred to as the "oak root fungus" or "honey fungus," is a fungal genus within the *Physalacriaceae* family. These fungi have a broad geographical distribution and are renowned for their remarkable wood decomposition abilities. Taxonomically, they are categorised as members of the *Armillaria* genus, situated within the kingdom Fungi, phylum *Basidiomycota*, class *Agaricomycetes*, and order *Agaricales*. The Armillarioid clade includes both *Armillaria* and *Desarmillaria* species, functioning as primary or opportunistic pathogens or saprotrophs (Koch *et al.,* 2017; Kedves *et al.,* 2021). These species are globally recognised as the cause of devastating root rot diseases, which impact hundreds of tree species, resulting in substantial economic losses worldwide. Pathogenic *Armillaria* species are responsible for infecting woody plants, leading to sudden death or, in certain instances, crown dieback, lesions, and reduced growth (Baumgartner *et al.,* 2011). The fungus employs a variety of virulence-related proteins to suppress its host, as well as utilising genes associated with wood-degrading abilities to decompose the pectin and lignocellulosic components of the plant cell walls (Sahu *et al.,* 2023). After the successful killing of the host plants, the infected stumps serve as an inoculum basis for their following infection, enabling them ultimately to survive for decades in the soil.

This dissertation primarily aims to investigate and elucidate the function of putative secretory genes, lncRNAs, and the associated microbiomes in the interplay between fungi and plants and their impact on fungal virulence.

1.1. Identification and nomenclature of *Armillaria*

The initial step in identifying *Armillaria* or *Desarmillaria* species or subspecies frequently involves assessing morphological traits, such as the presence of a ring, stem structure, ornamentation, and the development of specialised root-like structures known as rhizomorphs. These rhizomorphs consist of densely packed fungal hyphae and are vital for understanding the species. As an apparent morphological feature, the fruiting body of *Armillaria* is ring-shaped and produces abundant rhizomorphs compared to its *Desarmillaria* counterparts. However, relying on morphological features to distinguish *Armillaria* species in the field environment would be challenging, as they tend to change with season and age. Furthermore, growing fruiting bodies in an *in vitro* environment is tedious, and resulting fruiting bodies would not necessarily resemble those in nature (Guillaumin *et al.,* 1985). In

addition, most related *Armillaria* species, such as *A. cepistipes and A. gallica,* have congruent fruiting bodies (Park *et al.,* 2018). To circumvent such problems, "biological" species concepts are applied, in which individuals of a species interbreed to produce offspring. This process involves testing somatic tolerance/incompatibility reactions such as hyphal mating (Kile, 1983). Although this test is convenient, many researchers observed that haploid-diploid crosses were difficult to interpret and led to controversial identification, raising doubts about the accuracy of the method (Guillaumin *et al.,* 1991).

Biochemical methods such as using monoclonal/polyclonal antibodies and isoenzymes also appeared to help identify *Armillaria* species (Burdsall *et al.,* 1983). For example, Bragaloni *et al.* (1997) used isoenzyme profiles to identify *Armillaria* species, and Bruhn *et al.* (1998) used esterase and polyphenol oxidase production from *A. mellea*, *D. tabescens*, and *A. gallica* to study facets of their mycelial growth. However, this method of species identification struggled to distinguish two closely related species, so its popularity waned. Another method to identify fungi could be the matrix-assisted laser desorption ionization (MALDI) time of flight (TOF) method, where mass spectrometry (MS) is used for surface analysis of the fungal culture. Carolis *et al.* (2012) attempted to use MALDI-TOF MS to identify and discriminate fungal species such as *Aspergillus*, *Fusarium,* and Mucorales from clinical microbiology laboratories. They identified 103 isolates, compared MALDI-TOF to sequence-based identification methods, and found that 96.8% of the examined strains could be identified down to the species level. Although this technique is efficient and cost-effective, the availability of a limited database for identification and comparison still poses a significant challenge with this method of fungal identification.

With the advancement in molecular biology techniques such as qualitative PCR, real-time quantitative PCR, or PCR-DGGE (PCR-denaturing gradient gel electrophoresis) and the reduction in the cost of deoxyribonucleic acid (DNA) sequencing, the subsequent tool of choice for most researchers is the phylogenetic method for species identification (Baumgartner *et al.,* 2011). Mulholland *et al.* (2011) used species-specific primers that bind to the translation elongation factor 1-alpha gene (*tef1*) to perform a PCR-based and pyrosequencing-based diagnostic screen on northern European *Armillaria* species. Although the method was fast and effective, sequence heterogeneity within the strain cannot be analysed.

Brazee *et al.* (2011) compared the three different markers *tef1*, RNA polymerase II (*rpb2*), and the nuclear large subunit to identify the most efficient markers that could differentiate six different *Armillaria* species (*A. calvescens*, *A. gallica*, *A. gemina*, *A. mellea*,

A. sinapina and *A. solidipes*). They found that *tef1* efficiently discriminated even between close *Armillaria* species such as *A. calvescens* and *A. gallica*. However, they suggested combining other highly conserved markers, such as internal transcribed spacer (ITS) and *rpb2*, for a better resolution. Although combining *tef1* with additional markers such as *rpb2* is very effective, determining the intraspecies boundary of *Armillaria* species from different continents is often problematic. For such problems, phylogenomic approaches such as utilising complete orthologous genes could prove decisive. The *Armillaria* and *Desarmillaria* clades could be easily separated using the orthologous genes in our analysis (Kedves *et al.,* 2021), and it also confirmed that there are three genera in the armillarioid clade, namely *Armillaria*, *Desarmillaria,* and *Guyanagaster* (Fig. 1).

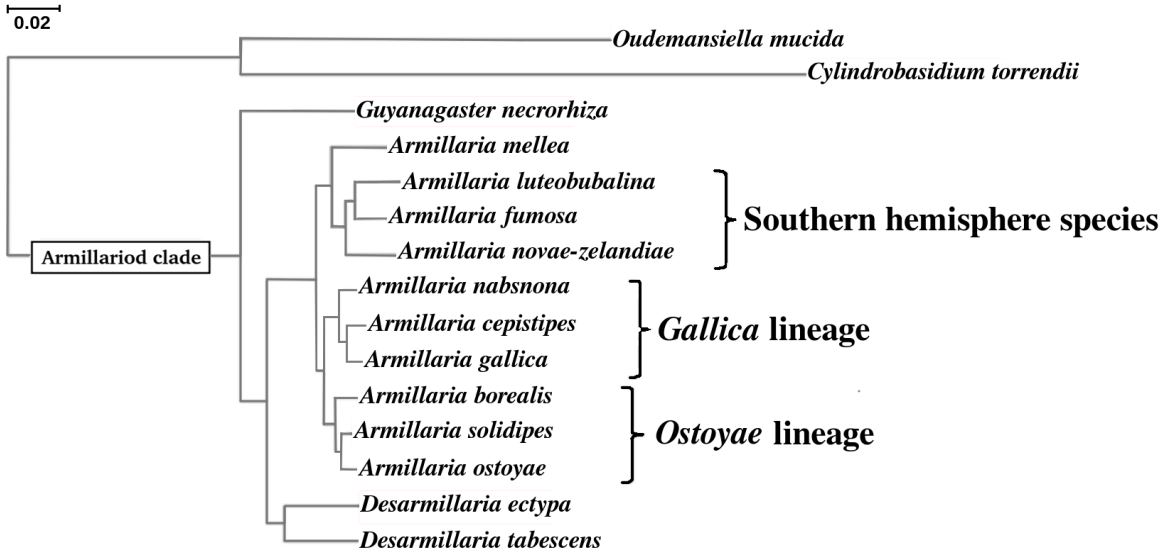

Fig. 1. Maximum likelihood phylogenetic tree of Armillaria species built using single copy orthologs (Kedves *et al.,* 2021).

1.1.1. *Armillaria* occurrence and lifestyle

Armillaria spp. are widely spread almost all over the world. Koch and Herr (2021) identified that the armillarioid species richness is high in the northern hemisphere especially in East Asia. The *Armillaria* species in China were significantly found to be conspecific to other *Armillaria* species in the northern hemisphere. In their study, they reiterated that "*Mellea"*, and "*Tabescens*" are collections of diverse species. This finding is in congruence

with our idea of possible "*Ostoyae*", "*Mellea*" and "*Gallica*" lineages, which are collections of complex species.

The distribution of *Armillaria* could depend on the type of the tree species; for example, *A. mellea*, *A. gallica,* and *D. tabescens* exist mainly on hardwood or broad-leaved species, while *A. ostoyae* and *A. borealis* on softwoods. *A. ostoyae,* which is a primary pathogen, has been reported from various high altitude and low altitude regions (100-1800 m) such as Switzerland, Ukraine, southern mountains of Serbia, England and the Balkan peninsula (Prospero *et al.,* 2004, Tsykun *et al.,* 2012, Keča *et al.,* 2006, Drakulic *et al.,* 2017, Grillo *et al.,* 1996). *A. solidipes* (another primary pathogen) is particularly common in Canada, North-Western and interior South-Western USA (Hanna 2005). *A. sinapina* (weak pathogen) has been reported from regions such as Alaska from a variety of hosts such as *Picea glauca*, hardwood-birch, willow, and Douglas-fir (Morrison *et al.,* 1985; Klopfenstein *et al.,* 2009). *A. gemina* (primary pathogen) is predominantly found in the Eastern United States, where it survives on a limited host range such as *Fagus grandifolia* and *Betula alleghaniensis* (Bérubé & Dessureault, 1989; Anderson, 1986.). *A. borealis* has been reported mainly from Slovenia, Albania and Scandinavian countries where it acts on woody plants as a weak secondary pathogen (Roll‐Hansen, 1985).

A. mellea strains are potent pathogens known to cause root rot diseases in various woody plants. They are dominant fungal pathogens in Greece, and they have also been reported from Central, Southern, and Western Europe, England, and North America (Cromey *et al.,* 2020; Storozhenko & Krutov, 2004; Bruhn *et al.,* 2000; Thomidis & Exadaktylou, 2012). They are also known to cause diseases in peach plants and are commonly reported from the south-eastern USA along with *D. tabescens (*Cox & Scherm, 2006; Beckman *et al.,* 1998*)*.

A. gallica strains are mostly opportunistic pathogens. The "Gallica" lineage includes *A. gallica*, *A. cepistipes*, *A. calvescens*, *A. nabsnona*, *A. altimontana* and "*Nag.E* " isolates from Japan (Coetzee *et al.,* 2018; Klopfenstein *et al.,* 2017). They grow along with *A. mellea,* targeting similar hosts such as oaks or other hardwood plants. They have been observed to share geographic regions with *A. mellea* in Central North America (Klopfenstein *et al.,* 2014). Isolates of *A. gallica* from central Mexico were found to be virulent pathogens on living plants (Duarte-Mata *et al.,* 2021), which was inconsistent with previous reports of a virulent attack by *A. gallica* on peach trees in Mexico (Elías‐Román *et al.,* 2013). The saprotrophic *A. cepistipes* is a frequently occurring armillarioid species throughout Europe (Kedves *et al.,* 2022). This species was sometimes found as a pathogen on grapevines (*Vitis*

spp.) at elevations of 800 to 1800 m, for the most part as a saprophyte on coniferous and deciduous trees in beech and silver fir woodlands (Lushaj *et al.,* 2010). *A. cepistipes* is commonly seen along with *A. ostoyae*, for instance in Serbia, they have been noticed together in silver fir and Norway spruce (Keča *et al.,* 2009). *A. calvescens* and *A. nabsnona* are to a great extent limited to certain hardwood tree species in the US, such as maple (*Acer macrophyllum*), vine maple (*Acer circinatum*), ruddy birch (*Alnus rubra*), etc. (Brazee *et al.,* 2011, Volk *et al.,* 1996) *A. altimontana* is found on hardwoods and conifers like western white pine along with *A. solidipes* (Brazee *et al.,* 2012).

D. tabescens or *D. caespitosa* (North American variant) is a worldwide saprotroph with many hosts (Antonín *et al.,* 2021). Hardwood forests, especially oak forests, are where they are most often spotted. They are frequented in the coastal area of Western Europe to Southern Britain (Guillaumin *et al.,* 1993; Drakulic *et al.,* 2017). Previous studies have discovered a distinct range of *Armillaria* species throughout the southern hemisphere (Koch *et al.,* 2017). Koch *et al.,* (2021) did not observe any shared *Armillaria* species between the South American and Australasian *A. novae-zelandiae,* as Coetzee *et al.* (2018) suggested. Their ITS-based phylogenetic analysis from sporocarps identified unique intraclade substrata from biogeographical areas. Some of the *Armillaria* species from Africa include *A. heimii* and *A. mellea* from the temperate regions.

1.1.2. Infection strategies of *Armillaria*

To date, about 13 *Armillaria* genomes have been reported, including novel genome reports (Collins *et al.,* 2013; Sipos *et al.,* 2017). Comparative genomic studies by Sipos *et al.* (2017) have revealed that plant cell wall degrading enzymes (CWDEs) and genes implicated in pathogenicity fully complement the four *Armillaria* genera. The result also showed that the chitin-binding and pectin degradation genes were among the top candidate genes. By characterising genomic and transcriptomic differences between pathogenic and saprotrophic activities, as well as virulent and non-virulent isolates of pathogenic species and their interactions with host-associated microbial communities, we can better understand the networks of genes involved in host interaction.

1.1.3. The life cycle of *Armillaria*

Armillaria breaks down residual wood in the soil during the saprophytic stage. This decomposing matter serves as a source of inoculum for *Armillaria*, which can then move to and parasitize living hosts. Rhizomorphs can penetrate the soil, and upon direct contact with the roots of susceptible trees, they can initiate infection (Fig. 2). To infect the host, the pathogen attaches itself to the host surface using rhizomorphs. Thomas (1934) and Yafetto *et al.* (2009) noted that *Armillaria* secretes glue-like sticky substances around its rhizomorphs to allow them to attach to host surfaces properly. Once the *Armillaria* attach to the host roots, the rhizomorphs employ a particular form of structures called hyphae that grow into the woody roots of the hosts (Baumgartner & Rizzo, 2006). The rhizomorphs can penetrate all types of roots of susceptible hosts, and a prior wound is not required for host penetration (Cleary *et al.,* 2012).

Armillaria can enter host tissues by a variety of methods, including (1) mechanical pressure to pierce the cells using hyphae from rhizomorphs or appressorium-like structures, (2) employment of toxins and plant CWDEs following attachment to provide a site of entrance, (3) exploiting the wounded surface of the cell wall to achieve access, and (4) exploiting natural cell junctions of cortical cells (Devkota & Hammerschmidt, 2020).

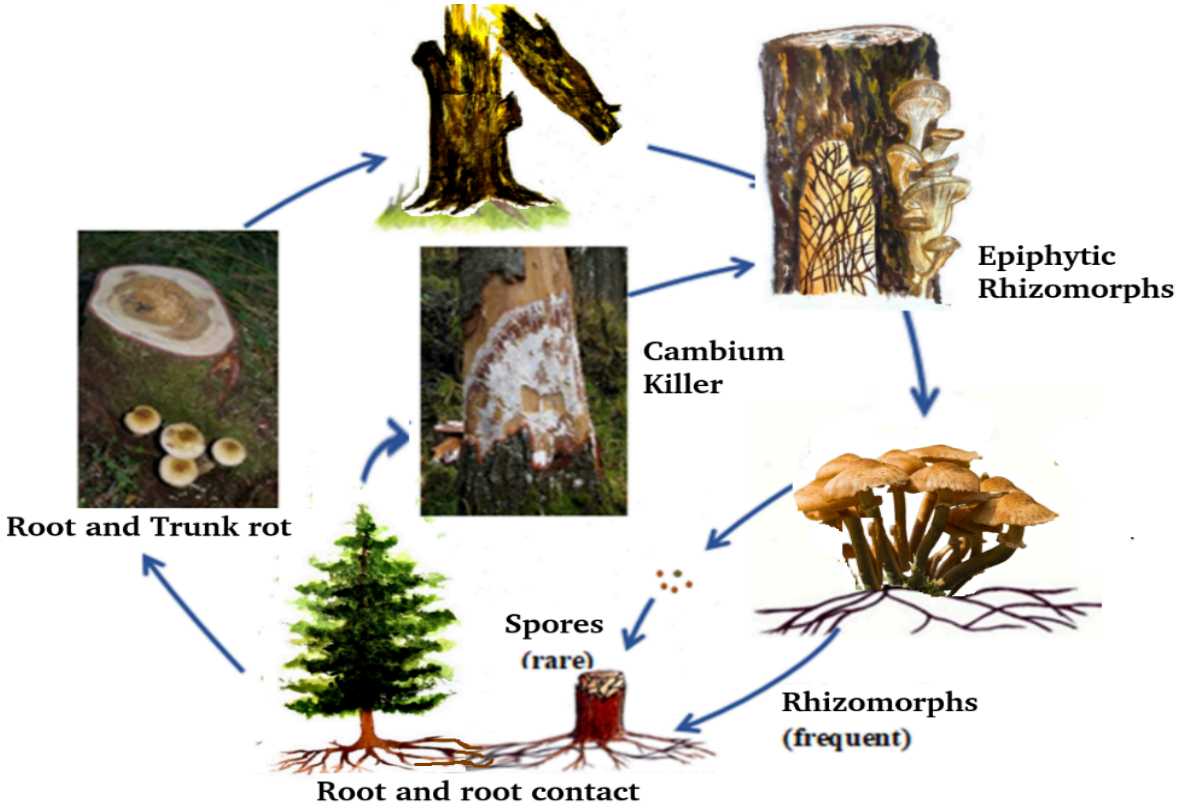

Fig. 2. Life cycle of *Armillaria* spp.

The utilisation of mechanical pressure to push through the host cell wall was first suggested by Thomas (1942) and later observed by Solla *et al.* (2002). In their microscopic study, they identified the cortical cells that were pushed inward by rhizomorphs, indicating their mechanical strength. The peripheral branch of the rhizomorph works as a unit to pierce through the host mechanically. The number of hyphae emanating from the rhizomorphs depended on the type of root structure of the host plants. For example, a single hypha grows from the tip of the rhizomorph in a host with rough bark (peach roots), while multiple branches of hyphae invade the roots of hosts with smooth papillary dermis (Persian walnut). Individual hyphae were considered essential for fungi when piercing thick roots, because the force of individual hyphae on a reduced diameter of the surface of the plant root cell wall has greater potential for piercing (Dickinson, 1960). Abundant melanin secretion by *Armillaria* might be responsible for the strength and agility of *Armillaria* rhizomorphs, hyphae, and appressoria (Howard & Ferrari, 1989). According to Sesma & Osbourn (2004), the development of melanized appressoria by *Magnaporthe grisea* was an essential prerequisite for leaf infection. It could be similar even in the case of *Armillaria* rhizomorphs and appressorium base penetration. Besides utilising mechanical pressure, *Armillaria* also employs toxic secondary metabolites such as oxalic acid (OA) and various proteinaceous secretory plant CWDEs to degrade plant cell walls and gain entry (Mallett & Colotelo, 1984; Collins *et al.,* 2013).

Once the host tree is infected, mycelial fans begin to spread in the host's vascular cambium, as seen in Fig. 2. *Armillaria* infection kills the tree, and once the tree is dead, the fungal mycelia can survive saprotrophically. The dead tree then becomes the disease centre, from which the fungi can explore and infect neighbouring areas with the rhizomorphs. Redfern (1973) reported that *Armillaria* rhizomorphs could expand up to a metre in a year, and therefore, the fungi can cause major problems by infecting lots of trees in the surroundings. *Armillaria* fruiting bodies, which produce sexual basidiospores, grow around the infected trees, and epiphytic rhizomorphs can be seen in the bark of the dead trees. Spores from the fruiting bodies are released into the environment, and they can establish themselves on dead hosts, and the cycle continues.

1.2. Molecular background of the plant-fungus interactions

During the plant-pathogen interaction, plants and fungi secrete proteinaceous and non-proteinaceous molecules to communicate. Fungi release effectors to trick/suppress the plant defense system and to establish infection (Franceschetti *et al.,* 2017). The small secreted proteins (SSPs) were initially identified as "effectors" that elicited host immune response when identified by the plant immune receptors. Since then, many systemic studies identified hundreds of fungal secretomes involved in plant-pathogen infection (Varden *et al.,* 2017). Fungal secretome refers to the diverse array of secretory proteins (soluble secreted or other extracellular proteins attached to the surface of cells), and chemicals that are involved in interacting with the external environment (Girard *et al.,* 2013). Secretory proteins, which comprise 4-5% of the total genes in the genome of fungi are involved in helping fungi to obtain nutrients from a range of surrounding substrates and protect them in extreme conditions. Hess *et al.* (2018) observed that "gene repertoire size" and "genome size" did not vary much between ectomycorrhizal and saprophytic fungi. It was observed that the symbiosis-related genes were also present in saprophytic fungal species, which could explain why fungi can switch between different lifestyles, such as pathogenic to saprophytic or *vice versa*, or even as mutualistic. Although their analysis explains how fungal species within a specific genus might switch between different lifestyles, it does not necessarily explain the lifestyles reflected by the secretory protein repertoires in diverse species of fungi from different genera. Krijger *et al.* (2014) identified that the secretory protein repertoires could be correlated to phylogeny rather than to the lifestyle of fungi. All these studies indicate that the composition of secretory proteins and their expression on the manifestation of a specific lifestyle may contribute to its behaviour dynamics. Secretory proteins can be categorized into two groups: a) Classically secreted proteins with an N-terminal signal and a cleavage site and b) proteins secreted using unconventional secretion pathways (LSP proteins).

1.2.1. SSPs and other classically secreted proteins

Small secreted proteins (SSPs) refer to classically secreted proteins whose length is less than 300 amino acids. Most SSP functions are unknown, as orphan genes encode them and they are specific to fungal species. They also show no sequence similarity and, hence, are less conserved. Although they do not show sequence conservation, some have been reported to exhibit structural conservation (Lo Presti *et al.,* 2015; Lo Presti & Kahmann, 2017). The

structural conservation could be due to the strong selective pressure leading to divergent evolution. Some SSPs could be expanded due to events like HGT (horizontal gene transfer), duplication, or speciation. SSPs help the fungi cope with the harsh environment and are involved in offensive and defensive actions. Cysteine-rich (3% cysteine residues) SSPs have been of great interest to researchers as they are involved in modulating host physiology and suppressing the host immune responses during host-pathogen interaction. Mycorrhiza-induced small secreted proteins (MiSSPs) were identified as responsible for controlling plant defense response by symbiotic fungi (Plett *et al.,* 2011; Pellegrin *et al.,* 2015; Martin *et al.,* 2016). MiSSP7, which was highly upregulated in the root tips of the ectomycorrhizal fungi *Laccaria bicolor,* is involved in manipulating the jasmonate signaling pathways in plants and helping them establish colonies. Kloppholz *et al.* (2011) observed another SSP called SP7 manipulating ethylene signaling pathways in plants to alter their defense mechanism. Some necrotrophic pathogenic fungi, such as *Stagonospora nodorum,* secrete toxic peptides SnTox1, SnToxA, and SnTox2 that cause plant necrosis. Another necrotrophic fungus, *Pyrenophora tritici-repentis,* was found to secrete a 13.2-kDa protein called ToxA that causes necrosis in wheat. Wheat mesophyll cells have a high-affinity binding site for ToxA that interacts with it via the Arg-Gly-Asp (RGD)-containing, solvent-exposed loop, triggering toxin uptake and cell death. All these findings suggest that SSPs are crucial for establishing infection by hijacking the plant's immune response (Moffat *et al.,* 2014). Caballero *et al.* (2022) compared the genomes of weak opportunistic pathogen *A. altimontana* and virulent pathogen *A. solidipes*, and they identified that genomes of both *Armillaria* species had similar gene sets and were very much comparable despite *A. altimontana* having larger genome size. To their surprise, they identified that most of the SSPs they harboured were species-specific genes, and their functions were primarily unknown.

Likewise, Sahu *et al.* (2023) explored the PiSSPs (pathogenicity-induced small secreted proteins) expressed by *A. luteobubalina* and *A. ostoyae* during the infection of the host system. Their study meticulously identified the two most robustly expressed, yet unannotated PiSSPs from *A. luteobubalina*. Taking their investigation further, they cloned and introduced these PiSSPs into the non-host *Nicotiana benthamiana* and *Eucalyptus grandis* (the natural host). This endeavor yielded an unexpected outcome: the cloned PiSSPs promptly instigated necrosis in the plant tissues. The study of these SSPs secreted by *Armillaria* spp. during infection holds the promise of unraveling the intricate pathosystem these organisms weave.

1.2.2. Leaderless secretory proteins (LSPs)

LSP proteins are secreted using unconventional protein secretion pathways (Krause *et al.,* 2013). They lack an N-terminal signal peptide sequence and are endoplasmic reticulum (ER)/Golgi independent. They are exported directly via vesicular or non-vesicular transport systems. The vesicular system involves autophagy-based secretion, and the non-vesicular pathway is a direct transport across the plasma membrane. The exact mechanism of UPS is unknown; however, UPS (unconventional protein secretion) can be studied using brefeldin A, which blocks the transport of proteins from ER to Golgi (Rabouille, 2017). Some chitin synthases, cellobiase, and PepN have been identified to be secreted via the UPS pathway in fungi like *Aspergillus* spp., *Ustilago maydis,* and *Neurospora* spp. Chitinases in *U. maydis* are reported to be secreted using the fragmentation zone during the division of mother and daughter cells (Robinson *et al.,* 2016). Another pathway for protein secretion is peroxicretion, observed by Sagt *et al.* (2009). In their study, they found that proteins tagged with peroxisome import signal (SKL tag) were imported to peroxisomes and secreted to the extracellular space from the peroxisomes, which were anchored to the plasma-membrane using V-SNARE proteins. Even in *Armillaria* spp. host-pathogen interactions, LSP proteins might play a central role, and hence, we reported the putative LPS proteins in our current work reported in this thesis.

1.2.3. Secreted proteases as virulence factors

Plant pathogenic fungi secrete diverse PCWDEs to break down cell wall components of plants and to aid invasion of host cells. Protease enzymes along with glycanases play a major role in plant cell-wall degradation and interaction with hosts (Kubicek *et al.,* 2014; Jashni *et al.,* 2015). They also act as virulence factors and have a role in pathogenesis of plant-pathogenic fungi (Jashni *et al.,* 2015b; Saitoh *et al.,* 2009). It has been observed that saprophytic fungi produce proteases according to their nutrient demand, therefore the variety and proportion of protease churned out determines the nature of a fungus to be saprophytic or pathogenic. Categorization of proteases can be predicated on the functional group that occurs in its active site, such as aspartic proteases, serine proteases, metalloproteases, glutamic proteases, cysteine proteases, threonine proteases and unknown (Rawlings *et al.,* 2014). Movahedi & Heale (1990) observed that *Botrytis cinerea* secreted aspartyl proteases in the tissues of infected carrots whereas it was not present in the uninfected carrots. This indicated

that aspartyl protease is crucial for establishing infection. Similar observation was made by Gregori *et al.* (2010), who identified abundant production of cysteine, serine and aspartic proteases by the soft-rot fungus *Glomerella acutata*. Redman & Rodriguez (2002) studied the importance of an extracellular serine protease encoding gene in the tomato pathogen *Colletotrichum coccodes* by silencing the gene, and discovered that silencing that gene converted the virulent pathogen into a nonvirulent endophytic fungus. The importance of extracellular proteases for virulence and pathogenicity has been observed in a range of fungal species including *Pyrenopeziza brassicae*, *Verticillium dahliae*, *Magnaporthe oryzae*, *U. maydis* and *F. oxysporum* (Batish *et al.,* 2003; Zhang *et al.,* 2019; Saitoh *et al.,* 2009; Mueller *et al.,* 2013; Jashni *et al.,* 2015). A novel class of metallo endopeptidase produced by the fruiting bodies of *A. mellea* was identified by Healy *et al.* (1999). In their study, Perazzolli *et al.* (2010) observed that grapevine roots expressed defence-related genes when infected by *A. mellea* and the list included protease inhibitors genes as well. The upregulation of protease inhibitor-related genes in grapevine roots may be attributed to the inhibition of proteases associated with *A. mellea*, which could have been expressed as a defence mechanism during the infection process, aimed at protecting the plant from the invading fungal pathogen.

1.2.4. Role of plant cell wall degrading enzymes during infection

Cell wall degrading enzymes (CWDEs) constitute carbohydrate-active enzymes (CAZymes) that are released by plant pathogens to invade and break down plant cell walls, and these CAZymes are tied directly to severe plant disease (Zhang *et al.,* 2014; Somai-Jemmali *et al.,* 2017; Gawade *et al.,* 2017). Phytopathogenic fungi belonging to phyla such as Ascomycota, Basidiomycota, Chytridiomycota, and Mucoromycota have been shown to possess a vast arsenal of CAZymes (Zhao *et al.,* 2014; Kubicek, Starr & Glass, 2014). Changes in wood component composition and structure are frequently paralleled by the kinds of lignocellulolytic enzymes secreted by the overwhelming pathogenic fungus (King *et al.,* 2011). Compared to saprotrophs, several phytopathogens, notably white rot fungi, have been identified to secrete a diverse array of lignocellulolytic enzymes for attacking specific hosts and degrading plant biomass. It is interesting to note that various profiles of CAZymes were released by pathogenic fungi at different phases of the transition from biotrophic to necrotrophic lifestyles, according to genome and transcriptome investigations (O'Connell *et al.,* 2012; M'Barek *et al.,* 2015). CWDE synthesis of pathogenic fungi has been revealed to be connected to the pathogenicity and cell wall of the infected plant hosts (Kang &

Buchenauer, 2000; Wanjiru *et al.,* 2002; Lyu *et al.,* 2015; Somai-Jemmali *et al.,* 2017). Given the importance of CWDE in nutrient acquisition from plant hosts, these hydrolytic enzymes are regarded as the primary pathogenicity determinant among plant diseases (Brito *et al.,* 2006; Kubicek *et al.,* 2014; Bravo *et al.,* 2016). Some of the PCWDE act on the mucilaginous cuticle of plant cell wall by secreting cutinase enzyme during the start of infection while some others act on lignocellulose, pectin, or other polysaccharides by secreting endoglucanases, laccases, pectinases. During the process of plant cell wall breakdown, specific oligosaccharides like the tetrasaccharide 31-β-D-cellobiose/ 31-β-D-cellulosic glucose are released, and they act as PAMPs (pathogen-associated molecular patterns) or DAMPs (danger-associated molecular patterns). DAMPs released via β-1,3-glucan degradation using secreted GH17 and GH15+CBM20 by the fungi *Cladosporium fulvum* and *B. cinerea* cause plant cell necrosis (Ökmen *et al.,* 2019; Yang *et al.,* 2018). PCWDEs help *Armillaria* spp. to promote infection by efficiently degrading the lignocellulose components of plants. Sipos *et al.* (2017) reported that pectin-degrading CAZymes (GH28,78,88 and PL1,3,4,9) were overrepresented in *Armillaria* spp. compared to other white-rot species. The availability of a broad repertoire of pectinolytic genes might provide *Armillaria* spp. the ability to act as powerful necrotrophic fungi. On comparing the secretory CAZymes of saprophytic *A. altimontana* and *A. solidipes,* Caballero *et al.* (2022) identified that *A. solidipes* possessed more prominently cellulose-, hemicellulose- and lignin-degrading CAZymes in contrast to *A. altimontana*, which had larger pools of hydrophobins, cerato-platanins and fungal cell wall associated enzymes. Even though this is an interesting finding, further studies are needed to understand how the regulation of CAZymes changes depending on the phylogeny and lifestyles.

1.2.5. Role of secondary metabolites in fungus-plant interaction

Only a few fungal secondary metabolites with known biological functions have been identified in *in vitro* studies and *in vivo* plant-fungus interactions. However, transcriptomic studies have identified many secondary metabolites gene clusters expressed in fungi during plant-fungus interaction. For instance, six secondary metabolite genes were found to be expressed during the early stage of wheat infection by Boedi *et al.* (2016). Numerous genome-wide expression research indicated that the expression of secondary metabolites in fungi peaked during the early infection stage of the plant-fungus interaction. These secondary metabolites expressed during the initial stage may act as virulence factors that interfere with

the normal functioning of the host cells and aid in fungal invasions. Antipova *et al.* (2022) studied the *in vitro* toxicity of the secondary metabolites in six *Armillaria* species (*A. mellea, A. gallica, A. cepistipes, A. borealis, A. ostoyae,* and *A. sinapina*). All the *Armillaria* species synthesized melleolide D and melledonal C. Then, they tested the effects of those two metabolites in *Pinus sylvestris* and *Larix sibirica* and found that only 0.5% concentration of the mixture of the two metabolites at a 1:1 ratio inhibited the growth of both conifer seedlings. *P. sylvestris* was more susceptible than *L. sibirica* as it started manifesting several symptoms compared to control in 5 days, whereas in the case of *L. sibirica* it took 21 days.

1.2.6. Role of lncRNA (long non-coding RNAs) in fungal plant pathogenesis

Studies on the role of long non-coding RNAs in the pathogenesis of plant pathogenic fungi are limited. Liu *et al.* (2022) attempted to study the role of lncRNAs in *Verticillium dahliae* and identified two lncRNAs (XLOC_006536, XLOC_000836) that were involved in the regulation of pathogenesis in cotton. Mutating the two lncRNAs reduced the virulence and pathogenicity of the fungi to invade the cotton. Previously, mutation studies identified lncRNA RZE1 in *Cryptococcus neoformans* as involved in the regulation of Znf2, which was involved in the fungal switch from yeast to hyphae (Lin *et al.,* 2010). Donaldson *et al.* (2013) and Goulet *et al.* (2020) observed that a lncRNA, ncRNA1 was the regulator of pathogenesis in *Ustilago maydis* by controlling the level of antisense transcript expression and deletion of ncRNA1 reduced virulence of *U. maydis*. Nonsense-mediated decay (NMD) pathway might be involved in maintaining the expression levels of lncRNAs, and deletion of the NMD pathway-related gene *xrn1* exonuclease resulted in reduced virulence of *Cordyceps militaris* (Wang *et al.,* 2019). Additional analysis revealed that around ten lncRNAs were upregulated on deletion of *xrn1* and eight genes involved in pathogenicity and virulence were downregulated. Choi *et al.* (2022) identified the lncRNAs expressed in *Magnaporthe oryzae* during the different stages of infection (vegetative mycelia, pre-penetration stage, biotrophic stage, necrotrophic stage). They observed that effectors and PCWDEs could be associated with the lncRNAs. In *Armillaria* spp., the role of lncRNAs in virulence and pathogenesis has not been previously reported. Therefore, here we first report the genome-wide existence of lncRNAs in the *A. ostoyae* genome and their potential role in the molecular pathogenic interactions between *A. ostoyae* and *P. abies*.

1.3. Interaction of *Armillaria* with the microbiome

Soil habitats are continually being studied to learn more about the multiple functions played by microorganisms, parasites, and their metabolites (Song *et al.,* 2020; Wrzosek *et al.,* 2017; Heinzelmann *et al.,* 2018). Many types of primary pathogenic fungi might also influence armillarioid species when infecting trees. Some examples are *Phaeolus schweinitzii* that causes butt rot in Douglas-fir, or *Ophiostoma wageneri* that produces black stain root disease in conifers. Several studies have also observed that *Heterobasidon annosum* and the parasitic plant dwarf mistletoe (*Arceuthobium*) frequently co-occur with armillarioids (Wargo *et al.,* 1992). Besides them, some other fungi that exist in stumps, trees or in the rhizosphere may also act as stimulants of armillarioids. Studies by Percival *et al.* (2011), Pellegrin *et al.* (2015), and Chen *et al.* (2019) demonstrate that some of the soil's resident fungi, such as *Trichoderma* spp., play a central role in the growth and development of *Armillaria* rhizomorphs. Additionally, non-harmful *Armillaria* species like *A. altimontana* may be able to restrain the spread of *Armillaria* species that cause root diseases like *A. solidipes* (Warwell *et al.,* 2019). Soil *Armillaria* growth may be stifled by the presence of other antagonistic fungi, such as *Rhizoctonia lamellifera*, *Coriolus versicolor*, *Xylaria hypoxylon*, *Hypholoma fasciculare* and *Entoloma abortivum* (Mercado-Blanco *et al.,* 2018; Stevens *et al.,* 2020; Koch & Herr, 2021). Lalande *et al.* (2019) studied the microorganisms that could be associated with the highly virulent plant pathogen *A. solidipes* and the less virulent *A. altimontana.* They reported that *Pseudomonadaceae* and *Spartobacteria* were linked to thriving trees, while *Acidobacteria* were associated with decaying ones. *Acidobacteria* and *Enterobacteriaceae* were linked with *A. solidipes*, whereas more *Pseudomonadaceae* and Rhizobiales were associated with *A. altimontana*. Przemieniecki *et al.* (2021) reported the microbiome inhabiting the rhizomorphs of *A. ostoyae* killing Scots pine. They observed that with the progression of tree dieback, the number of Bacillales increased. The presence of bacteria involved in cellulose and hemicellulose degradation in the rhizomorphs might aid them in decomposing wood materials and sharing nitrogen.

1.4. Biocontrol of *Armillaria*

Chemical methods of eradicating armillarioids are largely ineffective. Using efficient biocontrol strategies, either alone or in tandem with other control measures, is increasingly gaining momentum. Paper birch fosters a more bacterially favourable environment than Douglas-fir, attracting fluorescent pseudomonads and positively affecting the tree's susceptibility to Armillaria root disease (De Long *et al.,* 2002). To a large extent, the development of *A. solidipes* was stunted in several tree species by several isolates of fluorescent bacteria. Besides bacteria, different species of *Trichoderma* are well-known for their ability to act as antagonists to a wide range of plant pathogenic fungi. Scanning electron microscopy images revealed that *Trichoderma* hyphae penetrated the melanized exterior tissue of the rhizomorphs of the host fungus, and they destroyed the hyphae of *Armillaria gallica* via twisting and lysing of hyphal cells (Dumas & Boyonoski, 1992). It was also observed that metabolites produced by *Trichoderma* spp. prevented infection of *Camellia sinensis* roots (Onsando & Waudo, 1994). *Trichoderma* species are also known to hydrolyze and break down host cells and feed on them (Elad *et al.,* 1983). It was also observed that the plants quickly improved in health and leaf production in the presence of *Trichoderma* antagonists. In order to prevent grapevine root rot, the *Trichoderma atroviride* SC1 isolate was used in a controlled experiment. When *T. harzianum* was added to the soil around the inoculum of *Armillaria* that had been introduced through wood, the pathogen's viability was drastically reduced (Savazzini *et al.,* 2009). Keeping an adequate population after the initial inoculation, which is necessary for managing *Armillaria*, is the main challenge in using them as BCAs (biocontrol agents). Besides mycoparasites like *Trichoderma*, plants' resistance to certain fungal pathogens is increased by arbuscular mycorrhizal fungi and saprophytic basidiomycete fungi. They were proven effective as biocontrol agents in reducing and even preventing armillarioid invasion and colonisation (Bruisson *et al.,* 2016).

1.5. Prospects using armillarioids in mycoremediation

Mycoremediation uses fungi and their enzymes to cleanse polluted soil or water using biodegradation or biosorption processes (Barr & Aust, 1994; Kulshreshtha *et al.,* 2014). *Armillaria,* as a white rot fungus, uses enzymes like laccases, cytochrome p450 monooxygenases, FAD monooxygenases, cutinases, peroxidases, hydrolases, and antioxidants to degrade lignin (Akhtar & Mannan, 2020). Those enzymes that are secreted by

the *Armillaria* cells can also be used for bioremediation. Yildirim *et al.* (2018) found that one armillarioid species, *Desarmillaria tabescens*, effectively broke down malathion pesticides in liquid media, showing that the fungi could be used to treat wastewater. Rigling *et al.* (2006), who were studying the biosorption abilities of *Armillaria* species, found that the rhizomorphs of *A. ostoyae* and *A. cepistipes* cleared heavy metals from contaminated soils very efficiently. Similarly, Xu *et al.* (2019) recently used *A. cepistipes*, *Amanita muscaria*, *Xerocomus badius*, and *Bjerkandera adusta* to identify the fungi that could clear vanadium contamination. Their study interestingly highlighted that *A. cepistipes* could remove vanadium from the media. Krijger *et al.* (2014) found that a fungus's ability to grow and survive in a challenging environment is directly linked to the repertoire of specific genes and protein families. Hence, screening for the xenobiotic-degrading enzyme repertoires in the armillariod species and contrasting them with other fungal species can help us understand its bioremediation potential.

1.6. Application of Machine Learning in modelling the white-rot infection strategy of *Armillaria*

Machine Learning (ML) is a subfield of AI (Artificial intelligence) that uses algorithmic frameworks to gain insights into data and lay the groundwork for identifying relationships (Myszczynska *et al.,* 2020) among features and the source itself. The first step in analysing ML data includes identifying the most critical features which significantly impact the predicted outcome. Second, various ML techniques are applied to the set of chosen features to combine them into a single predictive model. There are two main types of ML training: supervised and unsupervised.

1.6.1. Supervised Machine Learning

In supervised learning, the model is first trained using the available training samples (known data and their corresponding outputs) to obtain an optimal model under a certain evaluation criterion, and then the model is used to achieve the purpose of classification. Once trained, the model can sort unidentified information into categories (Cios *et al.,* 2012). With supervised learning, we can teach a computer to use the established classification scheme. For example, these algorithms can be used to infer where the protein is targeted based on known annotated data (Horton *et al.,* 2007).

1.6.2. Feature Engineering

Feature engineering transforms raw data into features that better describe potential problems to the prediction model and improves the model's accuracy for unseen data and is thus an integral part of the process of building ML models. It is possible to improve model performance by implementing Feature extraction (FE) or feature selection (FS), two types of feature engineering that focus on minimising the effects of overfitting and increasing the model's accuracy and generalizability, respectively. When a function is fitted to a small or specific data set, a modelling error known as overfitting occurs. When developing ML models, it is important to identify and prioritise the most pertinent variables to ensure that simpler models can accurately predict and estimate disease risk. The purpose of feature engineering in life science is to extract, select, and identify key features to discover correlations in genomics, proteomics, and metabolomics datasets. Several ML feature selection algorithms, such as the random forest (RF) algorithm and XGBoost can filter out irrelevant features from multi-omics data while keeping the relevant ones.

1.6.3. Unsupervised Machine Learning

In unsupervised ML, the input data is not labelled, and the result is clusters of entities with shared similarities that the user may not have known about before running the analysis (Hastie *et al.,* 2009). The primary goals of unsupervised learning are to discover novel patterns in the data and to organise the data into meaningful groups. Some examples of unsupervised learning algorithms are: clustering, dimensionality reduction, and association rules. Clustering is grouping data based on similarities or differences, including methods like hierarchical clustering, k-means clustering, density-based clustering, etc. Dimensionality reduction methods like Principal Component Analysis (PCA), Linear Discriminant Analysis (LDA), etc., the process of transforming data from a high-dimensional space to a low-dimensional one while retaining certain relevant aspects of the original data and association rule learning examines the reliance of one data element on another and attempts to uncover some interesting relationships or links between the dataset's variables. It depends on various rules to discover interesting connections between variables in a database (Cios *et al.,* 2012).

1.6.4. Performance assessment of Machine Learning models

Overfitting the data and needing more generalisation ability are common issues for ML models trained with a given set of samples. As a result, there is a trade-off between model complexity and adaptability to new data. One solution is to employ models with fewer features and representations, which may lead to poorer performance on the training set. Regularisation is a technique used in ML models that sacrifices some precision on the training set in exchange for improved generalisation on the test data (Deo, 2015). Whichever ML model most closely corresponds to the underlying model of the generated data is the best. The standard method for finding the best ML model involves trying several different ones and saving the test data to compare how well they performed.

2. AIMS OF THE STUDY

Armillaria ostoyae is a fungus that is known for wreaking havoc on forests all over the world. The fungus is highly virulent, which means it is very effective at infecting and harming host trees. Its pathogenicity, or ability to cause disease, is influenced by a variety of factors, including the expression of protein-based virulence factors, long non-coding RNAs (lncRNAs) that regulate the expression of various genes involved in pathogenicity, and the microbiomes associated with the fungus during the invasion of the host plants. Understanding the molecular mechanisms that contribute to the virulence and pathogenicity of *A. ostoyae* is critical for developing effective strategies to control its spread. Exploring the microbiome associated with pathogenicity and virulence can also provide insights into the fungus's ecological context and how it interacts with other microorganisms in the soil. Finally, identifying the biodegradation prospects of *Armillaria* may offer significant implications for developing long-term management strategies for the fungus and utilising the fungus' full potential for minimising the impact of the environmental contaminants/pollutants. Keeping that in mind, the following were my aims and objectives:

1. To employ *in vivo* interaction studies between Norway spruce (*Picea abies*) and *A. ostoyae*, based on mimicking the natural environment, to unveil the genetic factors driving virulence and pathogenicity in *A. ostoyae*. In addition, this study aims to deepen our understanding of the complex molecular machinery used by the fungus during the infection process of spruce seedlings.
2. To identify lncRNAs in *A. ostoyae* genome and elucidate their role in pathogenicity and virulence.
3. To identify the microbes that are associated with *A. ostoyae* during the plant infection process and study their possible functional intervention.
4. To identify the biocontrol-related genes expressed during the interaction of haploid *A. ostoyae* and *Trichoderma atroviride*.
5. To investigate the mycoremediation potential of armillarioids through comparative analysis with other widely utilised fungi in biodegradation.

3. MATERIALS AND METHODS

3.1. Inoculum preparation

The inoculum preparation method was according to Rigling *et al.* (2003). When preparing inoculum, hazelnut stem segments of 10 cm and the diameter of 3-4 cm were used. They were placed in a polypropylene dish atop of Norway spruce (*Picea abies*) wood chips. Double sterilisation of the box was done after adding distilled water at 120°C for 30 mins. The gap between consequent sterilisation was 24 hours. To facilitate better moist heat sterilisation, sterile distilled water was added carefully before each sterilisation. After sterilisation, *A. ostoyae* C18 (AO) culture was added, and the box was kept in the dark at 25°C for about 4 months. In order to avoid dryness, sterile distilled water was added after two months.

3.2. Preparation of host plants and *A. ostoyae* control

The host plants utilised in the study were spruce seedlings cultivated in the soil of the nursery from the seeds. In March 2018, five bare-rooted seedlings were transferred into each 3.5 litre plastic container as part of the growing process. The soil that was employed as a substrate in the containers consisted of 20% peat and 80% commercial "container soil for shrubs," both of which had a pH of 5.8 and were acquired from Okohum GmbH (Germany). In addition, the substrate was treated with a slow-release fertiliser (Osmocote Exact Standard 5-6 M, Everris International B.V, the Netherlands) at a rate of 3 kg/m^3 and horn powder at a rate of 2 kg/m^3. To serve as a stand-in for the AO inoculum, a plastic pipe (20 cm × 3 cm in diameter) was put in the centre of each pot. For isolating AO control rhizomorphs, similar pots were prepared but without the seedlings.

3.3. Inoculation of seedlings with fungi and incubation

From the centre of each pot, the plastic pipe was removed and replaced with a piece of hazelnut stem that had been colonised by AO, and the soil was used to cover the inoculum segment. The pots with inoculated seedlings were kept outside in the forest nursery and got watered whenever it was necessary.

3.4. Assessment of fungus-inoculated seedlings

After inoculation, the seedlings were monitored monthly for signs of Armillaria root rot, including chlorotic foliage and death. When seedlings died, the *Armillaria* mycelial fans in the cambial region of the root collar were promptly examined. Throughout the experiment, dead seedlings were not removed. Each seedling was categorised into one of the following groups after the experiment: healthy-looking, symptomatic with wilting symptoms and/or chlorotic foliage, or dead.

3.5. Sample collection and RNA-sequencing

Sixteen months after inoculation, rhizomorphs (3 × Rhizo) of *A. ostoyae* were removed from the soil substrate and collected from 3 pots without seedlings. With a dissecting microscope, 10 to 20 rhizomorph tips (1 cm long) were cut. They were then instantly frozen in liquid nitrogen and kept at -80°C. Two years after the first inoculation, the seedlings in the inoculated pots were harvested. Three categories were used to evaluate each seedling's symptoms above ground: healthy-looking, symptomatic (3 × Symp) with wilting symptoms and/or chlorotic foliage, or dead (3 × Necro) with brown needles. The presence of white mycelial fans under the bark at the stem base and roots of the seedlings served as a warning sign for *Armillaria* infection. The mycelial fans (approximately 2 cm long, including the advancing edge) were removed with a scalpel for RNA extraction, then promptly frozen in liquid nitrogen and kept at -80°C.

The frozen samples were pulverised in liquid nitrogen using a mortar and pestle, and total RNA was extracted using a Qiagen RNeasy Plant Mini Kit (Hilden, Germany). The Agilent 2100 Bioanalyzer and Invitrogen QubitTM 3 Fluorometer were used to assess the RNA extracts' concentration and quality, respectively. Paired-end sequencing was carried out on the Illumina Nextseq platform after library preparation was completed using Lexogen's CORALL Whole RNA-Seq Library Prep Kit.

3.6. Bioinformatics analysis of virulence- and pathogenicity-related genes expressed in *A. ostoyae*

3.6.1. Analysis of the fungal transcriptome for identifying pathogenicity- and virulence-related genes

The read quality was initially examined using Fastqc v0.11.9 (Andrews, 2010). Using BBDuk (Bushnell, 2014), low-quality bases, adapters, and overrepresented sequences were eliminated. Bowtie2 (Langmead & Salzberg, 2012) removed host RNA, ribosomal RNA, and other contamination such as PhiX. The STAR (Dobin *et al.,* 2013) aligner was used to align the filtered reads to the *Armillaria ostoyae* v2 reference genome (GenBank accession: GCA 900157425.1). The reads were quantified using the RSEM (Li & Dewey, 2011) software, and differential expression analysis was performed in edgeR after TMM (weighted trimmed mean of M values) normalisation. The *A. ostoyae* genes that were upregulated ($\log_2$FC> |1| & $p < 0.05$) were further categorised into three groups based on their expression patterns: Rhizo, Symp, and Necro specific. This classification was performed using a Venn diagram. To achieve this, we considered three sets of upregulated genes: genes upregulated in Symp versus Rhizo, genes upregulated in Necro versus Rhizo and genes upregulated in Rhizo vs Symp and Necro. Genes that were downregulated in both Symp and Necro were classified as Rhizo specific. The Superseq R package (Robinson et al., 2023) was used to calculate the edgeR differential expression analysis's power.

3.6.2. Functional annotation and enrichment analysis

All protein sequences were annotated using InterProscan v5.38-76.0 (Jones *et al.,* 2014) and diamond blast (Buchfink *et al.,* 2015) against the UniProtKb database (Boutet *et al.,* 2016). DBCAN2 (http://bcb.unl.edu/dbCAN2/blast.php) (Zhang *et al.,* 2018) was used for annotating CAZymes. In order to predict peptidases, lipases, and effectors, Diamond BLAST was employed against the Merops (https://www.ebi.ac.uk/merops) (Rawlings *et al.,* 2010), Lipase Engineering (Fischer and Pleiss, 2003), and Phi-base databases (Urban *et al.,* 2020). BigPI Fungal site (Eisenhaber *et al.,* 2004) was used to identify GPI-anchored proteins. Then, by doing an extensive literature search, all the annotated protein sequences were manually curated. Kegg enrichment analysis was carried out using the clusterProfiler R package (Yu *et al.,* 2004), while GO enrichment analysis was done using BinGO (Maere *et*

al., 2005) in Cytoscape v3.4 (Shannon *et al.,* 2003). Orfanfinder (Ekstrom and Yin, 2016) was used to predict orphan genes. The ggplot2 R tool was used to create the charts, and Rv4.2.1 was utilised for data exploration.

3.6.3. Identification of secretory proteins and comparative secretome analysis

The pipeline for secretome predictions is shown in Fig. 3 and 4. Using the pipeline we predicted the G-secretome proteins in 60 more fungal species (Supplementary Table 1) besides *A. ostoyae*. The MycoCosm database of the Joint Genome Institute (JGI) (https://genome.jgi.doe.gov/portal/) retrieved the protein sequences. Orthologous proteins to other fungal species were identified using the Orthofinder software (Emms and Kelly, 2019). We compared our list of differentially expressed secretory genes with results from dead root and *in vitro* stem invasion experiments performed by Sahu *et al.* (2021, 2023). The list of secretory genes from the *in vitro* dead root invasion experiment was called "IM" (Sahu *et al.,* 2021). Using the ComplexUpset package (Krassowski, 2020) in R version 4.2.1, we examined the InterPro gene families that were specific to the conditions or were shared between groups specific using the upsetR plot.

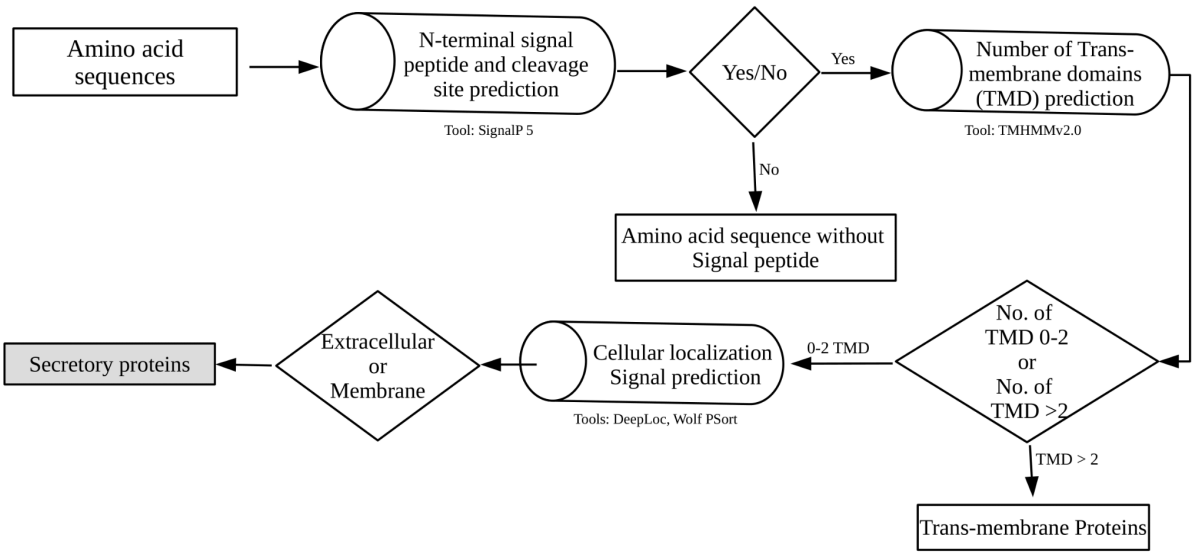

Fig. 3. Pipeline for predicting classically secreted proteins.

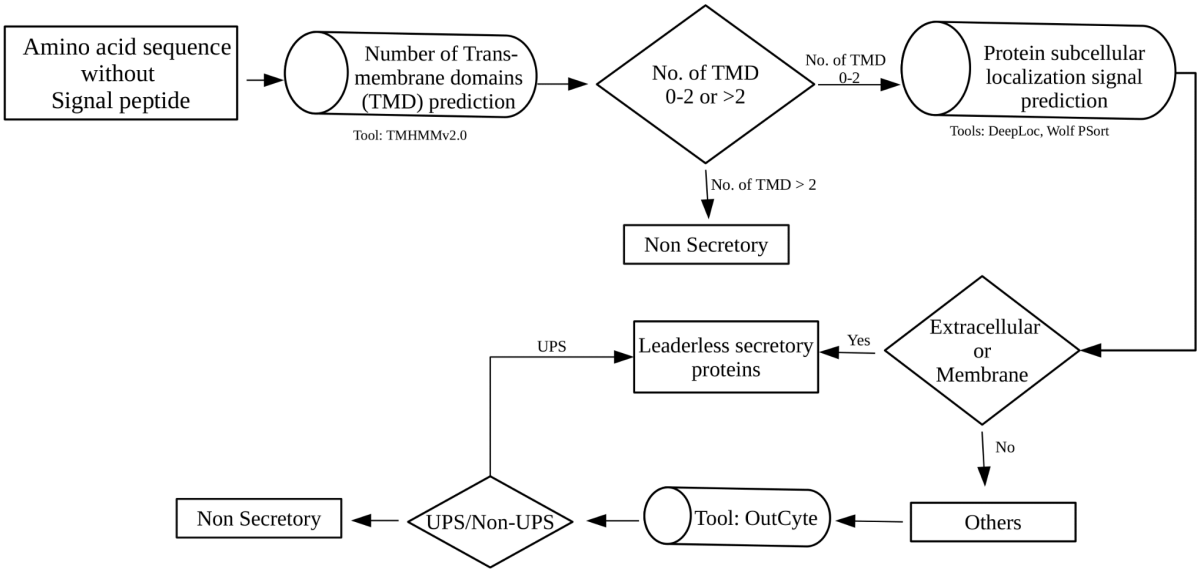

Fig. 4. Pipeline for predicting leaderless secretory proteins.

3.6.4. Building a Machine Learning model and feature extraction

After performing Bartlett's test of sphericity, all the differentially expressed genes ($p < 0.05$) with the highest expression in Symp, Necro, and Rhizo were used for hierarchical clustering based on principle components (HCPC) (Fig. 5). The number of principal components was selected in such a way that 85% of the variance was captured. Following clustering, the genes were manually filtered based on TMM-normalised $\log_2$CPM values and the conditions in which they displayed the highest expression. The condition for the gene to be regarded as highest expressed was that the minimum gene expression difference between two condition was greater than |1.0| $\log_2$CPM. Following that, the orthogroup repertoire to which those genes belonged to was identified for each species of white rotting, brown rotting, soft rotting, and mycorrhizal fungi. Boruta package (Kursa and Rudnicki, 2010) in R was used to find the orthogroups necessary for distinguishing white rotting from brown rotting, soft rotting, or mycorrhizal fungi. In order to determine the variable's significance, Boruta creates shadow variables based on permutations and compares their feature relevance to true predictor variables. Additionally, it determines the importance of the variable and trains a RF model using an expanded dataset. The method continues to run until the specified number of iterations and the variable relevance of each variable has been determined. With R's set.seed(99), we performed 10000 iterations of the Boruta algorithm. After determining the

relevance of each feature, we created an RF-based model utilising those features and compared it to an RF model created by dividing the full dataset into 60% training data and 40% test data. We also predicted orthogroup features that would be responsible for differentiating fungus with various lifestyles using the XGBoost (Extreme Gradient boosting) (Chen *et al.,* 2015) ML technique. Bayesian optimization was initially performed to tune the hyperparameters. Following hyperparameter tuning, the following parameters were set: fold cross validation of five, eta range between "0.001-0.1," and "multi:softprob" as objective function. Correlation analysis was performed using the features that both Boruta and XGBoost predicted to be valid. Psych package in R 4.2.1 was used to perform correlation analysis.

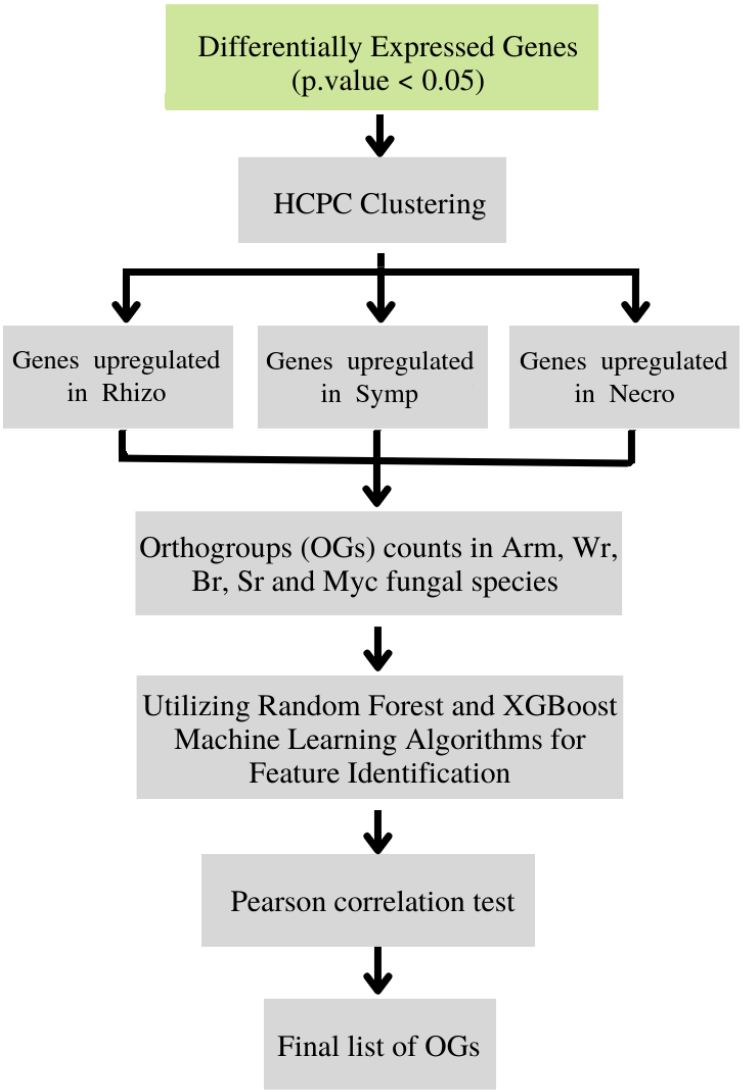

Fig. 5. Pipeline for identification of important orthogroup features.

3.7. lncRNA analysis in *A. ostoyae*

3.7.1. Differential expression analysis of lncRNA

HISAT2 (Kim *et al.,* 2015) and StringTie (Pertea *et al.,* 2015) were used to map filtered reads to the *A. ostoyae* genome (GenBank accession: GCA 900157425.1) and assemble the transcripts, respectively. Cuffcompare (Pertea & Pertea, 2020) was employed to evaluate assembly quality. Salmon (Patro *et al.,* 2017) was used for transcript quantification. After TMM normalisation, differential expression analysis was carried out using edgeR.

3.7.2. Identification of lncRNAs

The assembled transcripts with lengths shorter than 200 nucleotides (nt) were eliminated to find lncRNAs in *A. ostoyae*, and only transcripts with lengths greater than 200 nt were considered. CPC2 (Kang *et al.,* 2017) and CPPred (Tong and Liu, 2019) were used to determine coding potential. Only sequences whose $\log_2$CPM was more than 0.5 were considered for additional downstream analysis after being classified as non-coding by CPC2 (Kang *et al.,* 2017) and CPPred (Tong and Liu, 2019). Open reading frames (ORF) were detected using TransDecoder (http://transdecoder.sourceforge.net/), and only those sequences whose number of ORFs was < 100 were considered for Interproscan and CMSearch (Cui *et al.,* 2016) against Interpro and RFam (Kalvari *et al.,* 2021) databases, respectively (Fig. 6).

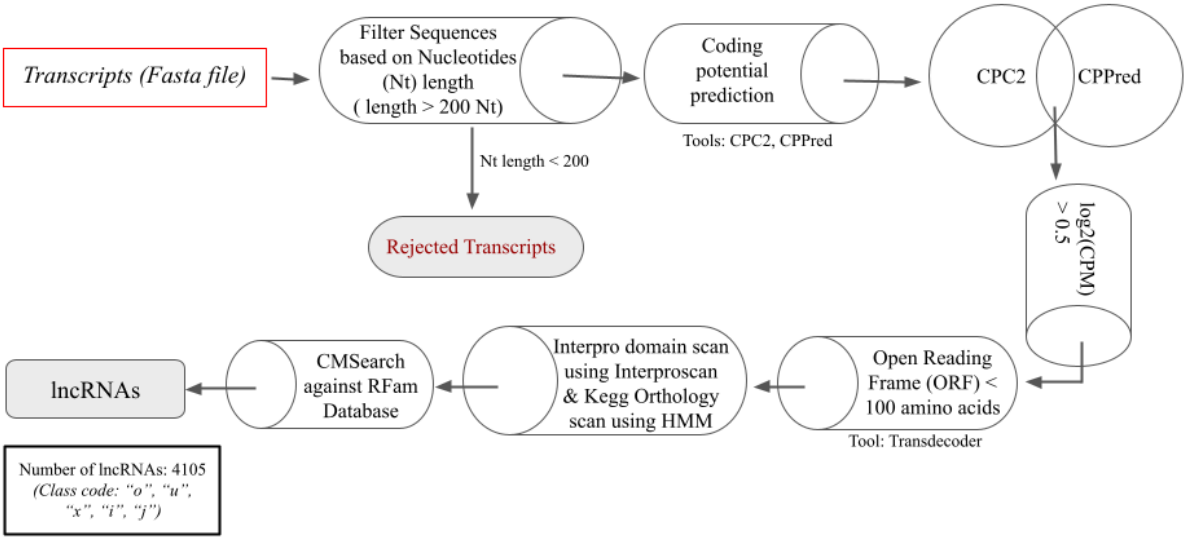

Fig. 6. Pipeline for predicting lncRNAs in *A. ostoyae*

3.7.3. lncRNA target gene prediction and functional enrichment analysis

To predict lncRNA functions, which might be either a cis or trans regulator of gene expression (Xu *et al.,* 2017), the FEELnc classifier (Wucher *et al.,* 2017) was used to predict the transcripts that were located in close vicinity to the lncRNAs. The lncRNA transcripts located within the range of 20 kb upstream/downstream of other mRNAs were considered cis-regulatory. The lncRNA transcripts located beyond the range of 20 kb upstream/downstream of other mRNAs were considered trans-regulatory if the binding free energy of lncRNA and the target mRNA was less than -40 kcal/mol. RIsearch (Wenzel *et al.,* 2012) version v1.2 was used to predict the binding free energy between lncRNAs and other transcripts. The co-expression correlation (Pearson correlation) between the lncRNAs and the targets was calculated in Rv4.2.

Gene ontology (GO) enrichment analysis of the target genes was carried out using BiNGO (Maere *et al.,* 2005) and Cytoscape v3.7.2 (Shannon *et al.,* 2003), in order to make predictions regarding the functions of lncRNAs. EnrichmentMap (Merico *et al.,* 2010) application was used in Cytoscape (Shannon *et al.,* 2003) to visually represent the GO Enrichment map.

3.8. Analysis of the *A. ostoyae* microbiome and differential expression of metatranscriptome

Reads coming from the host and fungi were identified and removed after aligning with the *Picea abies* (GenBank accession: GCA_900067695.1) and *A. ostoyae* genome using bowtie2 (Langmead & Salzberg, 2012) aligner respectively. CCMetagen (ConClave-based Metagenomics) (Marcelino *et al.,* 2020), which uses the ConClave sorting scheme, implemented in the KMA software, was used to identify the bacterial communities in the fungal reads. For the metatranscriptome differential expression study, Trinity v2.15.0 (Grabherr *et al.,* 2011) was used to assemble the transcripts, and bowtie2 (Langmead & Salzberg, 2012) was used to align the reads to the assembled transcripts. Prior to finalising only the protein-coding transcripts, the non-coding transcripts were removed after aligning to the RFam (Kalvari *et al.,* 2021) database. Annotation of the transcripts were done using gene ontology (GO), carbohydrate-active enzymes (CAZyme), and InterPro databases.

3.9. Transcriptomic analysis of haploid *A. ostoyae* biocontrol using *Trichoderma atroviride*

Armillaria ostoyae SZMC 23085 (AOS) and *Trichoderma atroviride* SZMC 24276 (TA) were grown together on a Petri plate for dual-culture assays. The control was grown on a plate separately and mycelia of the dual-cultured samples were collected at 0th (Control), 53rd (Metabolite interaction stage) and 62nd (Mycoparasite interaction stage) hours for both AOS and TA by scrapping. Most of the work mentioned in this section was done along with Chen (2021). This section will primarily focus on the bioinformatics analysis of the data.

Fastq reads were pre-processed using BBDuk (Bushnell, 2014) and quantified using Salmon v3.10 (Patro *et al.,* 2017). The quantified reads were then used for unsupervised fuzzy C-means clustering. Clustering analysis was performed to identify the members of the clusters control (C), metabolite interaction stage (MetS), and mycoparasite interaction stage (MycS) clusters. However, as data points can belong to multiple clusters with varying degrees of membership, the top members for a particular group were identified using strict criteria. For example, to belong to MetS, the genes in that cluster had to be expressed higher in that stage, and at minimum, the fold change difference should be at least >= 2 vs. any one of the groups. Similar criteria were also used to identify members of other groups. Functional annotation of the genes was done using InterProscan (Jones *et al.,* 2014), GO (Gene Ontology Consortium, 2004), KEGG (Kanehisa & Goto, 2000), SMIPS (Wolf *et al.,* 2016), and DbCan (Yin *et al.,* 2012) database. R v3.6 was used for exploratory analysis and plotting.

3.10. Comparing biodegradation prospects of *Armillaria*

We downloaded amino acid sequences of seven *Armillaria* species, two *Desarmillaria* species, one *Guyanagaster* species, 14 white-rot basidiomycetous fungi, 12 ascomycetous fungi, as well as 1 mucormycete as outlier fungus (Supplementary material 1) to compare the biodegradation potential of *Armillaria* from JGI (https://mycocosm.jgi.doe.gov/mycocosm/home). The species were selected after performing bibliographic research.

For this study, the enzymes responsible for the breakdown of xenobiotics by several fungal species were analysed in depth. KofamScan (Aramaki *et al.,* 2020) based on KEGG orthology and hidden Markov model, was initially utilised to determine the KEGG orthology of the amino acid sequences. The Biocatalysis/Biodegradation Database (Ellis *et al.,* 2006)

was utilised to curate data manually, and the remaining notable hits that could not be curated using the Biocatalysis/Biodegradation database (Ellis *et al.,* 2006) were curated using the KEGG database. The enzymes identified in the KEGG database (Kanehisa & Goto, 2000) involved in xenobiotics degradation were selected and used for further analysis.

R v4.2 was used for computational and comparative analysis of the enzymes involved in xenobiotic breakdown amongst different fungal species. The R package adephylo v1.1-11 (Jombart *et al.*, 2010) was used to conduct the phylogenetic PCA analysis. The enzyme copy number was calculated for each fungal species and then transformed into a n × m matrix for building the phylogenetic PCA. The analysis relied on a phylogenetic tree (supplementary material 2) constructed from single-copy orthologs. For that purpose, the MAFFT v7 aligner (Katoh & Standley, 2013) was used for sequence alignment, and the FastTree v2.1 (Price *et al.,* 2010) tree-building program was used for producing the maximum-likelihood phylogenetic trees. The R tool ggplot2 was then used to plot each image. MEME Suite (Bailey *et al.,* 2015) was used for motif analysis.

The study also examined gene expression data from recently conducted *in vitro* stem invasion assays (Sahu *et al.,* 2023). This analysis aimed to explore the activity of mycoremediation-related genes within *Armillaria* isolates. The investigation focused on isolates growing on nutrient-rich RSTO media and mycelia invading and thriving within plant tissues. During the stem invasion assays, fresh segments of spruce stems were placed on the mycelial lawn cultivated on RSTO media. The gene expression patterns of highly virulent and less virulent isolates from two conifer-specific *Armillaria* species (*A. borealis* and *A. ostoyae*) were studied, particularly regarding the mycoremediation genes.

4. RESULTS

4.1. *In vivo* infection of spruce seedlings with *A. ostoyae* isolate

Two-year-old *P. abies* seedlings infected with the virulent AO inoculum revealed two different outcomes. One group displayed curled leaves and wilting symptoms (Fig. 7B). In contrast, the other group experienced sudden dieback with drying brown needles (Fig. 7C). Mycelia of AO harvested from the cambium of symptomatic *P. abies* seedlings are hereafter referred to as "Symp," and the sudden dieback-related samples to "Necro". The freely grown rhizomorphic samples from the soil that did not infect plants are then called ‘Rhizo’. This study aimed to identify secretory genes/proteins associated with virulence and necrotrophy. The goal was achieved by performing comparative transcriptomic analyses using biological triplicates of the Symp, Necro, and Rhizo samples, and subsequently comparing the expression of the genes of interest to those expression profiles previously analysed by Sahu *et al.* (2021, 2023).

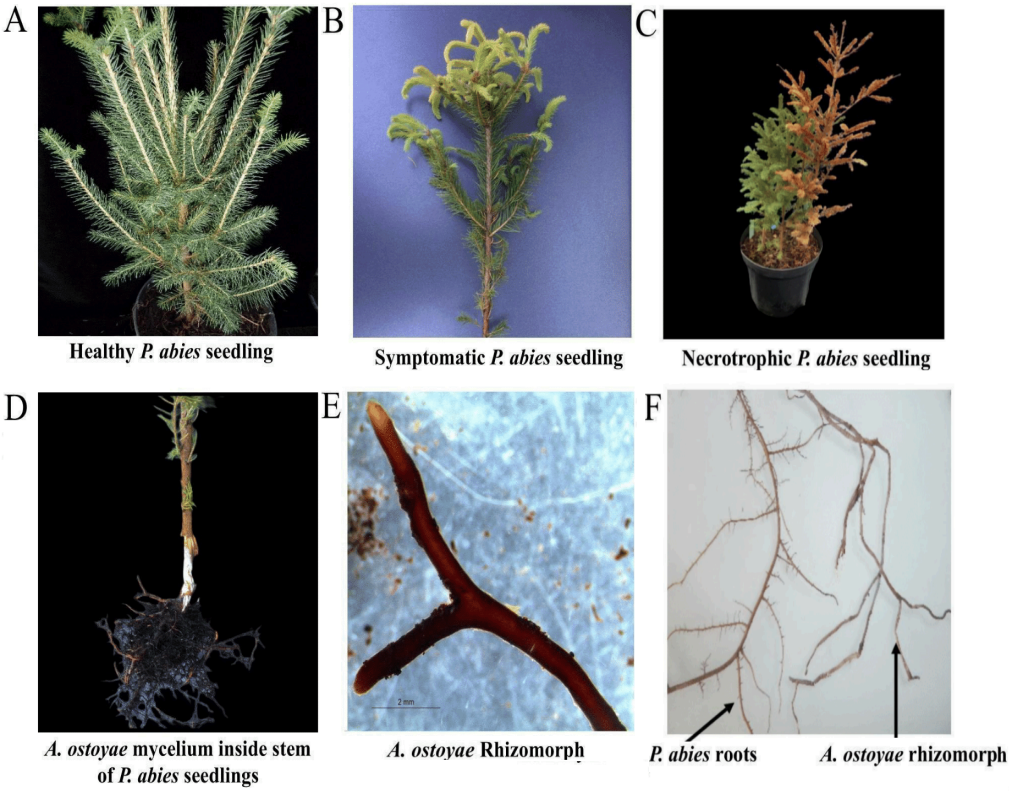

Fig. 7. Phenotypic differences in *P. abies* seedlings (A) healthy, B) symptomatic, C) sudden dieback, D) mycelium in the cambium of a *P. abies* seedling, E) microscopic image of a control rhizomorph, and F) *A. ostoyae* rhizomorphs attached to the roots of a *P. abies* seedling.

4.1.1. Differences in plant invasion tactics are shown by sample-specific gene expression

On average, 88% of the paired-end reads (13.5-24.9 million) from the three biological replicates could be mapped to the AO genome. Sample-wise Pearson correlation plot analysis showed that the different biological replicates grouped together, indicating similar gene expression patterns in AO tissues extracted from Symp, Necro, and Rhizo. Differential expression analysis identified upregulation ($\log_2$ Fold Change (logFC)>|1|, $p < 0.05$) of 463, 537, and 699 genes in Symp, Necro, and Rhizo, respectively (Fig. 8C). The statistical power for the differential expression analysis was 93%.

We compared the gene expression profiles of Symp, Necro, and Rhizo to identify the genes that are specifically expressed in each tissue type. We found 356, 262, and 605 genes uniquely upregulated in Symp, Necro, and Rhizo, respectively. Additionally, 144 genes were upregulated in both Symp and Necro compared to Rhizo (Fig. 8C).

We conducted a gene ontology (GO) enrichment analysis and identified 26 enriched GO terms (with $p < 0.05$) in Symp and 63 in Necro (Fig. 8B & 8D). The enriched GO terms in Symp were associated with aromatic degradation, hemicellulose, pectin degradation, fungal cell wall, secretory proteins, transport, transcription factors, tetrapyrrole, and heme binding. Similarly, in Necro, enriched genes were related to pectin, hemicellulose, aromatics degradation, and the apoptosis inducer KEX1 (EC. 3.4.16.6) (Hauptmann & Lehle, 2008), including carboxypeptidases. GO terms linked to transporter activities, such as amino acid, carboxylic acid, and phosphate transport, were overrepresented in down-regulated genes or Rhizo specific genes (Fig. 8A). Kofam enrichment analysis demonstrated that the Symp exhibited a significant enrichment of genes associated with detoxification, cellulose degradation, and MFS transporters (Fig. 9). In contrast, the Necro exhibited a more dominant enrichment of genes related to carboxypeptidase, pectin, and lignin degradation (Fig. 9).

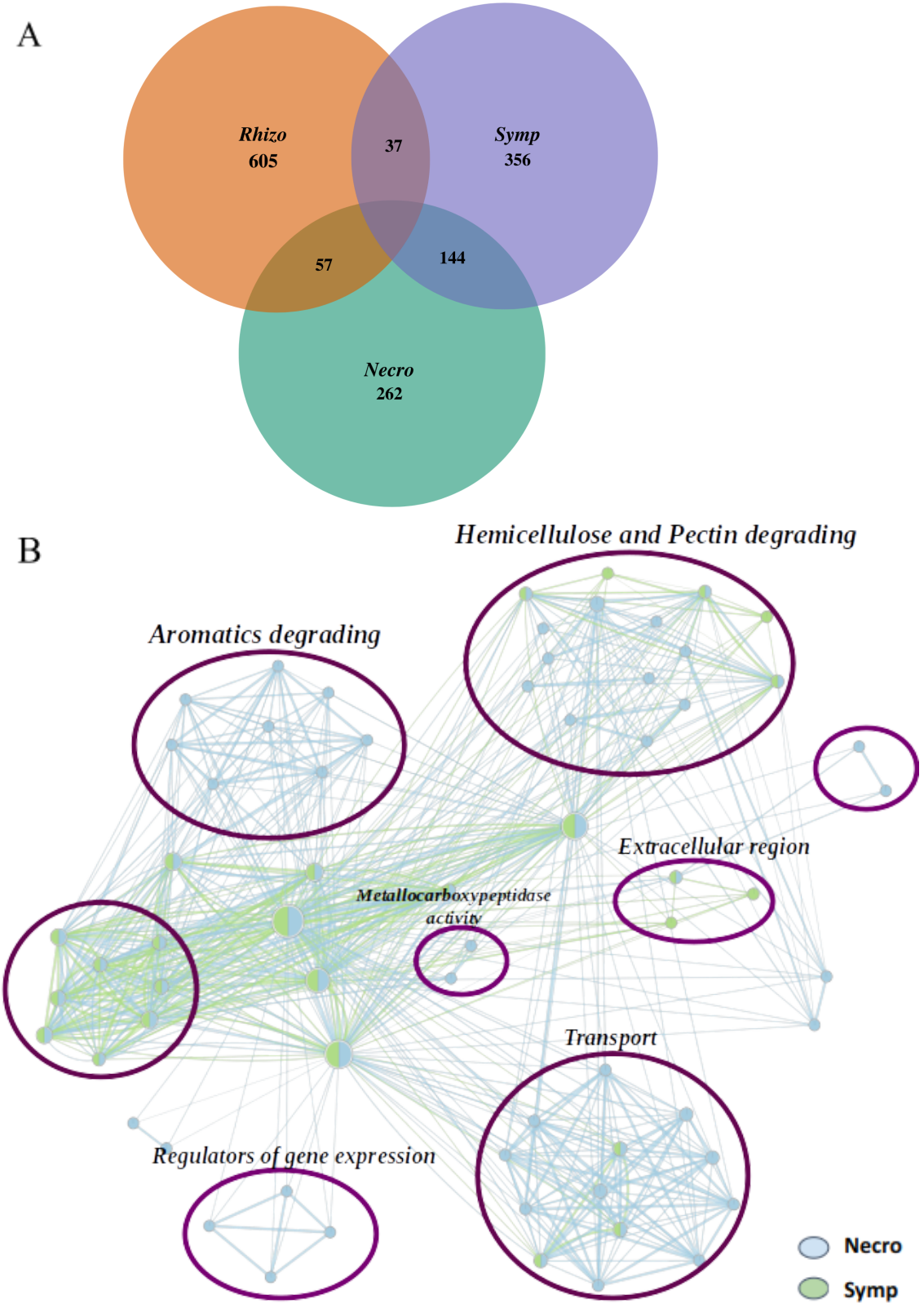

Fig. 8. Venn diagram and enrichment map of up-regulated genes specific to Symp, and Necro. A) Venn diagram of upregulated genes in Symp and Necro. B) Gene Ontology (GO) enrichment map of biological processes (BP) specific to Symp (green) and Necro (blue). The enrichment map was calculated based on uniquely upregulated genes in Symp and Necro identified from the Venn diagram. The node size corresponds to the number of genes associated with that node, and the edges represent the gene overlaps.

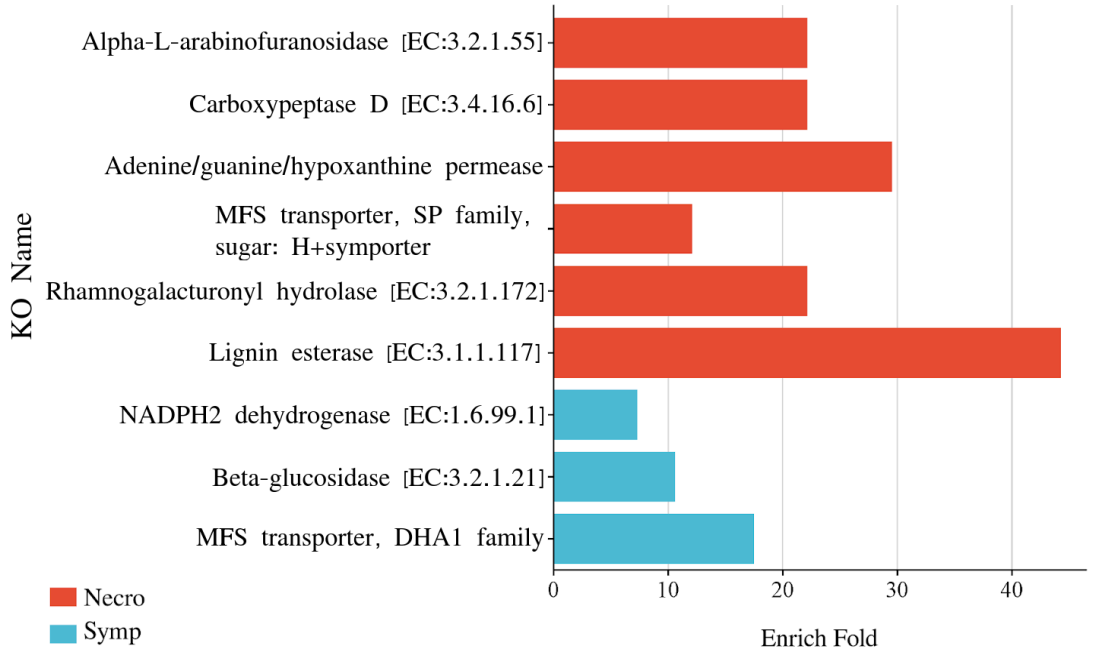

Fig. 9. The enriched KOfam in Symp and Necro. Kofam name is on the X-axis, and the enrich fold is on the Y-axis. Orange and green bar plots denote the KOfam enriched in Symp and Necro.

4.1.2. Investigation of potential virulence- and pathogenicity-related secretory proteins

The "Gsecretomes", consisting of GPI-anchored and non-GPI-anchored secretory proteins, were identified using the pipeline illustrated in Figures 3 and 4. The soluble secretome pool was expanded with the functional proteins anchored into the cell surface. In the AO genome, 2165 secretory proteins were identified, of which 279 were differentially expressed. During the host-pathogen interaction process, the Gsecretomes were significantly enriched in Symp (p= 1.24e-11, Fisher's exact test, FET) and Necro samples (p = 4.72E-06, FET).

To further analyse the differentially expressed Gsecretomes, they were classified into two major groups: classically secreted small proteins and leaderless secretory proteins (LSPs). Classically secreted proteins were further divided into two distinct groups, distinguished by their amino acid lengths: small secreted proteins (SSPs) containing fewer than 300 amino acids and non-small secreted proteins (non-SSPs) comprising more than 300 amino acids. Among the 471 putative SSP genes predicted in the *A. ostoyae* genome, 58 were differentially expressed. Enrichment analysis of the putative SSPs showed enrichment in *A. ostoyae* ($p < 0.05$, Fisher exact test, FET). 32 of 58 putative SSP genes had no functional

annotation, and Orfanfinder analysis of 32 unknown groups showed that 9 were genus ORFan, 4 class-, 3 subclasss-, 2 phylum-, 2 order- and 1 species-specific, and all the remaining genes were widely shared among all levels of taxonomy in the fungal kingdom. The remaining 26 corresponded to gene families such as cerato-platanins, hydrophobins, GH12 (β-1,4-endoglucanase), peptidase M43, fungal chitosanase, CAP domain, cysteine-rich secretory protein-related, LysM domain protein, kre9/knh1, glycosyl hydrolase catalytic domain, PriA protein, and intradiol ring-cleavage dioxygenases. 27 (46%) of the putative DE SSPs were cysteine-rich (cysteine percentage > 2%) proteins.

Table 1. The numbers of differentially expressed Gsecretory proteins.

Tissues	SSPs	CSP-non-SSPs	LSPs
Symp	19	36	24
Necro	13	40	20
Rhizo	13	37	26
Symp-Necro	7	21	6

In Symp, SSPs belonging to hydrophobin, cerato-platanins, chitosanase, GH12, and peptidase M43 were overrepresented ($p < 0.05$, Hypergeometric test, HT) (Fig. 10). Three SSPs that were highly represented in Necro were the LysM domain-containing protein, Kre9/Knh1 and hydrophobins (Fig. 10). The gene families shared by both Symp-Necro could be involved in plant invasion inside cambium. Overrepresentation analysis of the upregulated genes showed that certain hydrophobins and SGNH hydrolase-type esterases were prevalent in the Symp and Necro samples (Fig. 10).

The non-SSPs and LSPs overrepresented ($p < 0.05$, HT) Interpro terms that distinguished Symp from Necro and Rhizo included two pectins (PL8, Pectate lyase), one lignin (intradiol ring-cleavage dioxygenase), and two hemicellulose-degrading gene families (GH43, GH18). In addition to GH71, GH47, GH92, M20, GT61, GMC-oxidoreductases, and putative apoplast targeting guanine-specific ribonuclease N1/T1/U2, Symp also showed overrepresentation of two serine- (S8, S58) and metalloproteases (M35, M36) (Fig 10). Necro displayed overrepresentation ($p < 0.05$, HT) of protein families previously identified as virulence- or pathogenicity-related. An overrepresentation of the B-type carboxylesterase, known to cause hypersensitivity in tobacco plants, was found in Necro samples (Assis *et al.*, 2017). Besides, there were three pectin- (GH88, BNR repeat-containing family, alpha-l-arabinofuranosidases) and two lignin-degrading (fungal ligninase) Interpro terms, which were also prevalent (Fig. 10).

Fig. 10. Bubble plot of overrepresented interpro terms in Symp, Necro, Rhizo. The gene-ratio is in X-axis and interpro description in Y-axis. The size of the bubble denotes the gene count and color intensity of the bubble denotes the $\log_{10}$(p-value).

4.1.3. Comparative study of putative *A. ostoyae* secretory genes expressed during *in vivo* and *in vitro* plant tissue invasions

To identify the *A. ostoyae* genes necessary for the invasion of live *P. abies* tissues, we compared the secretory genes upregulated in the Symp and Necro mycelia to that of the genes upregulated in the. Analysing genes involved in the invasion and degradation of dead woods (Sahu *et al.,* 2021) and live stem tissues (Sahu *et al.*, 2023) can give us a better idea of genes that could be involved in virulence and pathogenicity.

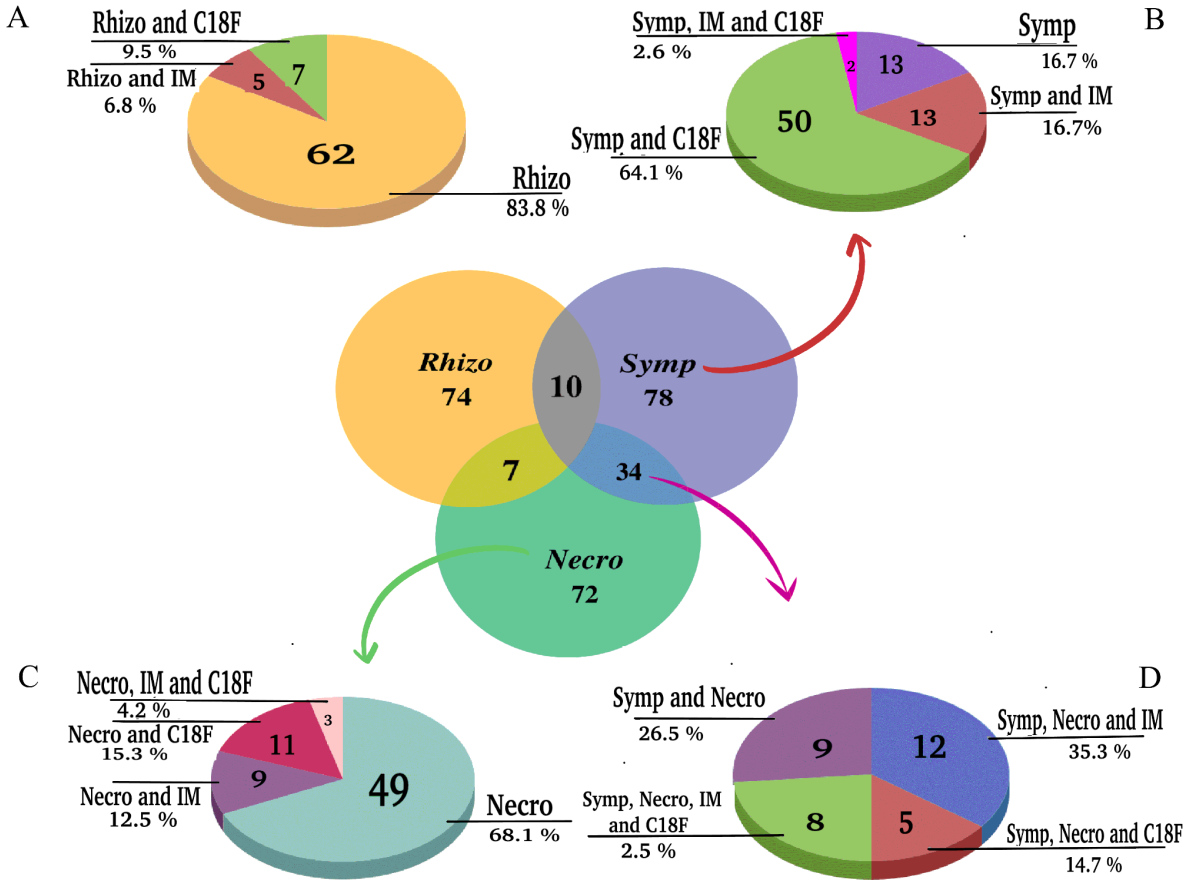

Fig. 11. The comparative distribution of secretory genes that are shared or unique in Rhizo, Symp, and Necro, compared to invasive mycelium (IM) and C18F (Sahu *et al.,* 2021, 2023). The unique G-secretome in A) Rhizo (yellow), B) Symp (green), C) Necro (light blue), and D) Symp and Necro (purple).

Our analysis showed that the *in vivo* invasion of *P. abies* showed a unique gene expression strategy compared to the wood-degrading experiment by Sahu *et al.* (2021). The majority of the genes (64.1 %) upregulated during Symp (Fig. 11b) showed a similar gene

upregulation pattern to that of the *in vitro* stem invasion experiment (Sahu *et al.,* 2023). However, during the Necro stage, *A. ostoyae* showed a unique gene expression pattern as 68.1% (Fig. 11C) of the genes were not observed in other experiments.

We separately performed UpsetR analysis of protein families (Fig. 12A) and CAZymes (Fig. 12B) to identify those families that were uniquely upregulated in Symp and Necro. From Fig. 13A, it could be observed that genes families such as glycoside hydrolase, family 61 and neutral/alkaline non-lysosomal ceramidase were unique to Symp and genes upregulated during Necro consisted of families like alpha/beta hydrolase fold-1, amidohydrolase 3, beta-glucan synthesis-associated, skn1, BNR repeat-containing family member, extracellular membrane protein, CFEM domain, fungal ligninase+haem peroxidase, glycoside hydrolase, family 20, 29, 115, peptidase M20, S28, S1/P1 nuclease and SMP-30/gluconolactonase/LRE-like genes. The signalling mucin MSB2 gene was present only in the *in vivo* experiment and was upregulated in both Symp and Necro.

Gene families such as endonuclease/exonuclease/phosphatase, fungal chitosanase, glycoside hydrolase family 12, 43, 47, 92, guanine-specific ribonuclease N1/T1/U2, haem peroxidase, intradiol ring-cleavage dioxygenase, lysine-specific metallo-endopeptidase, pectate lyase superfamily protein, peptidase M35, deuterolysin, peptidase M43, polysaccharide lyase family 8 and uncharacterized glycosyl hydrolase was shared between Symp, and C18F (Fig. 13A). DUF1996, GH127+beta-L-arabinofuranosidase, peptidase M36, fungalysin and serine carboxypeptidase S10 were shared among Symp, Necro and C18F (Fig. 13A) indicating that they might be crucial for invading raw plant tissues.

Differential expression analysis showed that 114 CAZyme-related genes were differentially expressed and could be grouped into 74 CAZyme families. Analysis of CAZyme families that might be specific to Symp, Necro, or shared with other groups such as C18F could provide useful clues about the genes involved in interaction with live tissues. CAZy comparison (Fig. 13B) showed that AA9 was uniquely observed only in Symp. In the Necro, CAZy groups such as CE15, CE17, GH115, GH13_32+CBM20, GH145/PL42, GH154, GH29, GH30_4, GH5_7 and GT48 were observed. CBM10 and GH5_22 were seen in both Symp and Necro. The 10 CAZymes shared between Symp and C18F were AA14, CBM5, GH12, GH128, GH43_5, GH47, GH55, GH75, GH92 and PL8. CAZymes families shared among Symp, Necro, and C18F were AA2, CBM50, GH1, GH127, and GH78.

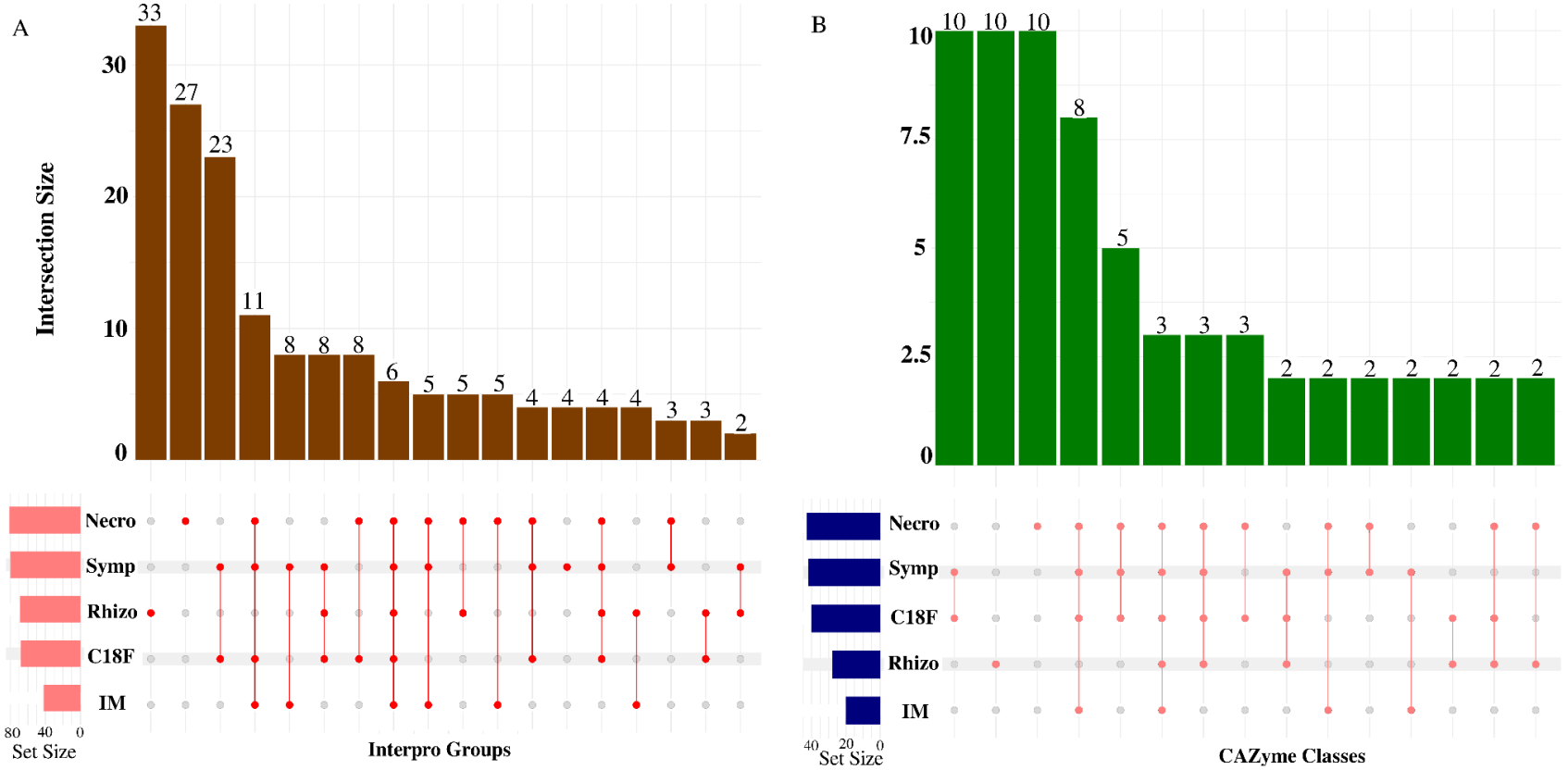

Fig. 12. Upset plot of shared and unique A) InterPro and B) CAZyme families in Necro, Symp, Rhizo, IM, and C18F conditions. The bar plots at the top represent the intersection indicated by the dots and the lines at the bottom. The size of the intersection is shown above the bar graph. The total number of Interpro families is indicated on the left side of the intersection diagram.

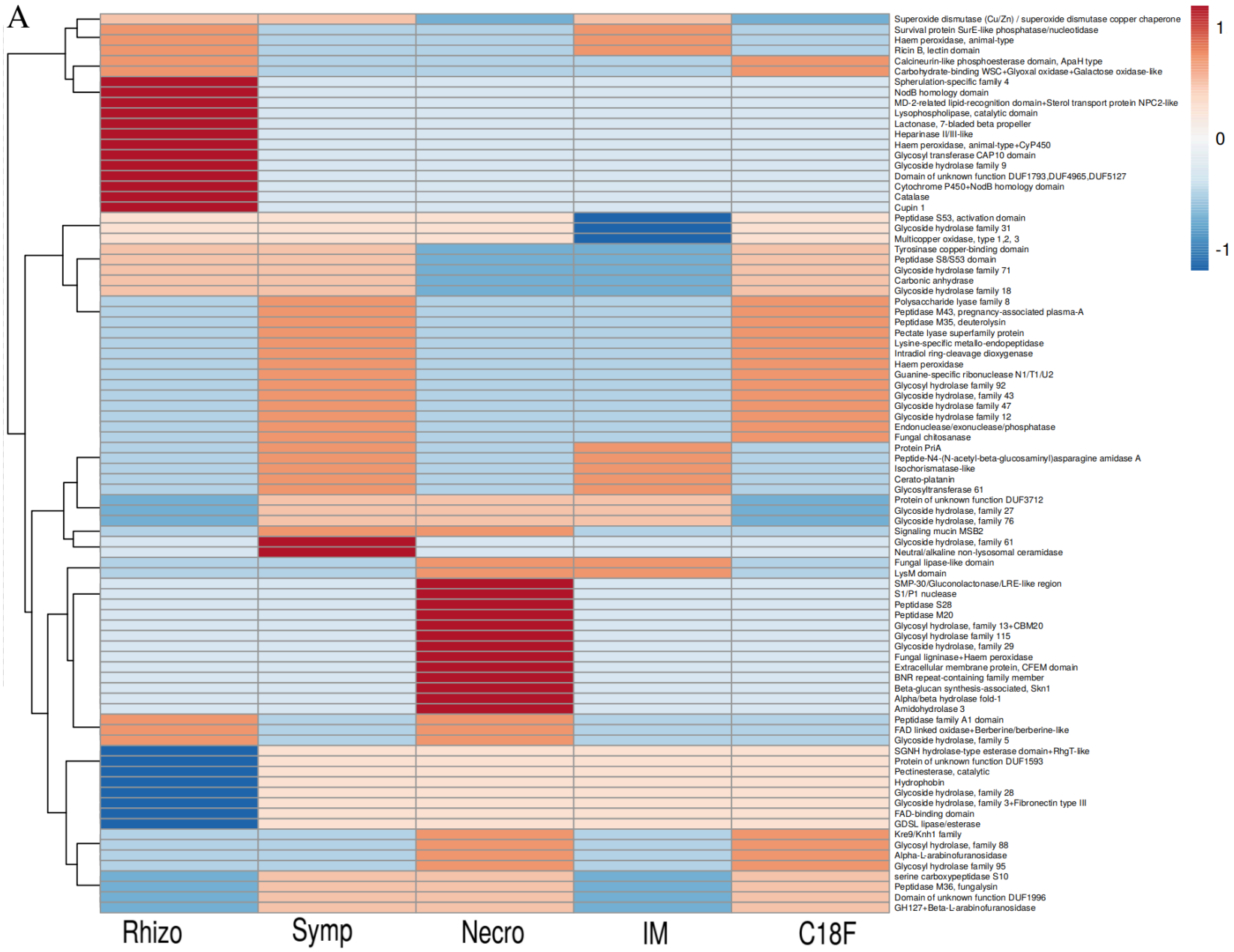
A
Superoxide dismutase (Cu/Zn) / superoxide dismutase copper chaperone
Survival protein SurE-like phosphatase/nucleotidase
Haem peroxidase, animal-type
Ricin B, lectin domain
Calcineurin-like phosphoesterase domain, ApaH type
Carbohydrate-binding WSC+Glyoxal oxidase+Galactose oxidase-like
Spherulation-specific family 4
NodB homology domain
MD-2-related lipid-recognition domain+Sterol transport protein NPC2-like
Lysophospholipase, catalytic domain
Lactonase, 7-bladed beta propeller
Heparinase II/III-like
Haem peroxidase, animal-type+CyP450
Glycosyl transferase CAP10 domain
Glycoside hydrolase family 9
Domain of unknown function DUF1793,DUF4965,DUF5127
Cytochrome P450+NodB homology domain
Catalase
Cupin 1
Peptidase S53, activation domain
Glycoside hydrolase family 31
Multicopper oxidase, type 1,2, 3
Tyrosinase copper-binding domain
Peptidase S8/S53 domain
Glycoside hydrolase family 71
Carbonic anhydrase
Glycoside hydrolase family 18
Polysaccharide lyase family 8
Peptidase M43, pregnancy-associated plasma-A
Peptidase M35, deuterolysin
Pectate lyase superfamily protein
Lysine-specific metallo-endopeptidase
Intradiol ring-cleavage dioxygenase
Haem peroxidase
Guanine-specific ribonuclease N1/T1/U2
Glycosyl hydrolase family 92
Glycoside hydrolase, family 43
Glycoside hydrolase family 47
Glycoside hydrolase family 12
Endonuclease/exonuclease/phosphatase
Fungal chitosanase
Protein PriA
Peptide-N4-(N-acetyl-beta-glucosaminyl)asparagine amidase A
Isochorismatase-like
Cerato-platanin
Glycosyltransferase 61
Protein of unknown function DUF3712
Glycoside hydrolase, family 27
Glycoside hydrolase, family 76
Signaling mucin MSB2
Glycoside hydrolase, family 61
Neutral/alkaline non-lysosomal ceramidase
Fungal lipase-like domain
LysM domain
SMP-30/Gluconolactonase/LRE-like region
S1/P1 nuclease
Peptidase S28
Peptidase M20
Glycosyl hydrolase, family 13+CBM20
Glycosyl hydrolase family 115
Glycoside hydrolase, family 29
Fungal ligninase+Haem peroxidase
Extracellular membrane protein, CFEM domain
BNR repeat-containing family member
Beta-glucan synthesis-associated, Skn1
Alpha/beta hydrolase fold-1
Amidohydrolase 3
Peptidase family A1 domain
FAD linked oxidase+Berberine/berberine-like
Glycoside hydrolase, family 5
SGNH hydrolase-type esterase domain+RhgT-like
Protein of unknown function DUF1593
Pectinesterase, catalytic
Hydrophobin
Glycoside hydrolase, family 28
Glycoside hydrolase, family 3+Fibronectin type III
FAD-binding domain
GDSL lipase/esterase
Kre9/Knh1 family
Glycosyl hydrolase, family 88
Alpha-L-arabinofuranosidase
Glycosyl hydrolase family 95
serine carboxypeptidase S10
Peptidase M36, fungalysin
Domain of unknown function DUF1996
GH127+Beta-L-arabinofuranosidase
1
0
-1
Rhizo
Symp
Necro
IM
C18F

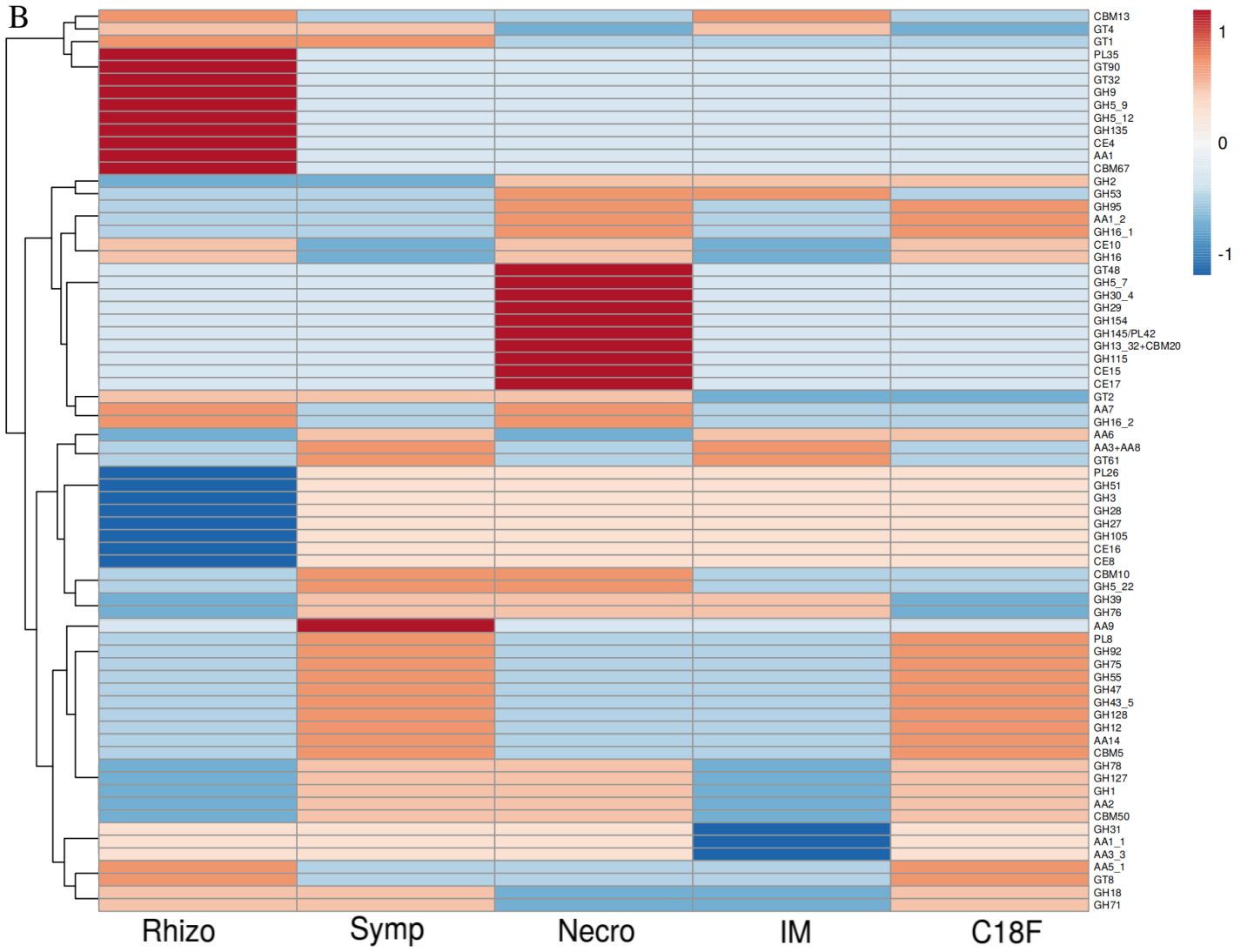

Fig.13. Heatmaps of interpro families and CAZymes identified in upsetR analysis. A) Correlation heatmap showing how the Interpro gene families were distributed in different conditions from left Rhizo, Symp, Necro, IM, and C18F. The conditions are on the X-axis, and Interpro gene families are on the Y-axis. B) Correlation heatmap showing how the CAZymes were distributed in different conditions from left Rhizo, Symp, Necro, IM, and C18F. The conditions are on the X-axis, and CAZyme is on the Y-axis.

4.1.4. Secondary metabolite genes upregulated in Rhizo, Symp and Necro stages

Seventy-two secondary metabolite-related genes were upregulated in the *A. ostoyae* mycelia during interaction with *P. abies*. Fischer's enrichment analysis indicated that secondary metabolite cluster genes were enriched in Rhizo (p= 1.72E-09, BH). Ten unique secondary metabolite-related genes were upregulated in Symp and Necro and nine were shared between Symp, and Necro. The distinguishing metabolites between Rhizo, Symp and Necro were terpene and NRPS-like cluster genes. The terpene-related gene cluster was the most dominant among all secondary metabolite-related genes in Rhizo (Fig. 14). In Symp and Necro, however, it was mainly NRPS-like genes (Fig. 14). NRPS- and siderophore-related cluster genes were specific to Necro. They were not observed in Rhizo and Symp (Fig. 14).

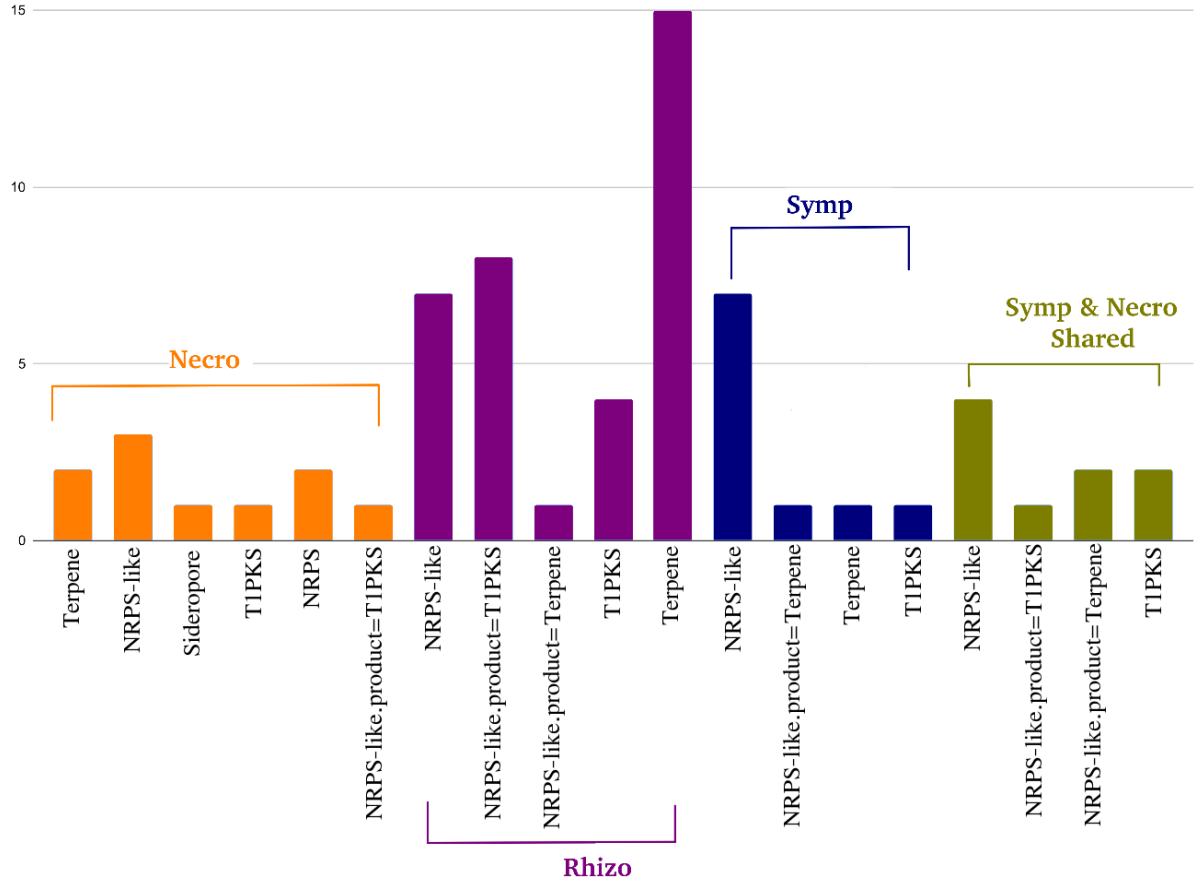

Fig. 14. Distribution of Secondary metabolites cluster genes in Rhizo, Symp and Necro. X-axis denotes the secondary metabolite gene and Y-axis denotes counts of those genes.

4.1.5 Pathogenicity model for *A. ostoyae* infection strategies as white rotting fungus

We investigated the repertoire of orthogroups that might contribute to the white-rot model of plant invasion strategies. Orthogroup analysis using Orthofinder identified 48573 different orthogroups in 61 (15 brown-rotting, 15 mycorrhizzal, 15 soft-rotting, 16 white-rotting) different fungal species. The differentially expressed genes corresponded to 529 different orthogroups. Comparing those orthogroup repertoires whose members were observed to be differentially expressed in *A. ostoyae* during the *P. abies in vivo* experiment could be crucial for unlocking the white-rot invasion strategy. Boruta and XGBoost identified 82 and 109 orthogroups as essential features. Among them, 43 orthogroups were identified by both ML algorithms (Fig. 15). Top 5 features identified by Boruta were OG0000871, OG0000258, OG0005476, OG0000253, and OG0000106 (Fig. 16A). The members of these orthogroups could be attributed to protein families such as major facilitator superfamily, fungal ligninase, zinc finger, ring-type, vilya/cst9/rnf212, GH28 and cupredoxin. OG0000002, OG0005476, OG0001881, OG0000253, and OG0001037 corresponding to GMC-oxidoreductases (AA3_2), zinc finger, ring-type vilya/cst9/rnf212, glycoside hydrolase, family 28 and glycoside hydrolase, family 76 were the top 5 orthogroups identified by XGBoost (Fig. 16B). The person's *r* between the orthogroups repertoire of white-rotting fungi and genes differentially expressed in the *in vivo* experiment was 0.8 (p-value = 1.2e-10) (Fig. 17A). Interestingly, the correlation of the DEGs with other groups were weakly correlated: soft-rotting (=0.69), brown-rotting (=0.61) and mycorrhizzal (= 0.64). Our results suggest that the critical features captured by our ML algorithms represent the fungal lifestyle, as reflected by the strong correlation between the captured repertoires of orthogroups and the orthogroups strongly manifested among the differentially expressed genes.

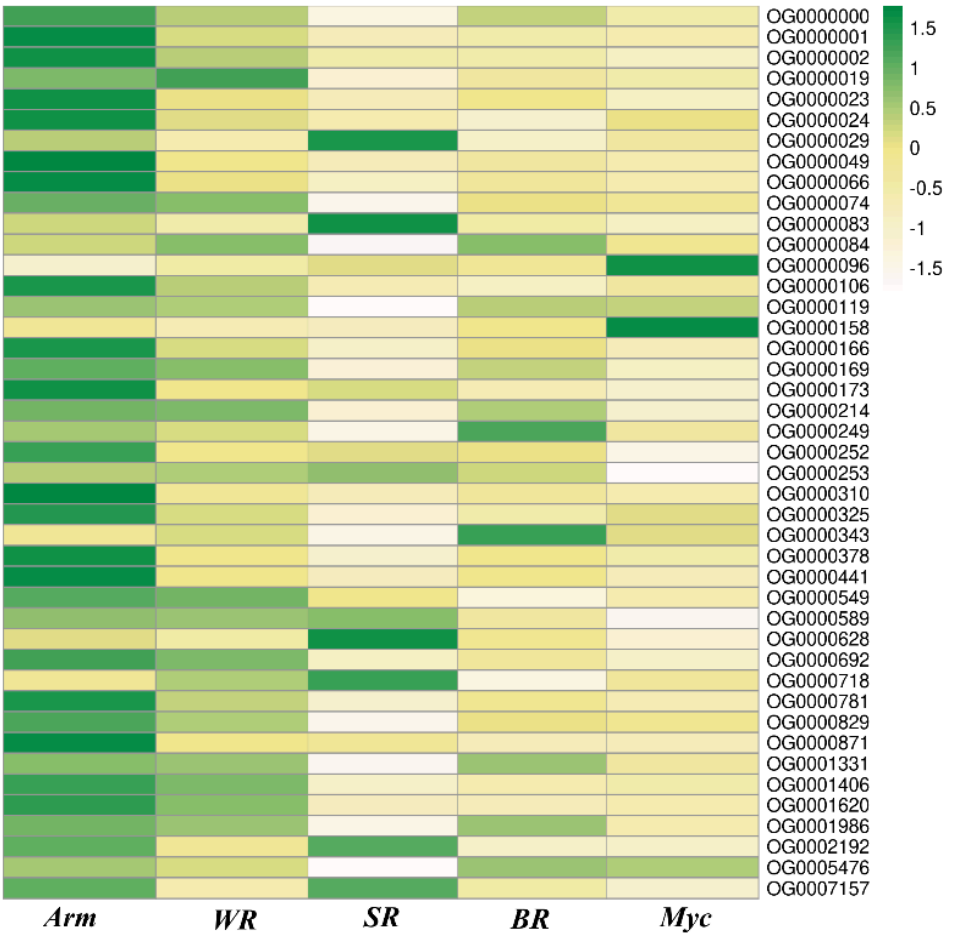

Fig. 15. Heatmap of important features identified by XGBoost and Boruta. The X-axis denotes the fungal groups, and the Y-axis identifies the Orthogroups (OGs) features. The intensity of the color depends on the mean OG counts in each group. The highest abundance is denoted in dark green, and the lowest is in White.

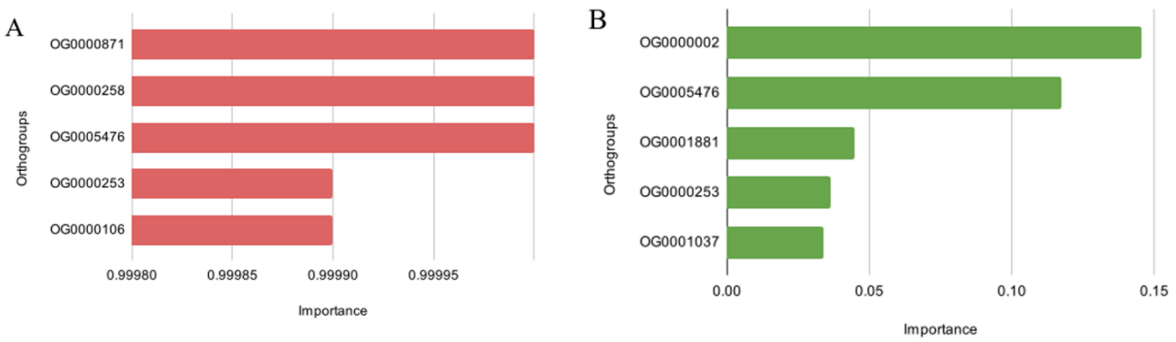

Fig. 16. Top 5 critical orthogroups identified by A) Boruta and B) XGBoost. The X-axis corresponds to the importance, and the Y-axis represents the orthogroups.

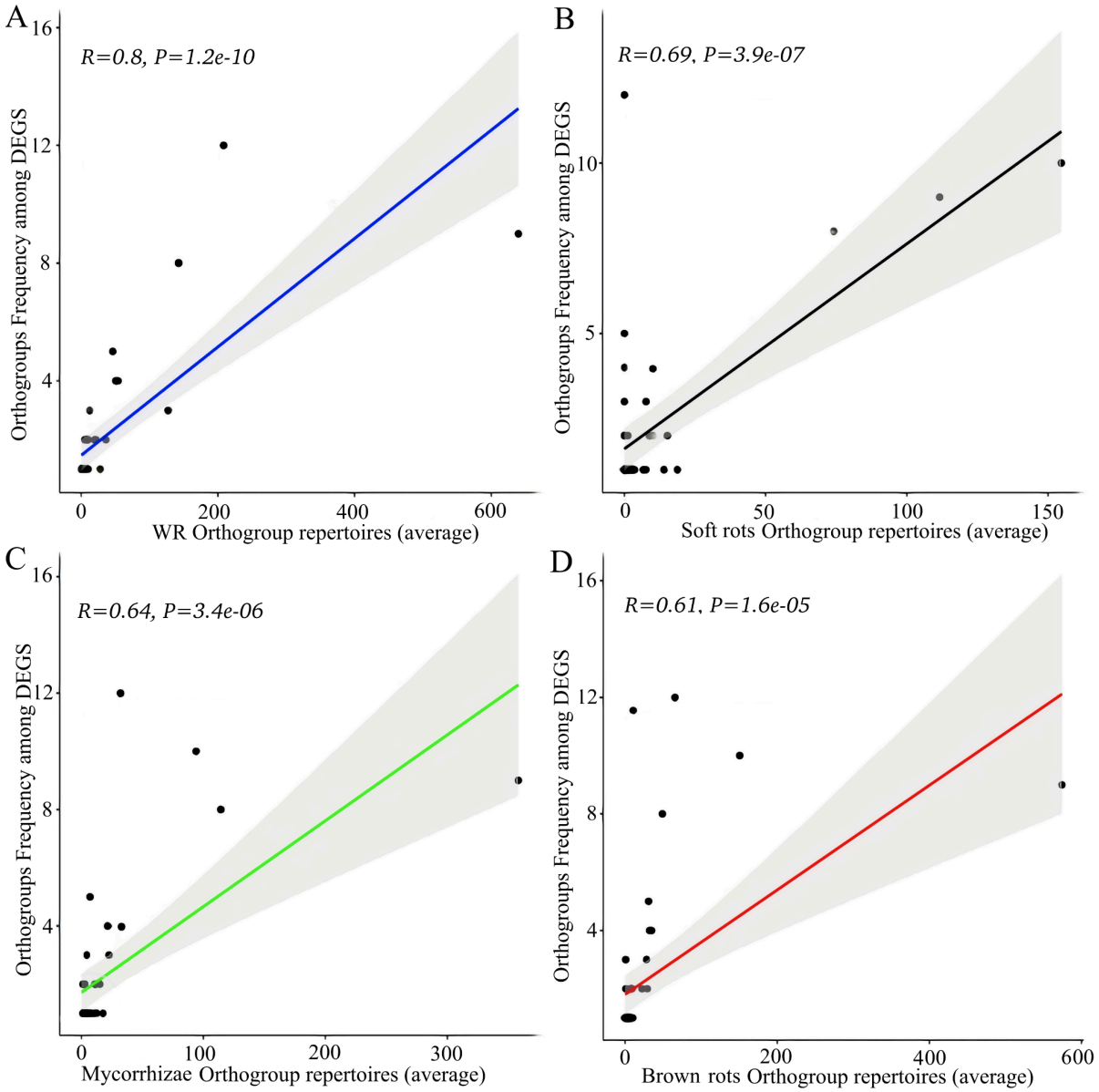

Fig. 17. Pearson correlation (r) between orthogroups identified as essential by both Boruta and XGBoost and differentially expressing gene orthogroups. r between differentially expressed orthogroup counts and (A) white-rot orthogroup repertoires, (B) soft-rot orthogroup repertoires, (C) mycorrhizae orthogroup repertoires, (D) brown-rot orthogroup repertoires.

4.2. lncRNAs in the *A. ostoyae* genome

The lncRNA predictions were carried out following the pipeline depicted in Fig. 6. There were 9351 and 7714 lncRNAs predicted by CPC2 and CPPred , respectively. CPC2 and CPPred consistently predicted 7678 different lncRNAs. The expression of the lncRNAs predicted by CPC2and CPPred was evaluated after trimmed mean of M values (TMM) normalisation, and only those transcripts were included whose $\log_2$ CPM expression > 0.5 and ORF < 100 amino acids. Eventually, using InterProScan and CMsearch, 4116 lncRNAs were discovered in the genome of *A. ostoyae* (Class Code: “o”, “u”, “x”, “i”, “j”). As shown in Fig. 18A, 292 novel long noncoding (class code “j”) isoforms were discovered with at least one shared splice junction with the reference transcripts, as well as 107 (class code "o") exonic overlap transcripts, 2921 (class code "u") intergenic lncRNA, 691 (class code "x") antisense transcripts, 105 (class code “I”) full intron overlap lncRNA were identified. Class code "u"/intergenic lncRNAs made up the majority of the lncRNAs found (70.9%), followed by antisense lncRNAs (16.7%), novel lncRNAs (7.09%), intronic and sense lncRNAs (2.6% and 2.5%, respectively).

In *A. ostoyae*, a significantly higher proportion of lncRNAs (83.01%) were composed of three or fewer exons, as opposed to protein-coding transcripts, where this figure was only about 21.8% (Fig. 18B).

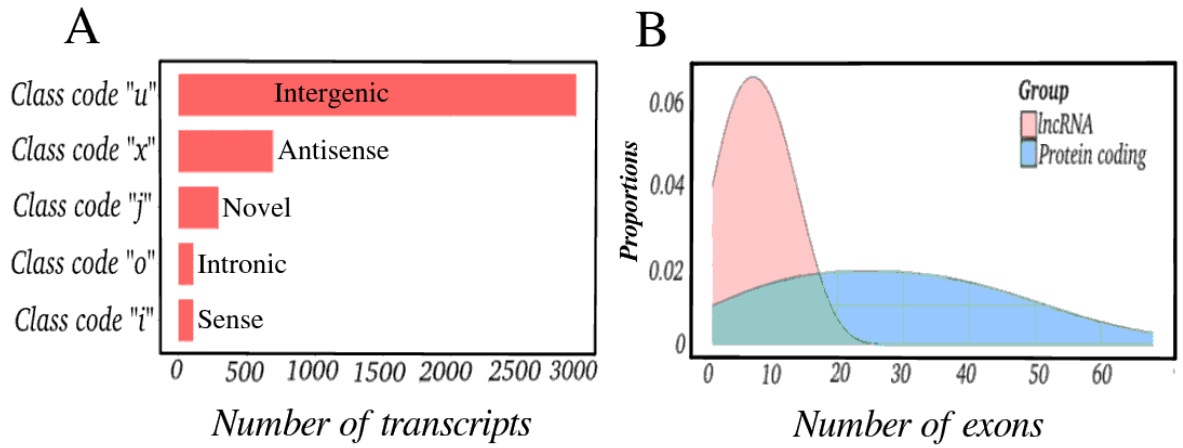

Fig. 18. lncRNAs distribution in the *A. ostoyae* genome. A) Horizontal bar plot of counts of lncRNA transcripts. The X-axis represents the number of transcripts, and the Y-axis the categories of lncRNA; B) Pie-chart plot of the different categories of lncRNA transcripts; C) Density plot of the comparison of lncRNA and protein coding transcripts based on the number of exons. The X-axis denotes the number of exons, and the Y-axis the proportion.

4.2.1. Differential expression analysis of transcripts

The alignment of Rhizo, Symp, and Necro to the genome of *A. ostoyae* v2 (GenBank accession: GCA 900157425.1) using HISAT2 showed an alignment percentage of approximately 86.1%. According to a Pearson correlation analysis of all samples, the biological replicates belonging to the same group had correlations between 0.84 and 0.89. Transcript differential expression analysis revealed 1617 (R versus N), 2324 (R versus S), and 182 (N versus S) transcripts that were differentially expressed (FDR 0.05). In Rhizo, Symp, and Necro, 59, 34, and 38 lncRNAs were upregulated, respectively. With log_2FC (log_2 fold change) > 4, the lncRNAs MSTRG.7390.2 and MSTRG.17337.1 exhibited the highest expression in Symp, whereas MSTRG.10210.4, MSTRG.15406.1 displayed log_2FC > 3.5 in Necro versus Rhizo.

4.2.2. lncRNAs, co-regulators of infection?

The functions of the target transcripts, which were either cis- or trans-regulated, were investigated to determine the role of the lncRNAs during infection. Across the whole *A. ostoyae* genome, 2939 cis- and 2185 trans-regulated targets of the DE lncRNAs could be identified. GO enrichment analysis of the cis/trans targets revealed enrichment of Biological Processes (BP) related to the "mitotic/meiotic cell cycle", "chromatin regulation", "methylation", "epigenetic gene regulation", "transport", "carbohydrate metabolism", "cell wall modification", "chitin metabolism", "pectin metabolism", "regulation of secretion", "xenobiotics degradation", "signalling", "mycotoxin biosynthesis", "hypusine metabolism"," 3-keto sphinganine metabolism", "cell-adhesion", and "response to stress". The top 5 BPs overrepresented in Cis targets were response to chemical stimulus, gene silencing, signal transduction, response to water deprivation, vacuole transport (Fig. 19A). Trans target overrepresentation analysis showed that gene silencing by rna, negative regulation of conjugation, regulation of mitochondrion organisation, regulation of cyclase activity and regulation of mitochondrion organisation (Fig 19B) were overrepresented.

The relationships between the differentially expressed cis/trans regulated genes and DE lncRNAs were carefully elucidated to identify the lncRNAs that may function as regulators of various genes. There were 164 cis-regulated and 73 trans-regulated DE genes

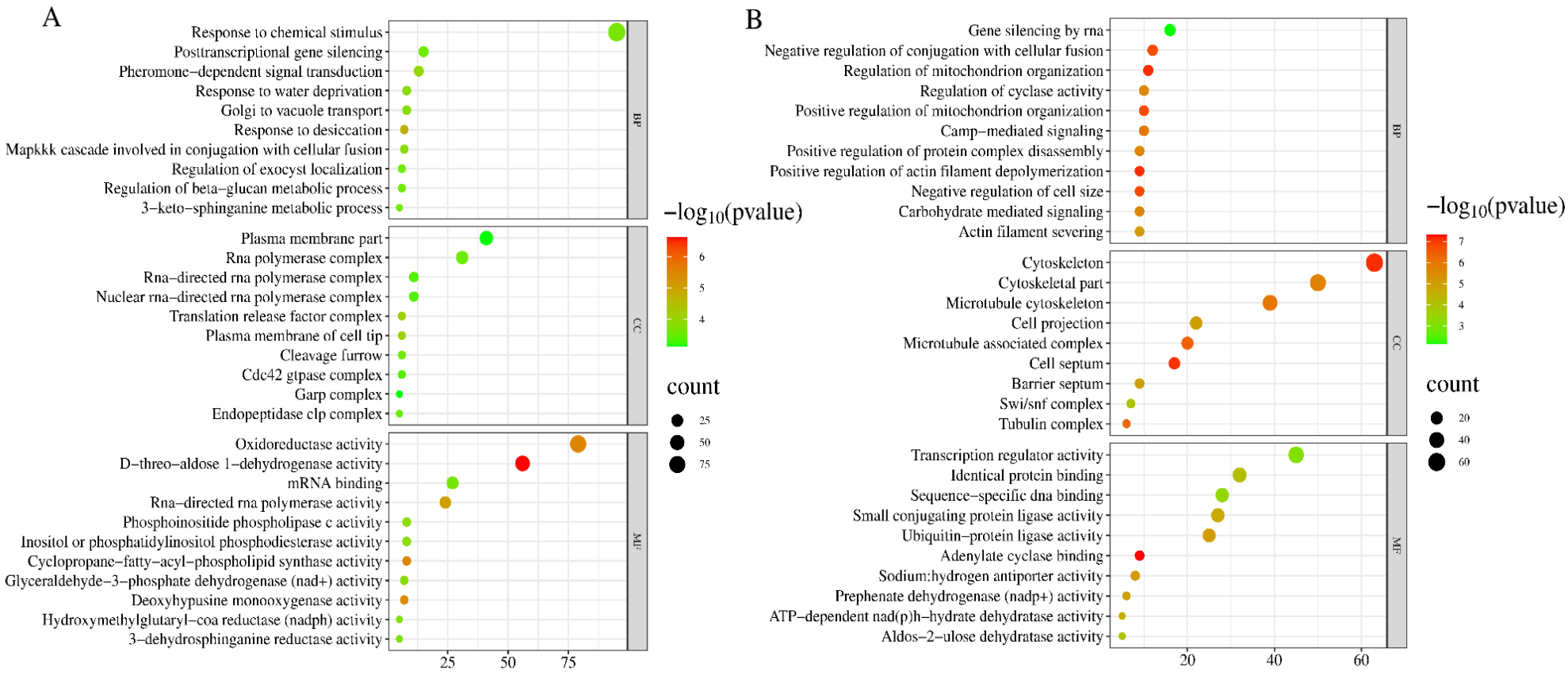

Fig. 19. GO bubble plot showcasing the top ten overrepresented biological processes (BP), cellular components (CC), and molecular functions (MF) for both A) cis-target and B) trans-target of differentially expressed lncRNAs. The X-axis indicates gene counts, while the Y-axis represents GO definitions. The color of each bubble corresponds to the negative log10 of the corrected p-value, and the size of the bubble indicates the number of genes associated.

correlating with DE lncRNAs. PAH-inducible cytochrome P450 monooxygenase PC-PAH (polycyclic aromatic hydrocarbons), predominantly highly expressed in Symp, correlated to the lncRNAs MSTRG. 14515.2, MSTRG. 19675.1, MSTRG. 14517.1 (Table 2). Similarly, NADP-dependent oxidoreductase genes, which were highly upregulated in Necro, correlated to lncRNAs MSTRG. 8611.8, MSTRG.17584.1, MSTRG.13953.4 (Table 2). Besides PAHs oxidising cytochrome p450 monooxygenases in Symp, other genes that were cis-regulated included methyltransferases, transcription factors, pectin/hemicellulose degrading genes, phospholipases, transporters and secondary metabolites biosynthesis genes. In Necro, other cis-regulated targets included genes responsible for signal transduction, peptidases transporters, and heterokaryon incompatibility systems (Fig. 20B).

Table 2. DE trans-regulated target genes and their potential lncRNA that could act as a regulator.

Target	Regulator Type	lncRNA
Pectinesterase	Cis	MSTRG.11084.2
Ureohydrolase	Cis	MSTRG.7390.3, MSTRG.7390.2
NADP-dependent oxidoreductase	Cis	MSTRG.16981.10, MSTRG.8611.8, MSTRG.17584.1, MSTRG.13953.4
Cytochrome p450	Cis & Trans	Cis: MSTRG.19675.1, Trans: MSTRG.4732.2
Major facilitator superfamily	Cis & Trans	Cis: MSTRG.18364.1, MSTRG.6246.1, MSTRG.1542.1, Trans: MSTRG.17232.1, MSTRG.10210.4, MSTRG.16981.10
GH28	Cis	MSTRG.15837.1
GH92	Cis	MSTRG.492.2
Laccase	Cis	MSTRG.18543.1
PAH-inducible cytochrome P450 monooxygenase PC-PAH 1	Cis & Trans	Cis: MSTRG.14515.2, MSTRG.19675.1, MSTRG.14517.1, Trans: MSTRG.16981.10
NADH:flavin oxidoreductase	Cis	MSTRG.15077.5
Short-chain dehydrogenase	Cis & Trans	Cis: MSTRG.20000.4, Trans: MSTRG.10081.1
SGNH hydrolase-type esterase	Cis	MSTRG.8611.8, MSTRG.8615.4
O-methyltransferase	Cis	MSTRG.18013.6, MSTRG.18013.5
Transcription factor	Cis	MSTRG.12128.1
Enoyl-CoA hydratase/isomerase	Cis	MSTRG.5782.1, MSTRG.5781.1
Alpha/beta hydrolase	Cis	MSTRG.1976.1
CBM21	Cis	MSTRG.15560.2
Biotinyl protein ligase (BPL) and lipoyl protein ligase (LPL)	Cis	MSTRG.12467.1
Class II aldolase/adducin	Cis	MSTRG.1542.1
GT48	Cis	MSTRG.3540.1
Heterokaryon incompatibility	Cis	MSTRG.19065.1
Peptidase S10	Cis	MSTRG.13953.4, MSTRG.12550.1
Phospholipase	Cis	MSTRG.5343.2
SRA-YDG	Cis	MSTRG.15406.1
cytochrome b5	Cis	MSTRG.5343.2
FAD binding	Cis	MSTRG.6512.1
Intradiol ring-cleavage dioxygenase	Trans	MSTRG.10080.1, MSTRG.19304.1
HSP70	Trans	MSTRG.19941.2
Dienelactone hydrolase	Trans	MSTRG.10210.4

Fig. 20. Differentially expressed targets that are cis-regulated. A) Symp; B) Necro. X-axis denotes counts and Y-axis denotes the interpro description

Many differentially expressed genes like phenol 2-monooxygenase, alpha-xylosidase with low binding energy (< -40 kcal/mol) did not correlate with the lncRNAs. However, the genes that showed correlation were involved in regulating gene expression, transport, aromatics degradation (intradiol ring-cleavage dioxygenases), secondary metabolite synthesis, and signal transduction.

4.3. Microbiome analysis of *A. ostoyae*

14-22 million metatranscriptome reads from each sample (Symp, Rhizo, Necro) were mapped to the NCBI-NT database using the KMA aligner, and the microbial community that occurred along with *A. ostoyae* was identified. Refraction analysis showed that the diversity richness flattened after a certain number of species, indicating that sampling was enough to capture most species diversity (Supplementary material 2). CCMetagen classified the reads to 55 phyla and 765 genera. The most dominant bacteria identified in *A. ostoyae* were Proteobacteria (> 48%), Actinobacteria (> 18%), Bacteroidetes (> 6%), and Firmicutes (>4%). Genera such as *Pseudomonas, Rhizobium, Bradyrhizobium, Sphingomonas, Streptomyces, Methylobacterium, Variovorax, Acidovorax,* and *Caulobacter* accounted for about 26 percent of the genera.

4.3.1. Bacterial community patterns

We investigated the diversity and dissimilarity of the microbial communities in: Rhizo, Symp, and Necro. The average observed microbial richness and faith diversity, for instance, stood at 1,745.3 and 2,476.08 in Rhizo, 703 and 1,428.7 in Symp, and 1,346.6 and 2,126.09 in Necro (Table 3, Fig. 21), suggesting that these two stages had more unique species. The average Shannon and Simpson diversity indices, 5.6 and 0.1 respectively, were slightly higher in stage Necro (Fig. 21), suggesting that this stage had a more even distribution of species. The average relative diversity index, which calculates the diversity of dominant species, was highest in stage Symp (0.9), followed by stage Rhizo (0.05) and stage Necro (0.03) (Table 3, Fig. 21). This suggests that stage Symp had a higher proportion of dominant species.

Table 3. Diversity indices for individual samples, including sample names, group membership, various diversity indices (Columns 3-7), and dominant family (Column 8)

Sample	Group	Observed	Shannon	Faith	Simpson	Relative	Dominant_taxa
R1030	Necro	1590	5.68	2350.37	0.09	0.03	Family: Sphingomonadaceae
R1035	Necro	1388	5.64	2174.08	0.10	0.03	Family: Sphingomonadaceae
R1038	Necro	1062	5.53	1853.82	0.11	0.04	Family: Sphingomonadaceae
R1073	Rhizo	2182	5.43	2822.27	0.04	0.05	Family: Pseudomonadaceae
R1071	Rhizo	1623	5.23	2389.12	0.05	0.06	Family: Rhizobiaceae
R1069	Rhizo	1431	4.95	2216.86	0.04	0.06	Family: Rhizobiaceae
R1034	Symp	893	5.23	1668.68	0.11	0.04	Family: Sphingomonadaceae
R1039	Symp	681	4.94	1410.27	0.07	0.10	Family: Frankiaceae
R1037	Symp	535	4.57	1207.19	0.06	0.15	Family: Sphingomonadaceae

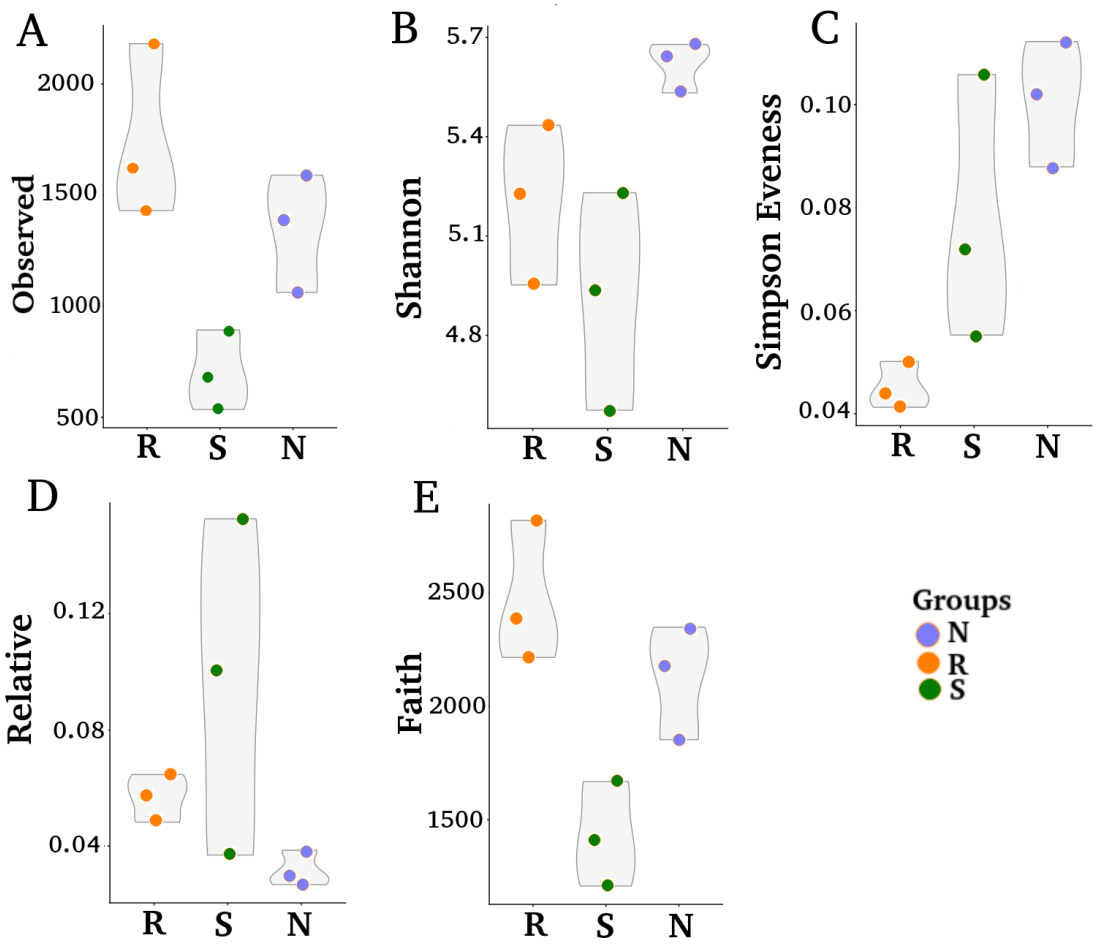

Fig. 21. Multiple violin plots of diversity indices in Rhizo (R), Symp (S), and Necro (N). From top left A) Observed richness, B) Shannon Diversity index, C) Simpson Evenness, D) Relative index and E) Faith diversity. The indices are in Y-axis and sample group in X-axis

The PERMANOVA test showed a significant ($p < 0.05$) difference in community composition among the three stages, likely due to the ongoing infection by the fungi. In Rhizo, the plant had a diverse range of microbial species. In stage Symp, a particular species took over and dominated the community. In stage Necro, the evenness of the community was restored. The top 20 taxa that contributed to discriminating the three different stages are shown in Fig. 22.

The results of this study suggest that the diversity and dissimilarity of microbial communities in plant infections are influenced by the stage of infection. The initial stage of infection is characterised by a high diversity of microbial species. As the infection progresses, a particular species may take over and dominate the community. However, in the final stage of infection, the evenness of the community may be restored. The bacteria from the genera *Sphingomonas* (*Sphingomonas* sp. 133, *Sphingomonas* sp., *Sphingomonas melonis*) and *Rhizobium* (*Rhizobium* sp. 34K_A, *Rhizobium* sp., *Rhizobium giardinii*) were observed to be top contributing taxa. There were also other bacteria such as *Frankia alni*, *Acidovorax* sp., as well as uncultured *Sphingobium* sp., *Nostocales cyanobacterium*, Betaproteobacteria, Alphaproteobacteria and Actinobacteria. The remaining four were unknown bacteria belonging to the Proteobacteria phylum.

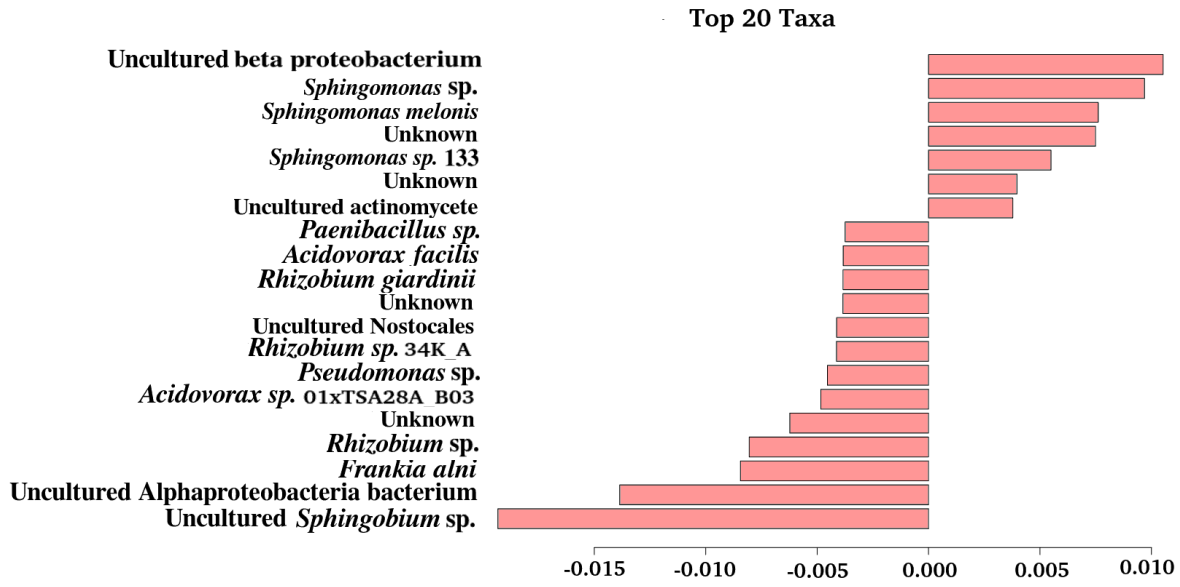

Fig. 22. Bidirectional bar plot of top 20 taxa that are involved in separation of the sample groups Rhizo, Symp and Necro. PERMANOVA model coefficients are in the X-axis and top contributing taxa in Y-axis.

4.3.2. Differential abundance analysis

There were significant differences between bacterial populations in different samples. A total of 258 and 154 bacterial taxa were found to have significant differences ($p < 0.01$) between the Rhizo vs. Symp and Rhizo vs. Necro, respectively. *Acidovorax, Rhodoferax, Bdellovibrio, Byssovorax,* and *Luteolibacter* were the top 5 most significant genera of bacteria present in Rhizo (Fisher's exact test, $p < 0.05$). Similarly, *Chroococcidiopsis, Geodermatophilus, Nevskia, Nakamurella,* and *Enterobacter* were found to be significantly occurring in Symp, while *Salinibacterium, Subtercola, Cryptosporangium, Methylobacterium*, and *Aeromicrobium* were found to be significant in Necro (FET, $p < 0.05$). Genera such as *Actinomycetospora, Friedmanniella, Hymenobacter, Microlunatu*s, and *Sphingomonas* (FET, $p < 0.05$) were significantly enriched in both Symp and Necro.

4.3.3. Differential metatranscriptome analysis

In this study, 42,374 transcripts were assembled and used for differential expression. It was observed in the analysis that 5,971 genes were differentially expressed (DE) between samples, with a statistical significance of less than 0.01. We discovered that 3,147 and 3,116 genes were upregulated in Symp and Necro, respectively. Among them, 1,844 genes were upregulated in both Symp and Necro.

4.3.4. Functional analysis of the metatranscriptome

The study involved the examination of a total of 5,971 transcripts, and it was found that only 527 transcripts, constituting 8% of the total, could be successfully annotated using the InterPro database. Unfortunately, the remaining 5,444 transcripts did not yield meaningful annotations or information regarding their functions. To gain insights into the biological processes associated with the upregulated genes in both Symp and Necro, a GO enrichment analysis was conducted. The results of this analysis, presented in Fig. 23, revealed that biological processes (BPs) related to membrane proteins and respiration were enriched in both Symp and Necro conditions. In addition to the GO analysis, the study focused on the expression of carbohydrate-active enzymes (CAZymes) in the Symp and Necro conditions. A notable finding was that 133 CAZymes were upregulated in the Symp, and 114 were upregulated in the Necro. Among these, the GT2 type of CAZyme was identified as the most

commonly upregulated in both Necro and Symp conditions, as illustrated in Fig. 24. This information suggests a potential involvement of these CAZymes in the biological processes associated with the studied conditions.

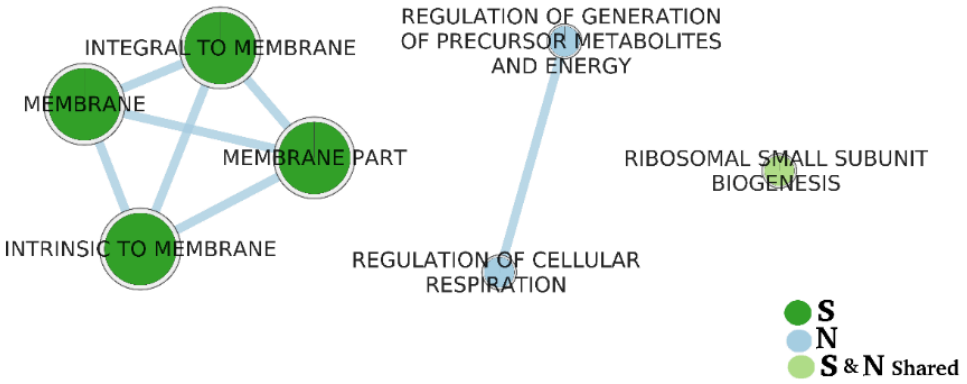

Fig. 23. Enrichment Map of Biological processes (BP) enriched in Symp(S), Necro(N) ($p < 0.05$). The enrichment map was constructed using the exclusively upregulated genes in Symp and Necro. Nodes represent the BP, and the size of the nodes denotes the number of genes. Edges represent the overlap, and the edge size represents the gene overlaps. Green nodes represent BP enriched in Symp and blue in Necro. Light green denotes the BP enriched in both Symp and Necro.

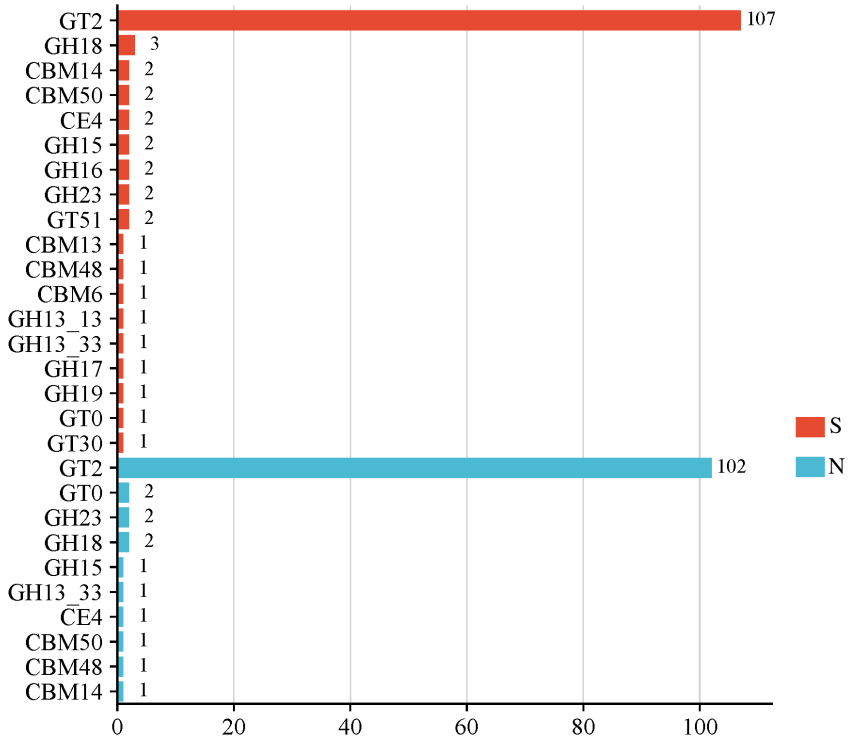

Fig. 24. Bar plot of upregulated CAZymes Counts in Symp (S) and Necro (N). The red color shows the CAZyme counts in Symp and blue in Necro. CAZymes counts are in the X-axis and CAZyme families in the Y-axis.

4.4. Interaction of *A. ostoyae* with *T. atroviride*

Time-course analysis of genes expressed during three time points (0^{th}, 53^{rd}, and 62^{nd} hour) revealed how the fungi talk to each other when brought together. In this thesis the main objective is to highlight the potential candidate genes that might be involved in the interaction between *T. atroviride* and *A. ostoyae*.

4.4.1. Identification and functional analysis of genes involved in the *A. ostoyae* and *T. atroviride* interaction

In A. ostoyae, 414 SSPs were found, 382 of which expressed themselves throughout the encounter. Out of the total 382 proteins, 202 were found to lack InterPro domains. *A. ostoyae* showed differential expression of 100 SSPs throughout the contact (Supplementary material 5). The SSPs associated with lectin activity, hydrophobin activity, and chitin binding were the most highly elevated. *T. atroviride* showed differential expression of 157 SSP-related genes during the 62^{nd} hour. Forty-three of the DEGs exhibited elevation in the interaction between the 0^{th} and 53^{rd} hour. The cerato-platanin, cerato-ulmin hydrophobin, RlpA-like protein, and peptidase S51 activities were the most highly elevated SSPs in *T. atroviride* (Supplementary material 6).

During the interaction, *A. ostoyae* showed an upregulation of 110 proteins with FCWD-related CAZyme annotation. 1 showed upregulation in 53^{rd} hour and 11 in 62^{nd} hour. Most expressed genes during this stage were CBM50, mannanases, glucanases, and chitin-binding proteins (Supplementary material 7). These proteins' overexpression may indicate that *A. ostoyae* attacks *T. atroviride'*s cell wall in order to defend itself. *T. atroviride* expressed forty genes associated to FCWD, of which thirty-three were elevated during the 0^{th}-53^{rd} hours of interaction (Supplementary material 8). These genes were associated with mannanases, glucanases, chitin-binding proteins, and other cell wall-degrading enzymes.

In *A. ostoyae*, 151 peptidase-related genes with differential expression were found; 39 of these genes showed upregulation during the 62^{nd} hour, and 37 genes showed differential expression in both the 53^{rd} and 62^{nd} hour. In the 62^{nd} hour of interaction, aspartic peptidase A1A and serine peptidase S12 showed the highest expression, whereas serine peptidases (S09, S33) and cysteine peptidase C12 were dominant(Supplementary material 9). In *T. atroviride*, 52 differently expressed secreted peptidases were found. Of these, four aspartic peptidases (A01A), three glutamic peptidases (G01), and five serine peptidases (S01A, S08A,

S09X, S12, and S54) were among the seventeen peptidases that were elevated during 62nd hour of contact. In both the 0th-53rd stages, there was an upregulation of one cysteine peptidase (C56) (Supplementary material 10). The pathogenicity and host adaptability of *T. atroviride* toward *A. ostoyae* may be attributed to the overexpression of A1 and G1 peptidases during the mycoparasite stage.

4.5. Identification of the biodegradation prospects of *Armillaria* species

4.5.1. Genome-level comparative analysis identifies specialisation of armillarioid fungi

The gene repertoire patterns of the primary enzyme classes were uniform across all fungal genomes, except for specific instances involving five basidiomycetous species (*B. adusta, T. betulina, T. versicolor, P. squamosus, I. lacteus*) and two ascomycetous species (*T. citrinoviride, G. candidum*), along with *M. lusitanicus*, where the count of transferase enzymes surpassed that of hydrolases. This observation is depicted in Fig. 25.

When investigating potential specialisation within white-rotting species, the quantities of 92 distinct enzymes encompassing a wide range of biodegradative activities were analysed and compared across the selected genomes (Fig. 26 & 27). The application of pPCA to prospective biodegradation genes revealed a distinct clustering of armillarioid species, clearly distinct from other white-rotting species (Fig. 28). Notably, based on individual copy number profiles, genes encoding benzoate-4-monooxygenase [EC: 1.14.14.92] and NADPH2 dehydrogenase [EC:1.6.99.1] (or xenobiotic reductase, "EAWAG-BBD enzyme, enzymeID# e0038") homologs, both characterised by notably high copy numbers in armillarioid genomes, significantly contributed to this distinctive clustering (Fig. 28).

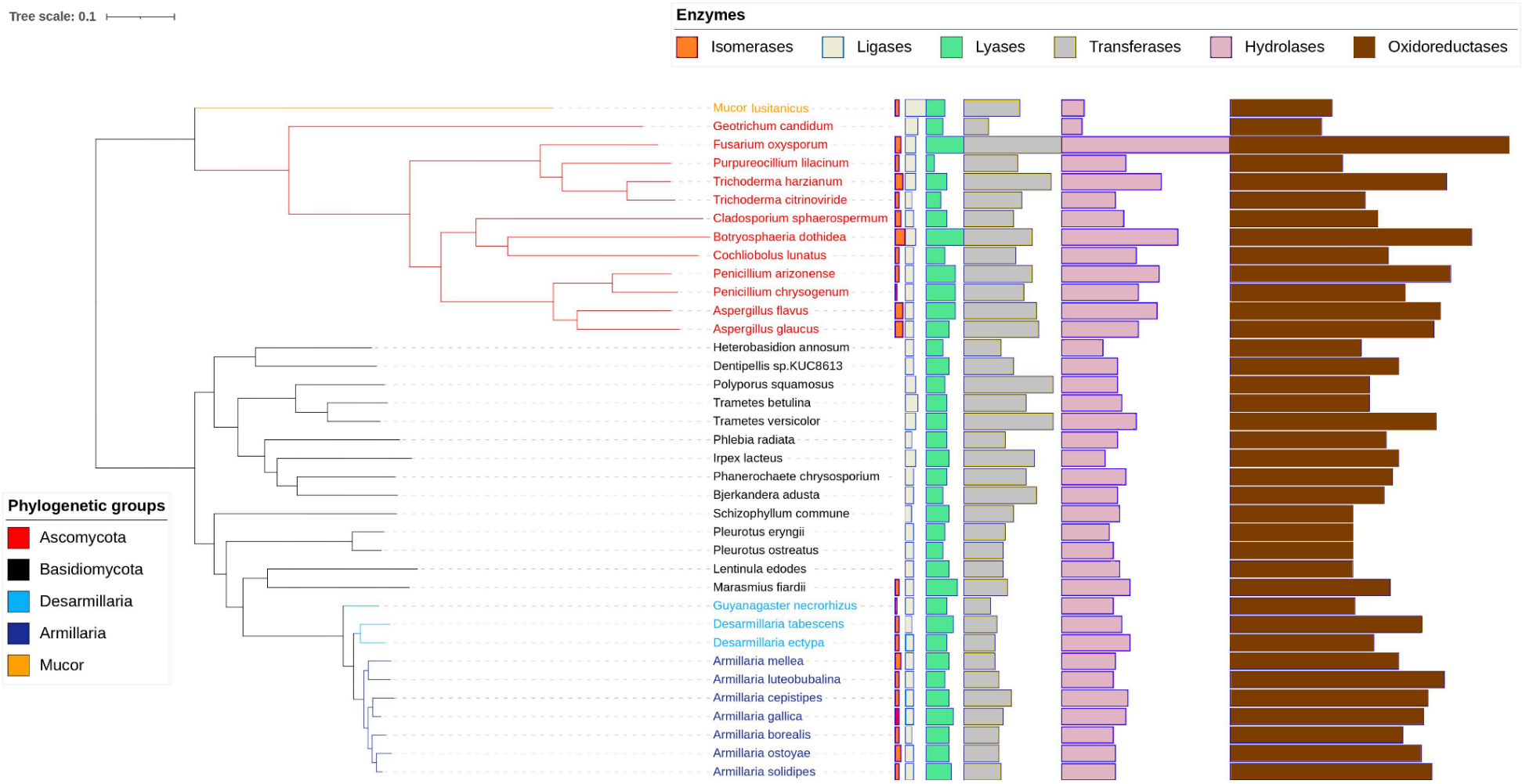

Fig. 25. Mycoremediation-related KEGG enzyme classes of fungi used in study. The enzyme classes are presented on the primary X-axis, and the fungal names are indicated on the Y-axis. The construction of the maximum likelihood phylogenetic tree for the fungal species was accomplished through the utilisation of orthologous proteins.

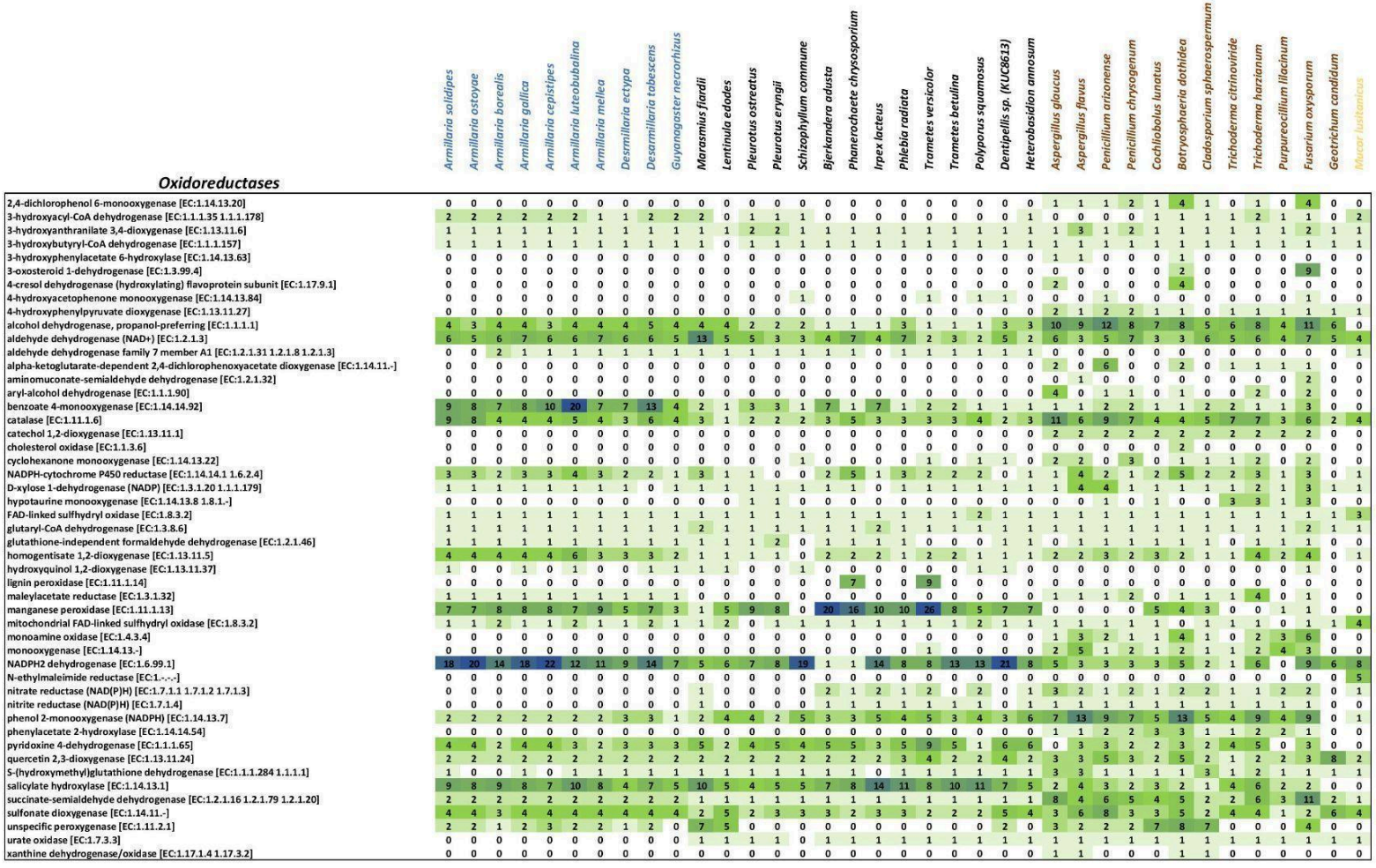

Fig. 26. Heatmap of mycoremediation-related oxidoreductase counts. Fungal species are on the top X-axis, and the enzyme names are listed along the Y-axis. The intensity of the cell colour correlates with the number of counts of a particular enzyme. # Enzyme clusters enriched in armillarioids. # Involved in PAH degradation. # Involved in degrading monocyclic aromatics.

B

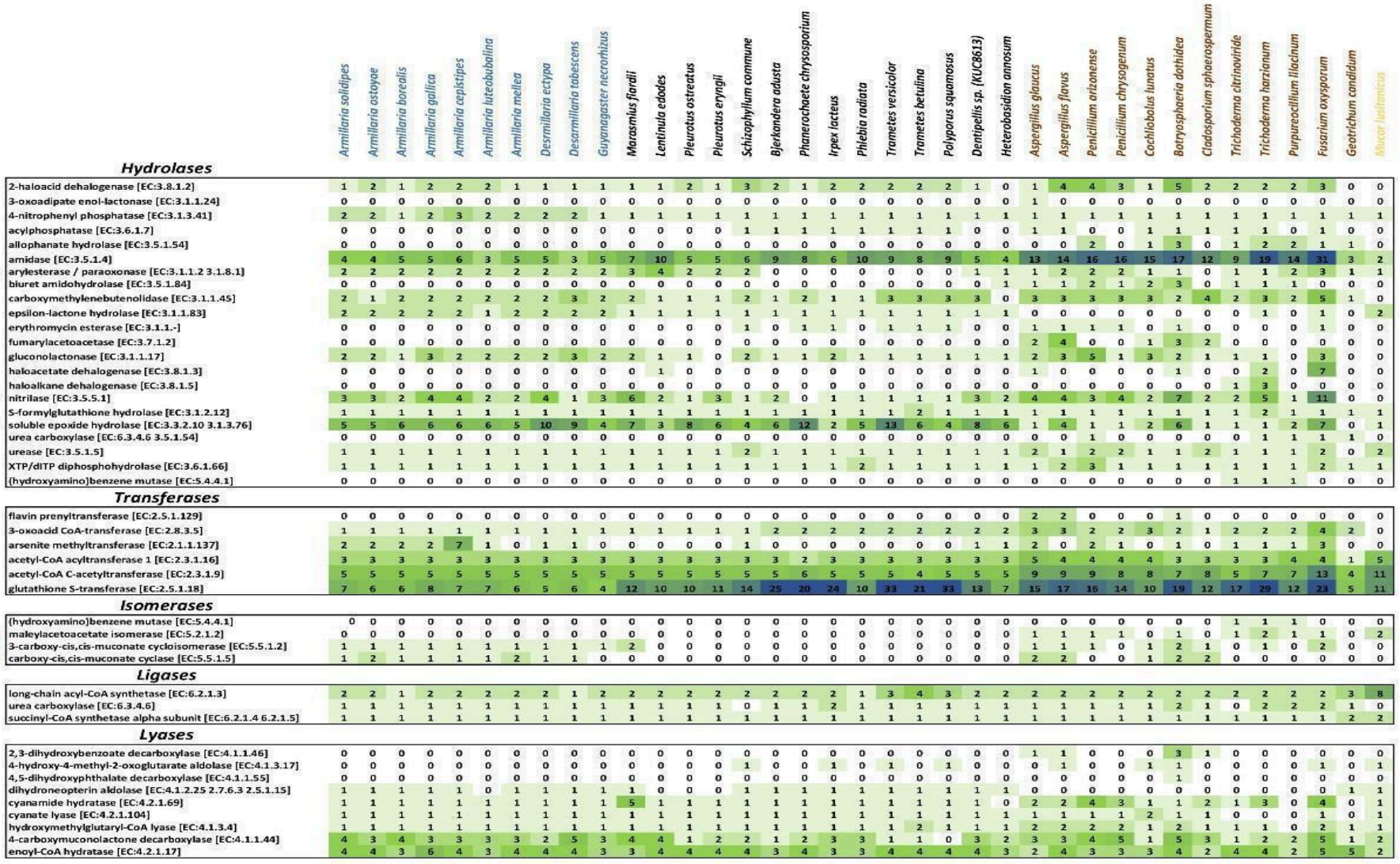

Fig. 27. Heatmap of mycoremediation-related hydrolase, transferase, isomerase, ligase and lyase counts. Fungal species are on the top X-axis, and the enzyme names are listed along the Y-axis. The intensity of the cell color correlates with the number of counts of a particular enzyme. # Enzyme clusters enriched in armillarioids. # Involved in PAH degradation. # Involved in degrading monocyclic aromatics.

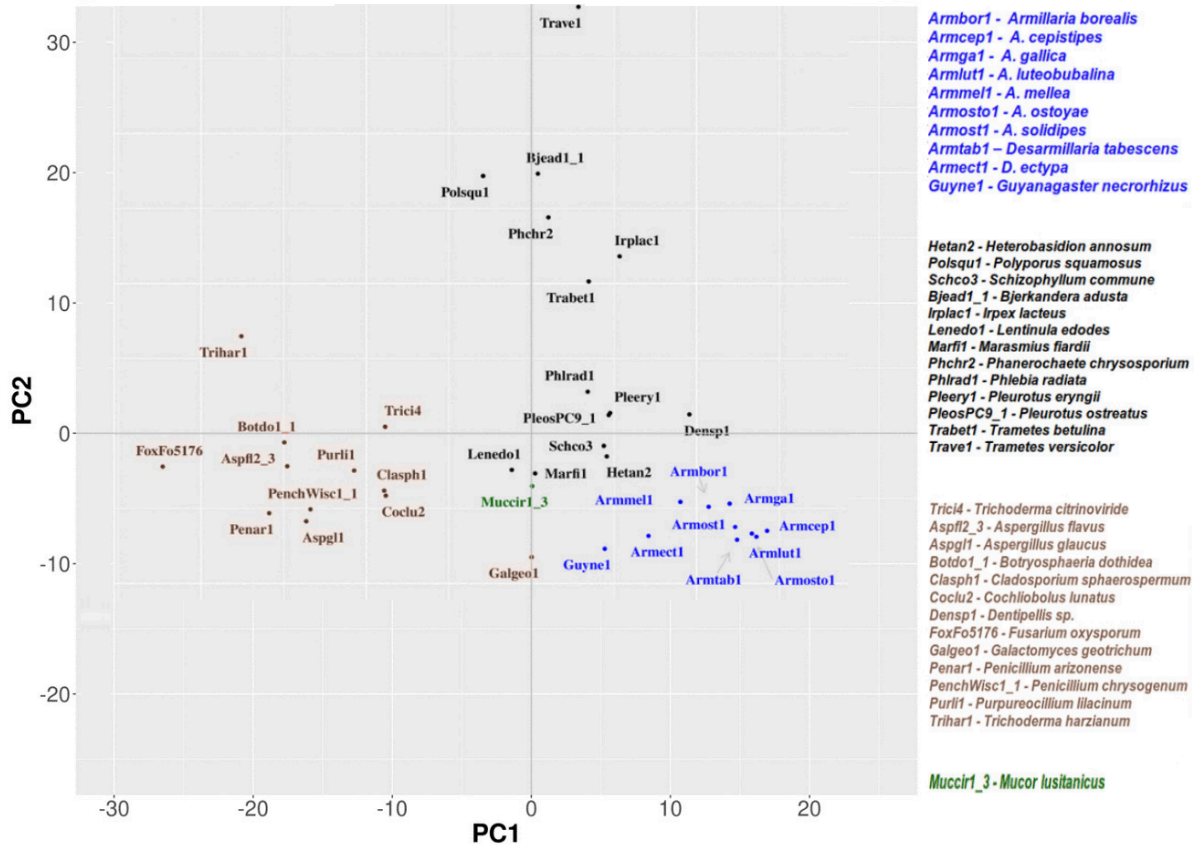

Fig. 28. Phylogenetic principal component analysis (PCA) plot depicting 37 diverse fungal species employed in a mycoremediation study. Armillariod species are represented by blue labels, black labels represent basidiomycetes other than armillariods, brown labels denote ascomycetes, and green labels identify mucoromycetes. The X-axis corresponds to PC1, and the Y-axis corresponds to PC2.

Through phylogenetic analysis, exploring 143 benzoate-4-monooxygenase and 331 NADPH2 dehydrogenase proteins across all fungi revealed diverse protein families. Despite the apparent structural diversity, thorough analysis of MEME motifs at the active site, substrate-binding, and cofactor-binding regions for armillarioid NADPH2 dehydrogenase proteins demonstrated no noteworthy substitutions in comparison to Ascomycota and Basidiomycota. However, scrutiny of multiple sequence alignments unveiled subtle yet significant disparities at the substrate- and heme-binding sites of benzoate-4-monooxygenases. Alterations in hydrophobicity and substitutions at the seventh and second positions of the substrate-binding site might influence the overall configuration of the substrate-binding surface, thereby impacting the specificity (Fig. 29).

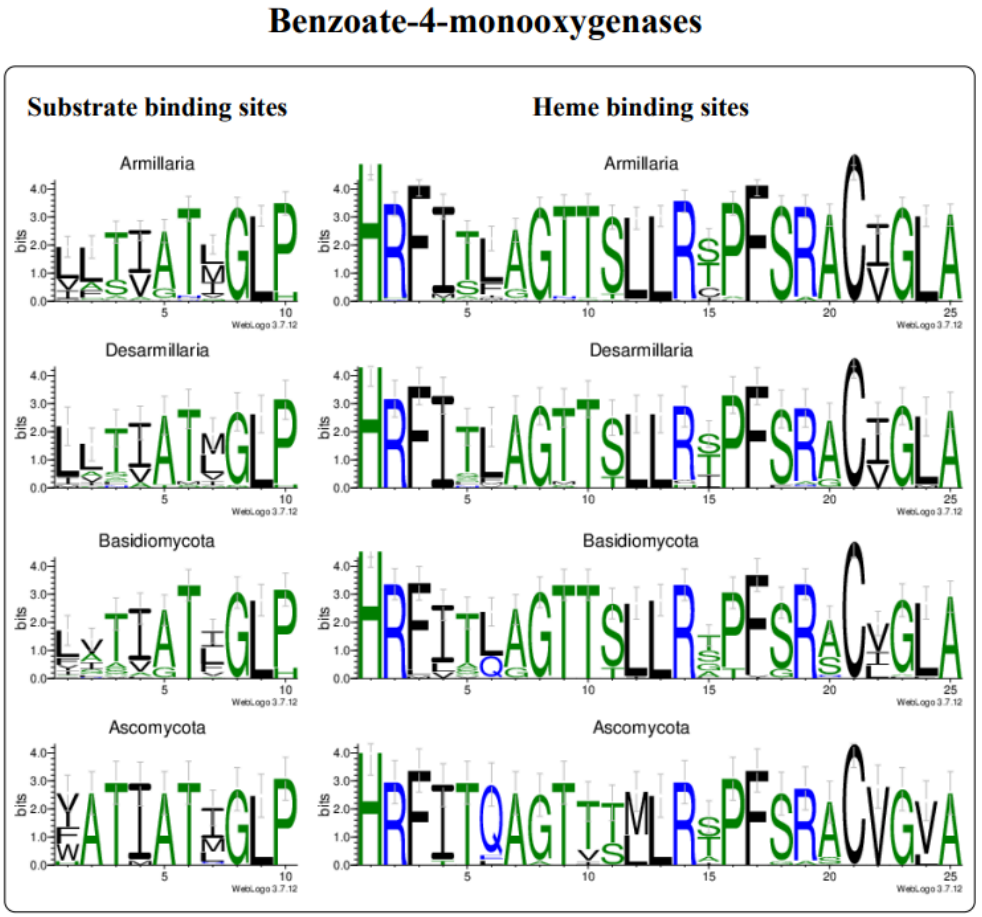

Fig. 29. Motif analysis of benzoate-4-monooxygenases

Additionally, at the sixth position of the heme-binding site, a hydrophobic leucine observed in armillarioids is exchanged for a polar, hydrophilic glutamine found in Basidiomycota and Ascomycota. It is recognized that a more hydrophobic milieu is preferable for heme interaction with the binding site (Liou *et al*., 2014). Further extensive experimentation is required to validate these potential implications.

4.5.2. Checking the expression profiles of the mycoremediation-related genes

Initially, the analysis of genes potentially involved in mycoremediation was conducted using raw RNA-Seq data from recent *in vitro* stem invasion assays (Sahu *et al.*, 2023). This analysis aimed to study the gene expression under native plant-interactive conditions and artificial, nutrient-rich media settings. The RSTO medium, which encompasses a diverse range of substrates, plays a pivotal role in initiating fruiting body formation for *Armillaria* species and acts as a crucial inoculum, enabling the invasiveness of

less virulent isolates in stem invasion experiments. Focusing on two conifer-specific species, *A. borealis,* and *A. ostoyae,* gene expression profiles were scrutinised for both highly virulent and less virulent isolates. Remarkably, a significant proportion of identified mycoremediation genes were active in both species: 95% (130/137) in *A. ostoyae* and 87% (126/145) in *A. borealis*. 75 % (6/8) and 100 % (7/7) of benzoate-4-monooxygenase [EC:1.11.1.13] were upregulated in A. ostoyae and A. borealis respectively.

In the comparative expression analysis of benzoate-4-monooxygenase genes, the study extended to the individual substrate and heme-binding sites of these genes. Intriguingly, among these genes, 4 out of 5 exhibited leucine or alanine at the second position and leucine at the seventh position within their substrate-binding sites – these positions are believed to represent the most likely armillarioid-specific residues (Fig. 29). Remarkably, these genes displayed a response within the plant environment, where they were upregulated under conditions of stem invasion across all isolates of both species. A noteworthy observation was made regarding one gene in *A. borealis* (Ambor|1721289), which seemed to contribute to virulence. Specifically, this gene was significantly overexpressed under conditions of plant invasion in the virulent isolate compared to the less virulent counterpart. In contrast, seven other genes with modified substitutions at the second and/or seventh positions or distinctly varied replacements at other binding site positions, remained inactive.

5. DISCUSSION

5.1. Comparative transcriptomic analyses of the *A. ostoyae* mycelia reveal specificities in the gene expression patterns

The purpose of this study was to investigate the effects of *A. ostoyae* C18 inoculum on two-year-old *P. abies* seedlings and also to identify the virulence and pathogenicity-related genes expressed in the mycelium of *A. ostoyae* inside the cambium of *P. abies*. Infected *P. abies* showed variation in outcomes as one group had curled leaves and wilting symptoms, while the other group showed sudden dieback with brown needles. This kind of intraspecies variation in infection strategies was observed by Prospero *et al.* (2004). It was also previously reported by Omdal *et al.* (1995) and Morrison & Pellow (2002) for *Armillaria* species.

The mycelium (Symp) of *A. ostoyae* extracted from the cambium of symptomatic *P. abies* and from sudden dieback (Necro) *P. abies* served as an excellent system to identify the set of genes that were differentially expressed in *A. ostoyae* that could lead to variation of outcome in *P. abies*.

Gene expression profiles of three different tissue types (Symp, Necro, Rhizo) were examined, and the genes with elevated transcription levels in Symp, Necro, and Rhizo were identified. Upregulation of genes related to cellulose, pectin, and hemicellulose degrading in Symp, and pectin, hemicellulose, and aromatics degradation in Necro indicated that the same fungi had a different strategy to invade the host plants, and possibly it resulted in the different phenotype of the host plant after infection. The analysis revealed that the fungi were invading the plant by destroying plant cell wall components. Degradation of those cell wall components might have led to tissue damage and loss of plant cell wall integrity.

The exact molecular mechanisms of how these genes cause symptoms such as wilting or sudden dieback in host plants are unclear; however, several factors could be associated with it. For example, the degradation of cellulose, pectin, and hemicellulose can release signalling molecules such as cellobiose, glucose, oligogalacturonides (OGs), and xyloglucan oligosaccharides (XGOs). These molecules have been shown to induce systemic defence by inducing the expression of pathogenesis-related (PR) genes and reactive oxygen species (ROS) in other plants like *Arabidopsis thaliana* (Souza *et al.,* 2017; Davidsson *et al.,* 2017; Claverie *et al.,* 2018). Similar triggers of PR in *P. abies* can also result in oxidative stress and cell death.

5.2. Unique sets of the Gsecretome were involved in the host-pathogen interactions

The contributions of secretory proteins in host invasion must be noticed as they are directly involved in the invasion of hosts (Yun *et al.,* 2023). This was proved by the overrepresentation of Gsecretome in *A. ostoyae* during its interaction with the host. Both Symp and Necro showed enrichment of different gene/protein families. For example, in Symp, putative GSecretome belonged to gene families like PL8, pectate lyase, intradiol ring-cleavage dioxygenase, GH43, GH18, S8, S58, M35, M36 while in Necro, carboxylesterase type B, GH88, BNR repeat-containing family, alpha-l-arabinofuranosidases, and fungal ligninase were overrepresented. Upregulation of genes related to intradiol ring-cleavage dioxygenase in Symp indicated ongoing degradation of aromatics in fungi, whereas upregulation of fungal ligninase in Necro indicated direct lignin degradation (Sariaslani & Dalton, 1989).

Gene families like PL8, pectate lyase, intradiol ring-cleavage dioxygenase, GH43, GH88, and fungal ligninase take part in plant cell wall degradation; however, what could be interesting is the gene families that are differently enriched in both tissues. In the Symp SSP pool, cerato-platanin, fungal chitosanase, M43, and GH12 were enriched, and in Necro, it was the kre9/knh1 family.

All though, the protein families uniquely enriched in different tissues were identified. The main question was, which genes or gene families would be crucial in the *in vivo* interaction environment. To answer that question, the genes expressed during *in vivo* interaction were compared to the *in vitro* wood invasion experiments. Surprisingly, it was discovered that the majority of the genes (64%) expressed in Symp was similar to those in the *in vitro* stem invasion experiments. In contrast, genes expressed in Necro and Rhizo were significantly different (Fig. 11). This could be due to epigenetic regulations or the defence response shown by the *P. abies* host. UpsetR analysis of gene families and CAZymes identified families uniquely upregulated in Symp and Necro. Gene families unique to Symp included the GH61, and the neutral/alkaline non-lysosomal ceramidase, while families unique to Necro included alpha/beta hydrolase fold-1, amidohydrolase 3, and beta-glucan synthesis-associated genes, among others. The signalling mucin MSB2 gene was upregulated in both Symp and Necro. Differential expression analysis of CAZyme related genes showed that AA9 was uniquely observed only in Symp, while CAZy groups such as CE15, GH115, and GH29 were observed in Necro. Shared CAZyme families were also identified, providing valuable clues about genes involved in interacting with live tissues.

5.3. Functional characterization of secreted proteins in *A. ostoyae* during plant pathogenesis

Several genes or gene families seem to be involved in the interaction between the pathogen *A. ostoyae* and the host *P. abies*. For instance, four SSP gene families, CAP domain containing cysteine-rich secretory proteins, the kre9/knh1 family, LysM domain containing genes, and superoxide dismutase that all being upregulated in the *A. ostoyae* mycelia potentially conferred resistance against *P. abies* defence response by trapping the hydrophobic substances released by plants, shielding from the plant defence by secreting polysaccharides, protecting from the hydrolytic enzymes by scavenging oliosaccharides and by breaking down the superoxide radicals, respectively (Darwiche *et al.,* 2017; Soanes *et al.,* 2008; Dubey *et al.,* 2020; Gleason *et al.,* 2014).

However, other gene families, such as cerato-platanins, GH12, M43 peptidases, and MD-2-related lipid recognition protein, may be involved in virulence and pathogenicity. Cerato-platanins serve as the initial line of plant-invading machinery by loosening the cell wall composition of plants and enabling easier penetration by fungal hyphae (Baccelli, 2015). Among the two cerato-platanins (ARMOST_11001, ARMOST_08316) expressed in the Symp stage in *A. ostoyae*, only one (ARMOST_08316) could be involved in invading live tissues as ARMOST_11001 was also seen in *A. ostoyae* invading dead wood. The glycoside hydrolase 12 gene, which was upregulated in Symp, was reported by Gui *et al.* (2017) to be associated with pathogen-associated molecular patterns (PAMPs) related to cell death. *Verticillium dahliae* GH12 proteins (VdEG1 and VdEG3) induced cell death and PAMP-triggered immunity (PTI) in *Nicotiana benthamiana*. GH12 (ARMOST_12600) upregulated by *A. ostoyae* might also have triggered a PTI response in *P. abies*. When *A. ostoyae* GH12 was searched against *Verticillium dahliae* using BLAST analysis, it showed that it was homologous to VdeG1 (E-value = 1e-43)) and VdeG3 (E-value = 4e-34).

Seven hydrophobins were upregulated in *A. ostoyae,* and four hydrophobins were also observed in a wood-decay experiment. We suspected that the hydrophobins expressed in the wood-degrading experiment and in the *in vivo* interaction experiment might differ from each other, and phylogenetic analysis of all the hydrophobins in *A. ostoyae* revealed that indeed the hydrophobin genes expressed during the *in vivo* plant-pathogen interaction were distant from the hydrophobins expressed in the wood-degrading experiment (Supplementary material 11). *A. ostoyae* hydrophobin genes, ARMOST_17948, ARMOST_11431, ARMOST_15834 might be crucial for adhesion and appressorium formation in live host-tissues.

Metallopeptidase M43 protein (ARMOST_05523), which is a putative apoplastic effector, was observed to be expressed in *A. ostoyae* only during *in vivo* interaction. M43 protein has been observed by Pan *et al.* (2020) to be involved in defence against plant chitinases and inducing plant cell death. One of the SGNH hydrolase-type esterase domain-containing genes (ARMOST_13144), which was predicted to be an apoplastic effector and involved in pectin-degradation was upregulated in both the wood degradation and our *in vivo* experiment. This gene could be involved in saprotrophy and pathogenicity (Kubicek *et al*., 2014).

In *A. ostoyae*, the secretion of putative classically secreted proteins (CSPs) seemed to be enriched (p-value < 0.05, FET) during the interaction with *P. abies*. Among 141 differentially expressed CSPs, 21 were observed during the wood degradation experiment. The remaining genes, which were uniquely upregulated in the *in vivo* experiment, could be associated with PCWD CAZymes, fungal cell wall remodelling enzymes, and virulence. PCWD genes included pectin-degrading InterPro families like alpha-L-arabinofuranosidase, BNR repeat-containing family member (GH145), GH88, polysaccharide lyase 8; oligosaccharide degrading beta-L-arabinofuranosidase (GH127), FAD linked oxidase, beberine-like (AA7); hemicellulose degrading GH47, GH43, GH5; cellulose degrading GH9, LPMO (AA9). InterPro families belonging to GH71 and GH92 might be involved in fungal cell wall remodelling.

Secreted GH18 upregulated in Symp might act as a sequester of free chitin to avoid plant response (Fiorin *et al.,* 2018). Peptidase M35 and M36 might be involved in deactivating plant-secreted chitinases and promoting infection (Zhang *et al.,* 2021). Upregulated catalase and haem-peroxidase might be involved in oxidative stress tolerance of fungi caused by PAMP/MAMP-triggered immune response initiated by fungi. Fungal ligninase, upregulated in Necro, might contribute to MAMP-triggered oxidative burst, host cell death, and necrosis, respectively (Xiao *et al.,* 2022). GH13+CBM20 (ARMOST_15344), specifically upregulated in Necro mycelia, could potentially be a virulence factor involved in necrosis. A similar protein, which comprised the GH15+CBM20 domain in the *Botrytis cinerea* gene (BcGS1), was found to be involved in inducing necrosis on tobacco and tomato leaves (Zhang *et al.,* 2015; Yang *et al.,* 2018). Pairwise alignment of both *B. cinerea* and *A. ostoyae* sequences showed only 36% similarity.

Upregulated protein families such as endonuclease/exonuclease/phosphatase and S1/P1 nuclease may be involved in degrading the DNA secreted by plants for neutrophil extracellular trapping and also inactivating plant ribosome-inactivating proteins, respectively (Park *et al.,* 2019; Pennington *et al.,* 2019). Laccases may also play a role in the infection of

spruce seedlings, and *A. ostoyae* showed upregulation of 7 genes related to laccases. Phylogenetic analysis of laccases from *Heterobasidion annosum* and *A. ostoyae* indicated that certain genes such as ARMOST_07310, ARMOST_08871, and ARMOST_12576 were close to *H. annosum* laccases jgi|Hetan2|181064 (HaLCC16), jgi|Hetan2|163392 (HaLCC6), and jgi|Hetan2|127340 (HaLCC13), (Supplementary material 11). In contrast, the remaining four genes/proteins upregulated in *A. ostoyae* were distant from *H. annosum* laccases. HaLCC16 and HaLCC6 were identified as being involved in the early stage of pine seedling infection by Kuo *et al.* (2015).

The protein MSB2 could play an essential role in the ability of *A. ostoyae* to penetrate and infect its host (Pérez-Nadales & Di Pietro, 2011). A knock-out study in *Fusarium oxysporum* by Pérez-Nadales & Di Pietro (2011) has shown that MSB2 is involved in invasion and virulence. Interestingly, a pairwise alignment of the mucin gene between *F. oxysporum* and *A. ostoyae* revealed only 38% similarity, suggesting that the two species have evolved distinct mechanisms for invasion and infection. Another protein with a potential role in *A. ostoyae* infection is cupin 1 (oxalate decarboxylase), as described by Liang *et al.* (2015) concerning appressorium development and infection. Further studies are needed to understand how MSB2 and cupin 1 contribute to *A. ostoyae* virulence.

Many gene families highlighted in this work may be of fundamental importance in the infection strategy of *A. ostoyae*. However, deeper investigations using gene knockout techniques are required to corroborate the findings and improve understanding. This thesis advocates for their selective targeting to understand better the role each of these genes plays in the progression of a fungal infection and to discover potential novel targets for antifungal medicines. In sum, the findings of this study lay a firm groundwork for further investigation of *A. ostoyae* and the methods it uses to infect hosts.

5.4. Decoding fungal lifestyles through orthogroup repertoires

Genes were grouped into orthogroups to determine whether orthogroup composition can distinguish between various fungi based on their lifestyle. The amino acid sequences from 61 different fungal species exhibiting different lifestyles (white rot, soft rot, brown rot and mycorrhizae) were utilized for this purpose. Using powerful ML algorithms such as XGBoost and Boruta, the orthogroup repertoires were identified, which were crucial to discriminating the fungi according to their lifestyles. On checking the correlation between the orthogroup repertoires and the differentially expressed genes in *A. ostoyae*, strong correlation

'*r'* between the white-rot orthogroup repertoire and *A. ostoyae* differentially expressed genes was observed. The results showed that the fungal lifestyle is reflected by their orthogroup repertoires and the genes expressed are in direct correlation with the size of orthogroup repertoire. The crucial orthogroups identified included protein families such as major facilitator superfamily (MFS), fungal ligninase, zinc finger, ring-type-vilya/Cst9/RNF212, GH28, cupredoxin, GMC-oxidoreductases (AA3_2), zinc finger, RING-type, GH28 and GH76.

The orthogroups OG0000871, OG0000258, and OG0000002, which are associated with the MFS, ligninase, and AA3_2 families, exhibited greater size in white-rot fungi. Additionally, these orthogroups were observed to play a pivotal role in distinguishing white-rot fungi from other species. The orthogroup OG0005476, whose members were associated with ring-type,vilya/cst9/rnf212 were completely absent in soft rot fungi but were present in white rot fungi. Our findings point to several previously unknown correlations between orthogroup repertoire and fungal life strategies, providing a foundation for future research.

5.5. Unravelling the complex molecular mechanisms of gene regulation during *A. ostoyae* infection through lncRNA

The importance of lncRNAs in regulatory mechanisms such as mitotic or meiotic cell cycle control, metabolism, cell-cell adhesion, stress response, pathogenicity, and several other functions is progressively becoming evident from a wide body of recently published studies (Till *et al.,* 2018; Li *et al.,* 2021). Since the lncRNAs expressed in *A. ostoyae* are largely unknown and have never been reported in previous investigations, they were investigated and reported in this study. In the *A. ostoyae* genome, 4116 lncRNAs were identified, of which 691 were antisense lncRNAs and 2921 intergenic lncRNAs. The distribution of different lncRNA counts followed a pattern that was remarkably similar to that of other fungal lncRNA publications, wherein lincRNAs (long intergenic non-coding RNA) were the most abundant, followed by antisense and other lncRNAs (Kyriakou *et al.,* 2016, Wang *et al.,* 2018). 83.01% of the lncRNAs in *A.ostoyae* had three exons or fewer, with a preference for two exon transcripts showing the highest incidence, as described in earlier studies (Wang *et al.,* 2018, Tucker *et al.,* 2021).

Symp vs. Rhizo, Necro vs. Rhizo, and Symp vs. Necro differential expression investigations yielded 131 DE lncRNAs that acted as cis- or trans-regulators of gene expression (Kopp & Mendell, 2018). Examining the genes nearby lncRNAs helped to identify their cis-targets (Martens *et al.,* 2005; Engreitz *et al.,* 227; Huang *et al.,* 2018), and analysing the binding energies of lncRNAs with distant transcripts helped discover their trans-regulated targets (Lamoth *et al.,* 2015). Enrichment of BPs such as "chromatin silencing," "posttranscriptional regulation of gene expression," "methylation/demethylation," and "acetylation/deacetylation" in cis-trans targets of lncRNAs corroborated with previous findings that lncRNAs act as epigenetic regulators of gene expression activity by recruiting histone-modifying enzymes and altering histone proteins, resulting in a change of chromatin structure (Huang *et al.,* 2018; Lamoth *et al.,* 2015; Berretta *et al.,* 2008; Nadal-Ribelles *et al.,* 2014).

In *A. ostoyae*, it is possible that the expression of the lncRNAs MSTRG.18013.6, MSTRG.15376.6, MSTRG.17015.1, and MSTRG.18013.5 regulates the activity of methyltransferase genes, which in turn affects the chromatin structure and controls the expression of genes. Examples of these types of lncRNAs found in *Saccharomyces cerevisiae* are Ty1AS and ncASP3, which are involved in changing gene expression by controlling chromatin structure alteration (Ribelles *et al.,* 2014; Morrison *et al.,* 2012). Antisense transcript in *Ustilago maydis* was discovered to be essential for maize infection and to play a significant role in virulence by Donaldson *et al.,* (2013) and Schaefer *et al.,* (2020). They discovered a substantial correlation between the expression of the antisense lncRNA ncrna1 and severity of the infection in the host. In this study it was also discovered that transcription factors, DE pectinesterase, serine carboxypeptidase (S10), intradiol dioxygenases, GH16, GH28, GH48, GH92, and others correlated with lncRNAs (Table 5). These lncRNAs might contribute to the pathogenicity and virulence of *Armillaria ostoyae.*

lncRNA MSTRG.7390.3, which was highest expressed in Symp showed strong positive correlation with ureohydrolase gene (ARMOST_08042), which has a crucial role in l-arginine, agmatine, guanidinobutyrate (GB), agmatinase, and 4-guanidinobutyrase (GBase) catabolism and also in virulence (Schaefer *et al.,* 2020). lncRNAs MSTRG. 19941.2, MSTRG.10080.1, MSTRG.19304, and MSTRG.10210.4 were identified to be trans-regulators of HSP70, intradiol ring-cleavage dioxygenase, and dienelactone hydrolase. Lamoth *et al.* (2015) and Tereshina (2005) previously reported that HSP70 has a role in stress adaptation and resistance to antifungal compounds, while intradiol ring-cleavage and

dienelactone hydrolase are involved in virulence and aromatics degradation (Joshi *et al.,* 2016; Berretta *et al.,* 2008; Semana & Powlowski, 2019; Schlömann *et al.,* 1993).

The findings of this study offer important new insights into the intricate regulatory networks involved in plant-fungal infections, even though the molecular mechanisms underpinning the regulatory roles of lncRNAs are still not entirely known. The mechanism of how the lncRNAs control gene expression still needs to be elucidated and studying the relationships between lncRNAs and additional regulatory components, like transcription factors and histone-modifying enzymes, may be necessary to achieve this.

In conclusion, a significant number of lncRNAs of the *A. ostoyae* genome have been discovered and described in this study, and their data revealed their possible contributions to control gene expression during a fungal infection. The findings of this study have significant ramifications for the design of novel approaches for managing fungal infections in plants and for improving our knowledge of the intricate regulatory networks involved in fungal pathogenesis.

5.6. Diverse microbial and gene expression patterns observed in Symp, Necro, and Rhizo

The objective of this study was to investigate the microbial community associated with Symp and Necro *A. ostoyae* mycelium. By comparing the microbial composition of Symp and Necro to that of freely growing *A. ostoyae* rhizomorphs in potting soil, The analysis revealed a total of 55 phyla and 765 genera. The results showed that Proteobacteria, Actinobacteria, Bacteroidetes, and Firmicutes were the most dominant bacteria identified in *A. ostoyae*, with genera such as *Pseudomonas*, *Rhizobium*, Brady*rhizobium*, *Sphingomonas*, *Streptomyces*, *Methylobacterium*, *Variovorax*, *Acidovorax*, and *Caulobacter* accounting for about 26% of the genera. Some genera, such as *Sphingomonas* and *Rhizobium*, were discovered to be the top contributing taxa in differentiating between the various groups of samples.

Sphingomonas and *Rhizobium* are two prokaryotic genera that play substantial roles in plant growth and development. *Sphingomonas* spp. are known to benefit plants in a variety of ways. They can aid plant growth by producing plant hormones like indole acetic acid (IAA), which stimulate root development (Ashaf *et al.,* 2020). By producing antimicrobial compounds, *Sphingomonas* spp. can also improve the plant's resistance to pathogens (Wang *et al.,* 2022). Furthermore, they have been shown to assist plants in coping with

environmental stresses such as drought and salinity. *Rhizobium* spp., on the other hand, are required for nitrogen fixation in leguminous plants. They form nodules on plant roots, converting atmospheric nitrogen into a form the plant can use for growth (Zahran, 1999). This process can reduce the need for nitrogen fertilisers, which can be costly and harmful to the environment. Rhizobium can contribute to the enhancement of soil health by increasing the organic matter content and improved nutrient availability. Furthermore, bacteria like *Rhizobium radiobacter,* formerly identified as *Agrobacterium tumefacien*st can also infect various plant species.

While both bacteria have beneficial effects on plants, they can also be harmful under certain conditions. Some *Sphingomonas* spp. have been reported as phytopathogens by Kini *et al.* (2017) and Buonaurio *et al.* (2002). The majority of the *Sphingomonas* species are potent degraders of aromatic and polycyclic compounds; hence, they could work alongside *A. ostoyae* synergistically in lignin degradation (Purahong *et al.,* 2022; Wilhelm, 2019). *Sphingomonas*, *Caulobacter*, and *Acidovorax* are potent lignin degraders, and some *Sphingomonas* spp. as are involved in nitrogen (N)-cycling. Purahong *et al.* (2022) showed that N-cycling bacteria are highly active in deadwood. They also found *Sphingomonas* in the early stage of wood decay and were substantial contributors to accelerated wood decay. The enrichment of *Sphingomonas* in Symp and Necro hints towards synergistic wood decay activities along with *A. ostoyae*.

Gene expression profiling revealed a difference in the expression of 5,971 genes between the samples, with 3,147 genes upregulated in sample S and 3,116 genes upregulated in sample Necro. As only 8% of the transcripts could be annotated, large sections of the differentially expressed genes were unknown. Glycosyltransferase 2 (GT2) CAZymes were found to be predominant in all Rhizo, Symp and Necro. GT2 enzymes are essential in a variety of cellular processes, including the synthesis of extracellular polysaccharides, lipopolysaccharides, and capsular polysaccharides (CPSs), which are involved in biofilm formation and bacterial attachment to host tissues (Oehme *et al.,* 2019). Since the majority of the metatrancripts could not be annotated, further research is needed to understand the functional role and significance of the differentially expressed genes.

5.7. *A. ostoyae* and *T. atroviride* genes in action

Both *A. ostoyae* and *T. atroviride* showed differences in gene expression during the 53rd and 62nd-hour stages of their interaction. Cerato-ulmin hydrophobin, which belongs to class II hydrophobins, was upregulated in *T. atroviride* during the 53rd hour. Ruocco *et al.* (2015) identified that the Hytlo1 gene, a class II hydrophobin in *T. longibrachiatum,* was crucial for mycoparasitism. Although it was observed to be directly involved in mycoparasitism, they were crucial for overgrowing the pathogenic fungi. Hence it can also be speculated that cerato-ulmin hydrophobin is involved in similar functions and might contribute to mycoparasitism. G1 peptidase, upregulated in *T. atroviride* during the 62nd hour, might also have similar functions. Although the involvement of G1 peptidases in mycoparasitism has not been reported before, this would be the first report of the involvement of G1 peptidases. *A. ostoyae* in response to *T. atroviride* expressed RlpA, CAP domain and cysteine-rich proteins, osmotin/thaumatin, LysM domain-containing and pectate lyase related genes. These genes might result from a desperate attempt by *A. ostoyae* to fight against the mycoparasite.

The study also investigated the dynamics of CAZymes and proteases during the interaction between *T. atroviride* and *A. ostoyae*. The transcriptomes of both fungi during the 0th hour (pre-contact), 53rd hour (metabolite), and 62nd hour (mycoparasite) stages of their interaction were analysed. In *A. ostoyae*, most of the FCWD enzymes were highly expressed during the 53rd hour (metabolite), and 62nd hour (mycoparasite) stages, whereas in *T. atroviride*, they were already highly expressed during the 0th hour. In accordance with Kullnig *et al.,* (2000), certain enzymes, including chitinases, were already secreted during the precontact phase. GH18 represents chitinases, the upregulation of which can enhance the ability of *T. atroviride* to colonize its prey cells (Fanelli *et al.,* 2018; Lienemann *et al.,* 2009; Kappel *et al.,* 2020). The activation of genes encoding chitinolytic enzymes and glucanases may play a significant role in *Armillaria*'s mycoparasitism by *T. atroviride*. During the 62nd hour, expression of GHs in *T. atroviride* decreased significantly with increasing incubation time, presumably due to a saturation of these enzymes in the medium. Most CAZymes exhibited no significant changes in the 62nd hour, except auxiliary activities (AAs) that were substantially upregulated at the 62nd hour. This phenomenon may be part of or a consequence of an oxidative stress defense.

The dynamics of secreted proteases was also studied to understand the mechanism of the degradation of cell wall glycoproteins (Flores *et al.,* 1997). Similar to CAZymes, many

secretory protease genes were already expressed by *T. atroviride* in 0th hour, but to a lesser extent in *A. ostoyae*. During the 62nd hour, the abundance and diversity of protease profiles increased substantially in *A. ostoyae*, possibly due to the direct contact of mycoparasite and its host. In previous studies by Viterbo *et al.* (2004), during plate confrontation assay of *T. asperellum* with *R. solani*, the gene *papA* encoding one of the extracellular aspartyl proteases was upregulated in *T. asperellum*. It was also observed by Szabó *et al.* (2013) that certain metalloendopeptidases, serine proteases, and aspartic proteases were induced in *T. harzianum* during *in vitro* nematode egg-parasitism of *Caenorhabditis elegans*. These observations reveal a significant biocontrol role of these proteases. It was observed in biocontrol experiments that the genera *Serratia* and *Bacillus* release specific peptidases and proteases that are involved in the detoxification of toxic molecules produced by *Aspergillus niger* and *R. solani* (Benoit *et al.,* 2015, Gkarmiri *et al.,* 2015). A similar gene expression indicated that *A. ostoyae* implemented a similar detoxification mechanism against *T. atroviride*. *A. ostoyae* exhibited an intense reaction by expressing diverse peptidases during *in vitro* plate assay to protect itself from the *T. atroviride* assault.

Although various gene candidates were identified in this study, further studies are required to validate the individual gene functions by performing knockout experiments. This study provides a reliable system to study the interaction of *A. ostoyae* and *T. atroviride* in the real time and to dive deeper to elucidate the roles of different genes of both partners.

5.8. The mycoremediation potentials of the armillarioids

Addressing environmental contamination is a worldwide concern demanding effective solutions, and mycoremediation has surfaced as a promising alternative that meets crucial criteria, including cost-effectiveness, environmental friendliness, and efficacy. The study underscores the potential of armillarioid species in facilitating the degradation of benzoic acid derivatives. This insight is derived from a comprehensive comparative genomics analysis, which assessed the copy counts of genes/proteins across 36 fungal species. It could be seen that expanded repertoires of benzoate 4-monooxygenase-degrading genes were present in the armillarioid species (Fig. 26). As a result, our findings imply that armillarioid species might well handle benzoate contaminations in the environment. Nevertheless, the high copy number of benzoate 4-monooxygenase [EC 1.14.14.92] genes only provides a single step in converting benzoate to 4-hydroxybenzoate (Fuchs *et al.,* 2011). The genes responsible for further conversion of 4-hydroxybenzoate have yet to be found, and the full degradation

process has to be thoroughly investigated. According to the investigation, armillarioids contain increased levels of the nitroglycerine-degrading enzyme [EC:1.6.99.1]. Thus, species of armillarioids *like A. cepistipes* and *A. ostoyae* would be promising candidates for *in vitro* investigations along with already known *P. chrysosporium,* previously employed by Pal & Christodoulatos (1995).

Maleyl acetate reductase that degrades chloroaromatic chemicals in the 3-oxoadipate pathway (Seibert *et al.,* 1993; Martins *et al.,* 2015) might have been horizontally transferred from bacteria. BLAST analysis of armillarioid maleyl acetate dehydrogenase genes with the nr database of NCBI (National Centre for Biotechnology Information) showed that the consensus sequence was 61% identical (E-value = 6e-145) to the maleyl acetate genes of *Pseudomonas* spp.

A. cepistipes, among all other *Armillaria* and *Desarmillaria* species, may be a potential option for arsenic biotransformation due to the abundance of arsenite methyl transferases. Previously it was discovered that *A. cepistipes* helped to remove vanadium from media and heavy metals from forest soil (Rigling *et al.,* 2006; Xu *et al.,* 2019). The tolerance index *of A. cepistipes,* as researched by Xu *et al.* (2019), was found to be similar to that of *A. muscaria*, *X. badius*, and *B. adusta*. *A. cepistipes* also showed tolerance towards vanadyl sulfate ($VOSO_4$) and sodium metavanadate ($NaVO_3$). The molecular mechanism that involves vanadium uptake is still unclear.

Fungal genome mining showed no fungi expressing polyethylene (PE) and polyurethane (PU) degrading enzymes. Hence, this finding is in concordance with the findings of Bruner *et al.* (2018) who could not find any potent PE- and PU-degrading fungi.
Our comparative genomics technique provided a high-level overview of the mycoremediation capability of several fungal species that might effectively break down various types of contaminants. Although mycoremediation appears promising, many physical and chemical factors have a substantial impact on how well fungal strains degrade, whether the process is carried out *in vitro* or *in situ*. For instance, Hefnawy *et al.* (2017) previously noted that the growth of *Aspergillus flavus* and *Penicillium canescens* was suppressed by a concentration of 0.05% direct brown (DB) dye. Senthilkumar *et al.* (2014) found that increasing the dye concentration had a comparable effect on *P. chrysosporium*. However, medium optimization and the addition of potential inducers, such as lignin, can assist to greatly enhance the tolerance of fungi.

All in all, bioremediation interventions primarily focus on the natural environment, although these techniques can also be simulated and executed within a controlled laboratory

setup. Such controlled environments offer optimal conditions for the growth and functionality of microorganisms or enzymes. Recent advancements in genetic and protein engineering have significantly contributed to laboratory procedures and bioengineering, leading to more robust strategies for enhancing mycoremediation solutions. In addition to utilising native fungal cells, genetic engineering utilising the versatile CRISPR-Cas targeted genome editing technology presents a potent alternative. This approach facilitates the expression of crucial genes or their modified variants in bacterial or fungal hosts that are better suited for environmental or biotechnological purposes (Song *et al*., 2019; Jaiswal *et al*., 2021; Singh *et al*., 2019). Notably, the recently developed "HACKing" strategy provides a highly dependable and efficient framework for co-expressing multiple genes in fungi employed for environmental mycoremediation (Yue *et al*., 2023). Building upon our current findings, the initial step towards a focused, efficient biodegradation of specific aromatic or xenobiotic compounds within the environment could involve evaluating the specialisation and effectiveness of genetically diverse benzoate-monooxygenase homologs from armillarioids within a heterologous system. This approach holds the potential for targeted and efficient bioremediation of these compounds.

SUMMARY

Armillaria ostoyae, a ubiquitous and ecologically significant fungal species, poses a significant threat to coniferous forests globally. Its broad parasitic range and facultative necrotrophic lifestyle contribute to its detrimental impact on these ecosystems. This facultative necrotrophic behaviour, the ability to utilise both live and dead organic matter for growth, allows *A. ostoyae* to infect trees both during their healthy state and after they have succumbed to other stressors. This duality of pathogenicity often leads to widespread damage and even mortality within affected coniferous stands. Several factors influence its pathogenicity and virulence, including secretory proteins, long non-coding RNAs, and associated microbiomes. Understanding the molecular mechanisms contributing to the virulence and pathogenicity of the fungus is critical for developing effective strategies to control its spread. Identifying the biodegradation prospects of *Armillaria* spp. can have significant implications in developing long-term management strategies for the fungus and utilising its full potential to handle the impact of specific environmental contaminants/pollutants effectively.

In this study, the effects of *A. ostoyae* C18 inoculum on two-year-old *P. abies* seedlings were investigated, and virulence- and pathogenicity-related genes expressed in the invasive mycelia of *A. ostoyae* inside the cambium of *P. abies* were identified. Infected *P. abies* showed variation in outcomes, with one group exhibiting curled leaves and wilting symptoms, while the other group showed sudden dieback with brown needles. The exact molecular mechanisms of how these genes cause symptoms such as wilting or sudden dieback in host plants are unclear, but several factors could be associated. The degradation of cellulose, pectin, and hemicellulose can release signalling molecules such as cellobiose, glucose, oligogalacturonides (OGs), and xyloglucan oligosaccharides (XGOs), which could act as elicitors of systemic response resulting in symptoms like wilting or sudden dieback.

The contributions of the extracellularly delivered secretory proteins in host invasion were demonstrated by the overrepresentation of secretory proteins in *A. ostoyae* during its interaction with the host. Symp and Necro samples showed enrichment of different gene/protein families, such as PL8, pectate lyase, intradiol ring-cleavage dioxygenase, GH43, GH88, and fungal ligninase. Upregulation of genes related to intradiol ring-cleavage dioxygenase in Symp indicated ongoing degradation of aromatics in fungi, whereas upregulation of fungal ligninase in Necro indicated direct lignin degradation. The study found that seven hydrophobins were upregulated in *A. ostoyae*, and the hydrophobins expressed in

in vivo infection were phylogenetically different from hydrophobins expressed during the wood-decay experiment.

The remaining genes that uniquely upregulated in the *in vivo* experiment could be associated with plant cell-wall degrading CAZymes, fungal cell wall remodelling enzymes, and virulence. *A. ostoyae* showed the upregulation of seven genes related to laccases. Phylogenetic analysis of laccases from *Heterobasidion annosum* and *A. ostoyae* indicated that genes from *A. ostoyae*, such as ARMOST_07310, ARMOST_08871, and ARMOST_12576 were closely related to *H. annosum* laccases expressed during the early period of their host invasions, indicating that laccasses may uniformly represent virulence factors. The MSB2 gene, which was highly expressed in *A. ostoyae*, could also be involved in invasion and virulence. However, further research is needed to determine which genes are responsible for the virulence of *A. ostoyae*, and knock-out experiments are mandatory in evaluating their ultimate role in virulence.

The study also looked at the expression of long non-coding RNAs in *A. ostoyae* and their possible functions. The analysis found that 131 differentially expressed lncRNAs acted as cis- or trans-regulators of gene expression, affecting biological processes such as chromatin silencing, post-transcriptional regulation of gene expression, methylation/demethylation, and acetylation/deacetylation. Our study identified several lncRNAs that regulate the activity of methyltransferase genes and control the expression of genes related to transcription factors, pectinesterase, serine carboxypeptidase, intradiol-dioxygenases, and various other proteins.

Analysis of microbiomes associated with *A. ostoyae* revealed that Proteobacteria, Actinobacteria, Bacteroidetes, and Firmicutes were the most dominant bacterial phyla. Several genera, including *Pseudomonas, Rhizobium*, *Bradyrhizobium, Sphingomonas*, *Streptomyces, Methylobacterium, Variovorax, Acidovorax,* and *Caulobacter,* that accounted for approximately 26% of the genera, could be identified. The high occurrence of *Sphingomonas* confirmed its role as a significant contributor to accelerated wood decay, and they acted synergistically with *A. ostoyae.*

Furthermore, the study investigated the interaction between *A. ostoyae* and *Trichoderma atroviride*, and found that secretory proteins, carbohydrate-active enzymes, and proteases played crucial roles in the fungus-fungus interactions. The study identified several genes that were upregulated in *T. atroviride*, including cerato-ulmin hydrophobins and G1 peptidases, which could aid *T. atroviride* in mycoparasitism. Haploid *A. ostoyae* hyphae expressed RlpA, CAP domain and cysteine-rich proteins, osmotins/thaumatins, LysM

domain-containing proteins, and pectate lyase-related genes that could help them to defend themselves from *T. atroviride*.

Finally, we have investigated the mycoremediation ability of armillarioid species and found that they had expanded repertoires of benzoate 4-monooxygenase-degrading genes and NADPH2 dehydrogenases, suggesting that armillarioid species may be exceptionally equipped to handle specific benzoate contaminations in the environment.

This study has shed light on the molecular mechanisms in *A. ostoyae* mycelia that contribute to its virulence and pathogenicity, including the role of secretory proteins, long non-coding RNAs, and the microbiome. Understanding these mechanisms is essential for developing effective strategies to control the spread of the fungus and mitigate its impact on the environment.

ÖSSZEFOGLALÓ

Az Armillaria ostoyae egy világszerte előforduló, ökológiailag fontos gombafaj, amely mindenhol jelentős veszélyt jelent a tűlevelű erdőkre. Parazitaként a széleskörű előfordulása és fakultatív nekrotróf életmódja együttesen hozzájárul ezekre az ökoszisztémákra gyakorolt kiemelten káros hatásához. Ez a fakultatív nekrotróf életforma, az élő és az elhalt szerves anyagok hasznosításának képessége lehetővé teszi, hogy az A. ostoyae megfertőzze az egészséges fákat, és azokat is, amelyeknek a stresszhatásoknak köszönhetően már legyengült az ellenállóképességük. A patogenitásnak ez a kettőssége gyakran széles körben megjelenő károkhoz, pusztulásokhoz vezet az érintett tűlevelű állományokban. Számos tényező befolyásolja a gomba patogenitását és virulenciáját, beleértve a szekréciós effektor fehérjéket, a hosszú, nem kódoló RNS-eket és az invázióban résztvevő, társult mikrobiális közösségeket. A gomba virulenciájához és patogenitásához hozzájáruló molekuláris mechanizmusok megértése rendkívül fontos a gomba terjedésének szabályozására szolgáló hatékony stratégiák kidolgozásához. Az Armillaria fajok biodegradációs profiljának, potenciáljának a felmérése pedig jelentős következményekkel járhat a gombával kapcsolatos hosszú távú felhasználási stratégiák kidolgozásában, és lehetővé teszi a bennük rejlő képességek, lehetőségek kihasználását bizonyos specifikus környezeti szennyezőanyagok célzott, hatékony lebontásában.

Inváziós kísérleteinkben az A. ostoyae C18 virulens izolátum kétéves P. abies palántákra gyakorolt hatását vizsgáltuk és azonosítottuk az invazív micéliumban expresszálódó, patogenitással, virulenciával kapcsolatos géneket. A fertőzött fenyőpalánták tüneteiben jelentős eltérések mutatkoztak, ugyanis az egyik csoportban hullámos levelek és hervadásos tünetek jelentkeztek, míg a másik csoportban az egyedek elhalt barna tűlevelekkel gyorsan kiszáradtak. Nem tisztázott a pontos molekuláris mechanizmusa annak, hogy ezek a gének hogyan okoznak olyan tüneteket, mint a hervadás vagy a gazdanövények hirtelen elhalása, de több tényező is összefüggésbe hozható a tünetekkel. A cellulóz, a pektin és a hemicellulóz lebomlása olyan jelzőmolekulákat szabadíthat fel, mint a cellobióz, glükóz, oligogalakturonidok (OG-ok) és xiloglukán-oligoszacharidok (XGO-k), amelyek a szisztémás válasz kiváltójaként működhetnek, olyan tünetek megjelenéséhez vezetve, mint a hervadás vagy a hirtelen halál.

Az extracellulárisan kiválasztott szekréciós fehérjék gazdaszervezet inváziójában betöltött potenciális, aktív szerepét ezen fehérjék túlreprezentáltsága bizonyítja a gombahifáknak a gazdaszervezettel való kölcsönhatása során. A szimptomatikus (Symp) és

nekrotróf (Necro) mintákban különböző gén/fehérjecsaládok, például PL8, pektát-liáz, intradiol gyűrűhasító dioxigenáz, GH43, GH88 (glikozil-hidroláz) és gombaligninász enzimek feldúsulását mutattuk ki. Az intradiol gyűrűhasító dioxigenázhoz kapcsolódó gének upregulálása a Symp-ben az aromás anyagok folyamatos lebontását jelezte a gombákban, míg a gomba ligninázok szintjének a növekedése a Necro-ban a lignin közvetlen lebontására utal. Az inváziós génexpressziós adatok analízise alapján kiderült, hogy hét hidrofobin gén volt upregulálva a növényi szövetekkel kölcsönható A. ostoyae mintákban, és az in vivo fertőzésben expresszált hidrofobinok filogenetikailag különböztek a fapusztulási kísérlet során expresszált hidrofobinoktól.

Az in vivo kísérletben egyedülállóan upregulált gének a növényi sejtfalat lebontó CAZyme, és a gomba sejtfalát adaptívan átalakító enzimekkel, illetve a gombahifák virulens aktivitásával hozhatók összefüggésbe. Az A. ostoyae hét lakkáz funkcióhoz kapcsolódó gént expresszált kiemelkedő szinten. A Heterobasidion annosum és az A. ostoyae lakkázainak filogenetikai analízise a továbbiakban azt mutatta, hogy az A. ostoyae gének, mint például az ARMOST_07310, ARMOST_08871 és ARMOST_12576 szoros rokonságban állnak a H. annosum azon lakkázaival, amelyek a gazdaszervezet hatékony inváziójában virulenciafaktorként viselkedve a szöveti invázió hátterét biztosítják. Az MSB2 gén, amely nagymértékben upregulálódott az A. ostoyae-ben, virulenciafaktorként szintén szerepet játszhat az invázióban. Azonban további vizsgálatokra van szükség annak meghatározásához, hogy mely gének felelősek az A. ostoyae virulenciájáért, és "knockout" gén hátterű kontroll kísérletek alapvetőek a virulenciában betöltött végső szerepük kiértékeléséhez.

Az in vivo kísérletes eredmények analízise során megvizsgáltuk a hosszú, nem kódoló RNS-ek expresszióját és lehetséges funkcióikat is A. ostoyae-ben. Az elemzés megállapította, hogy 131 eltérően expresszálódó lncRNS működött közre a génexpressziós folyamatok cisz- vagy transz-szabályozójaként, ezáltal befolyásolva a biológiai folyamatokat, mint például a kromatincsendesítés, a génexpresszió poszt-transzkripciós szabályozása, a metiláció/demetiláció és az acetilezés/deacetiláció. Vizsgálatunk számos lncRNS-t azonosított, amelyek szabályozzák a metiltranszferáz gének aktivitását, és a transzkripciós faktorokhoz, pektinészterázokhoz, szerin-karboxipeptidázokhoz, intradiol-dioxigenázokhoz és számos más fehérjéhez kapcsolódó gének expresszióját.

Az A. ostoyae micéliumok in vivo inváziójával kapcsolatos mikrobiómok elemzése feltárta, hogy a Pseudomonadota (korábban Proteobacteria), Actinomycetota (korábban Actinobacteria), Bacteroidota (korábban Bacteroidetes) és Bacillota (korábban Firmicutes) voltak a folyamatban résztvevő domináns baktériumtörzsek. Számos nemzetség közül a

Pseudomonas, Bradyrhizobium, Sphingomonas, Rhizobium, Streptomyces, Methylobacterium, Variovorax, Acidovorax és Caulobacter voltak többségben, amelyek a nemzetségek körülbelül 26%-át tették ki. A Sphingomonas nemzetség előfordulása megerősítette a szerepüket a felgyorsult fapusztulásban, amikor is domináns mértékben az A. ostoyae micéliumszövetek lebontó tevékenységeivel szinergisztikus aktivitást mutattak.

Az A. ostoyae és a Trichoderma atroviride izolátumok közötti kölcsönhatások vizsgálata során megállapíthatóvá vált, hogy különféle szekréciós fehérjék, a szénhidrát-aktív enzimek és proteázok alapvető szerepet játszanak a mikoparazita gomba-gomba interakciókban. Számos olyan gént sikerült azonosítani, amelyek a T. atroviride-ben upreguláltak voltak, beleértve a cerato-ulmin hidrofobinokat és a G1 peptidázokat, amelyek döntően segíthetik a Trichoderma micéliumok mikoparazitikus aktivitását. A haploid A. ostoyae hifák RlpA-t, CAP domént és ciszteinben gazdag fehérjéket, ozmotinokat/taumatinokat, LysM domént tartalmazó fehérjéket és pektát-liáz funkciókhoz kapcsolódó géneket expresszáltak, amelyek lehetőséget adtak a T. atroviride elleni védekezésben.

Végül megvizsgáltuk az armillarioid fajok mikoremediációs képességeit, és azt találtuk, hogy kibővült a benzoát 4-monooxigenázt lebontó gének és a NADPH2 dehidrogenázok repertoárja, ami arra utal, hogy az armillarioid fajok kivételesen jól fel vannak szerelve a környezetben előforduló specifikus benzoátszennyeződések kezelésére.

Az elért eredményeink rávilágítottak azokra az A. ostoyae gombaszövetekben található molekuláris mechanizmusokra, amelyek hozzájárulnak a faj kiemelkedő virulenciájához és patogenitásához, beleértve a különféle szekréciós fehérjék, a hosszú, nem kódoló RNS-ek és a társult mikrobiómok szerepét. E mechanizmusok megértése elengedhetetlen a gomba terjedésének megfékezésére és a környezetre gyakorolt hatásának mérséklésére szolgáló hatékony stratégiák kidolgozásához.

ACKNOWLEDGEMENTS

First and foremost, I would like to thank God for the successful completion of my thesis and then my Ph.D. supervisor, Prof. Dr. György Sipos for his expert mentorship and guidance. His expertise and important feedback kept me going during all times of my Ph.D. I would also like to thank the head of the Department of Microbiology of the University of Szeged, Prof. Dr. Csaba Vágvölgyi, for providing all necessary help and input during our discussions. I am also really grateful to Dr. László Kredics and Dr. László Nagy, who are fungal experts, and discussions with them always proved to be very fruitful and motivating. I also thank bioinformatics geniuses Dr. Martin Münsterkötter and Dr. Attila Szűcs for their technical support and guidance. I wish to thank my lab members and friends, especially Boris Indic, Dr. Garima Raj and Neha Sahu for their help, motivation and support. To all my friends, Tapan Kumar Baral, Savio Topno, Jugami Iswary, Dr. Michael Islary, and Tapan Roy, a big "Thank You" for always being there for me and listening to my nonsense talks. I am also thankful to Jyotismita Basumatary, Dr. Rinku Champramary (beloved brother), and my family for their prayers and emotional support.

FINANCIAL SUPPORT

This research was funded by the Hungarian Government and the European Union within the frames of the Széchenyi 2020 Program (GINOP-2.3.2-15-2016-00052). I am grateful to the Stipendium Hungaricum Scholarship program for the monthly allowances and the University Grants Commission of India for supporting my studies in Hungary.

LIST OF REFERENCES

Andrews, S. (2017). FastQC: a quality control tool for high throughput sequence data. 2010.https://www.bioinformatics.babraham.ac.uk/projects/fastqc/

Akhtar, N. Amin-ul Mannan M. (2020). Mycoremediation: Expunging environmental pollutants. *Biotechnol Rep*, *26*, e00425.

Anderson, J. B. (1986). Biological species of *Armillaria* in North America: redesignation of groups IV and VIII and enumeration of voucher strains for other groups. *Mycologia*, *78*(5), 837-839.

Antipova, T. V., Zhelifonova, V. P., Litovka, Y. A., Pavlov, I. N., Baskunov, B. P., Kokh, Z. A., ... & Kozlovsky, A. G. (2022). Secondary metabolites of six Siberian and Crimean *Armillaria* species and their in vitro phytotoxicity to pine, larch and poplar. *iForest-Biogeosciences and Forestry*, *15*(1), 38.

Antonín, V., Stewart, J. E., Ortiz, R. M., Kim, M. S., Bonello, P., Tomšovský, M., & Klopfenstein, N. B. (2021). *Desarmillaria caespitosa*, a North American vicariant of *D. tabescens*. *Mycologia*, *113*(4), 776-790.

Aramaki, T., Blanc-Mathieu, R., Endo, H., Ohkubo, K., Kanehisa, M., Goto, S., & Ogata, H. (2020). KofamKOALA: KEGG Ortholog assignment based on profile HMM and adaptive score threshold. *Bioinformatics*, *36*(7), 2251-2252.

Asaf, S., Numan, M., Khan, A. L., & Al-Harrasi, A. (2020). *Sphingomonas*: from diversity and genomics to functional role in environmental remediation and plant growth. *Critical Reviews in Biotechnology*, *40*(2), 138-152.

Baccelli, I. (2015). Cerato-platanin family proteins: one function for multiple biological roles?. *Frontiers in Plant Science*, *5*, 769.

Bailey, T. L., Johnson, J., Grant, C. E., & Noble, W. S. (2015). The MEME suite. *Nucleic Acids Research*, *43*(W1), W39-W49.

Barr, D. P., & Aust, S. D. (1994). Pollutant degradation by white rot fungi. *Reviews of Environmental Contamination and Toxicology*, 49-72.

Batish, S., Hunter, A., Ashby, A. M., & Johnstone, K. (2003). Purification and biochemical characterisation of Psp1, an extracellular protease produced by the oilseed rape pathogen *Pyrenopeziza brassicae*. *Physiological and Molecular Plant Pathology*, *62*(1), 13-20.

Baumgartner, K., & Rizzo, D. M. (2006). Relative resistance of grapevine rootstocks to *Armillaria* root disease. *American Journal of Enology and Viticulture*, *57*(4), 408-414.

Baumgartner, K., Coetzee, M. P., & Hoffmeister, D. (2011). Secrets of the subterranean pathosystem of *Armillaria*. *Molecular Plant Pathology*, *12*(6), 515-534.

Beckman, T. G., Okie, W. R., Nyczepir, A. P., Pusey, P. L., & Reilly, C. C. (1998). Relative susceptibility of peach and plum germplasm to *Armillaria* root rot. *HortScience*, *33*(6), 1062-1065.

Benoit, I., van den Esker, M. H., Patyshakuliyeva, A., Mattern, D. J., Blei, F., Zhou, M., ... & Kovács, Á. T. (2015). *Bacillus subtilis* attachment to *Aspergillus niger* hyphae results in mutually altered metabolism. *Environmental Microbiology*, *17*(6), 2099-2113.

Berretta, J., Pinskaya, M., & Morillon, A. (2008). A cryptic unstable transcript mediates transcriptional trans-silencing of the Ty1 retrotransposon in *S. cerevisiae*. *Genes & Development*, *22*(5), 615-626.

Bérubé, J. A., & Dessureault, M. (1989). Morphological studies of the *Armillaria mellea* complex: two new species, *A. gemina* and *A. calvescens*. *Mycologia*, *81*(2), 216-225.

Boedi, S., Berger, H., Sieber, C., Münsterkötter, M., Maloku, I., Warth, B., ... & Strauss, J. (2016). Comparison of *Fusarium graminearum* transcriptomes on living or dead wheat differentiates substrate-responsive and defense-responsive genes. *Frontiers in Microbiology*, *7*, 1113.

Boutet, E., Lieberherr, D., Tognolli, M., Schneider, M., Bansal, P., Bridge, A. J., ... & Xenarios, I. (2016). UniProtKB/Swiss-Prot, the manually annotated section of the UniProt KnowledgeBase: how to use the entry view. *Plant Bioinformatics: Methods and Protocols*, 23-54.

Bragaloni, M., Anselmi, N., & Cellerino, G. P. (1997). Identification of European *Armillaria* species by analysis of isozyme profiles. *European Journal of Forest Pathology*, *27*(3), 147-157.

Bravo Ruiz, G., Di Pietro, A., & Roncero, M. I. G. (2016). Combined action of the major secreted exo‐and endopolygalacturonases is required for full virulence of *Fusarium oxysporum*. *Molecular Plant Pathology*, *17*(3), 339-353.

Brazee, N. J., & Wick, R. L. (2011). *Armillaria* species distribution and site relationships in *Pinus*- and *Tsuga*-dominated forests in Massachusetts. *Canadian Journal of Forest Research*, *41*(7), 1477-1490.

Brazee, N. J., Hulvey, J. P., & Wick, R. L. (2011). Evaluation of partial *tef1*, *rpb2*, and nLSU sequences for identification of isolates representing *Armillaria calvescens* and *Armillaria gallica* from northeastern North America. *Fungal Biology*, *115*(8), 741-749.

Brazee, N. J., Ortiz-Santana, B., Banik, M. T., & Lindner, D. L. (2012). *Armillaria altimontana*, a new species from the western interior of North America. *Mycologia*, *104*(5), 1200-1205.

Brito, N., Espino, J. J., & González, C. (2006). The endo-β-1, 4-xylanase Xyn11A is required for virulence in Botrytis cinerea. *Molecular Plant-Microbe Interactions*, *19*(1), 25-32.

Bruhn, J. N. (1998). Identification of *Armillaria* field isolates using isozymes and mycelial growth characteristics. *Mycopathologia*, *142*(2), 89-96.

Bruhn, J. N., Wetteroff Jr, J. J., Mihail, J. D., Kabrick, J. M., & Pickens, J. B. (2000). Distribution of *Armillaria* species in upland Ozark Mountain forests with respect to site, overstory species composition and oak decline. *Forest Pathology*, *30*(1), 43-60.

Bruisson, S., Maillot, P., Schellenbaum, P., Walter, B., Gindro, K., & Deglène-Benbrahim, L. (2016). Arbuscular mycorrhizal symbiosis stimulates key genes of the phenylpropanoid biosynthesis and stilbenoid production in grapevine leaves in response to downy mildew and grey mould infection. *Phytochemistry*, *131*, 92-99.

Brunner, I., Fischer, M., Rüthi, J., Stierli, B., & Frey, B. (2018). Ability of fungi isolated from plastic debris floating in the shoreline of a lake to degrade plastics. *PLoS One*, *13*(8), e0202047.

Buchfink, B., Xie, C., & Huson, D. H. (2015). Fast and sensitive protein alignment using Diamond. *Nature Methods*, *12*(1), 59-60.

Buonaurio, R., Stravato, V. M., Kosako, Y., Fujiwara, N., Naka, T., Kobayashi, K., ... & Yabuuchi, E. (2002). *Sphingomonas melonis* sp. nov., a novel pathogen that causes brown spots on yellow Spanish melon fruits. *International Journal of Systematic and Evolutionary Microbiology*, *52*(6), 2081-2087.

Burdsall Jr, H. H., Banik, M., & Cook, M. E. (1990). Serological differentiation of three species of *Armillaria* and *Lentinula edodes* by enzyme-linked immunosorbent assay using immunized chickens as a source of antibodies. *Mycologia*, *82*(4), 415-423.

Bushnell, B. (2014). BBDuk: adapter/quality trimming and filtering. https://jgi.doe.gov/data-and-tools/software-tools/bbtools/bb-tools-user-guide/bbduk-guide/

Caballero, J. R. I., Lalande, B. M., Hanna, J. W., Klopfenstein, N. B., Kim, M. S., & Stewart, J. E. (2022). Genomic comparisons of two *Armillaria* species with different ecological behaviors and their associated soil microbial communities. *Microbial Ecology*, 1-22.

Chen, L., Bóka, B., Kedves, O., Nagy, V. D., Szűcs, A., Champramary, S., ... & Kredics, L. (2019). Towards the biological control of devastating forest pathogens from the genus *Armillaria*. *Forests*, *10*(11), 1013.

Chen, T., He, T., Benesty, M., Khotilovich, V., Tang, Y., Cho, H., ... & Zhou, T. (2015). Xgboost: extreme gradient boosting. *R Package Version 0.4-2*, *1*(4), 1-4.

Choi, G., Jeon, J., Lee, H., Zhou, S., & Lee, Y. H. (2022). Genome-wide profiling of long non-coding RNA of the rice blast fungus *Magnaporthe oryzae* during infection. *BMC Genomics*, *23*(1), 1-12.

Cios, K. J., Pedrycz, W., & Swiniarski, R. W. (2012). Data mining methods for knowledge discovery. *Springer Science & Business Media*, 458.

Claverie, J., Balacey, S., Lemaître-Guillier, C., Brulé, D., Chiltz, A., Granet, L., ... & Poinssot, B. (2018). The cell wall-derived xyloglucan is a new DAMP triggering plant immunity in *Vitis vinifera* and *Arabidopsis thaliana*. *Frontiers in Plant Science*, *9*, 1725.

Cleary, M. R., Van Der Kamp, B. J., & Morrison, D. J. (2012). Effects of wounding and fungal infection with *Armillaria ostoyae* in three conifer species. II. Host response to the pathogen. *Forest Pathology*, *42*(2), 109-123.

Coetzee, M. P., Wingfield, B. D., & Wingfield, M. J. (2018). Armillaria root-rot pathogens: species boundaries and global distribution. *Pathogens*, *7*(4), 83.

Collins, C., Keane, T. M., Turner, D. J., O'Keeffe, G., Fitzpatrick, D. A., & Doyle, S. (2013). Genomic and proteomic dissection of the ubiquitous plant pathogen, *Armillaria mellea*: toward a new infection model system. *Journal of Proteome Research*, *12*(6), 2552-2570.

Cox, K. D., & Scherm, H. (2006). Interaction dynamics between saprobic lignicolous fungi and *Armillaria* in controlled environments: Exploring the potential for competitive exclusion of *Armillaria* on peach. *Biological Control*, *37*(3), 291-300.

Cromey, M. G., Drakulic, J., Beal, E. J., Waghorn, I. A., Perry, J. N., & Clover, G. R. (2020). Susceptibility of garden trees and shrubs to Armillaria root rot. *Plant Disease*, *104*(2), 483-492.

Cui, X., Lu, Z., Wang, S., Jing-Yan Wang, J., & Gao, X. (2016). CMsearch: simultaneous exploration of protein sequence space and structure space improves not only protein homology detection but also protein structure prediction. *Bioinformatics*, *32*(12), i332-i340.

Darwiche, R., El Atab, O., Baroni, R. M., Teixeira, P. J., Mondego, J. M., Pereira, G. A., & Schneiter, R. (2017). Plant pathogenesis–related proteins of the cacao fungal pathogen *Moniliophthora perniciosa* differ in their lipid-binding specificities. *Journal of Biological Chemistry*, 292(50), 20558-20569.

Davidsson, P., Broberg, M., Kariola, T., Sipari, N., Pirhonen, M., & Palva, E. T. (2017). Short oligogalacturonides induce pathogen resistance-associated gene expression in *Arabidopsis thaliana*. *BMC Plant Biology*, *17*, 1-17.

Davis, J. R., Goodwin, L., Teshima, H., Detter, C., Tapia, R., Han, C., ... & Sello, J. K. (2013). Genome sequence of *Streptomyces viridosporus* strain T7A ATCC 39115, a lignin-degrading actinomycete. *Genome Announcements*, 1(4), e00416-13.

De Carolis, E., Vella, A., Vaccaro, L., Torelli, R., Spanu, T., Fiori, B., ... & Sanguinetti, M. (2014). Application of MALDI-TOF mass spectrometry in clinical diagnostic microbiology. *The Journal of Infection in Developing Countries*, *8*(09), 1081-1088.

DeLong, R. L., Lewis, K. J., Simard, S. W., & Gibson, S. (2002). Fluorescent pseudomonad population sizes baited from soils under pure birch, pure Douglas-fir, and mixed forest stands and their antagonism toward *Armillaria* ostoyae in vitro. *Canadian Journal of Forest Research*, *32*(12), 2146-2159.

Deo, R. C. (2015). Machine learning in medicine. *Circulation*, *132*(20), 1920-1930.

Devkota, P., & Hammerschmidt, R. (2020). The infection process of *Armillaria mellea* and *Armillaria solidipes*. *Physiological and Molecular Plant Pathology*, *112*, 101543.

Dickinson, S. Y. D. N. E. Y. (1960). The mechanical ability to breach the host barriers. *Plant Pathology*, 2, 203-231.

Dobin, A., Davis, C. A., Schlesinger, F., Drenkow, J., Zaleski, C., Jha, S., ... & Gingeras, T. R. (2013). STAR: ultrafast universal RNA-seq aligner. *Bioinformatics*, *29*(1), 15-21.

Donaldson, M. E., & Saville, B. J. (2013). *Ustilago maydis* natural antisense transcript expression alters mRNA stability and pathogenesis. *Molecular Microbiology*, *89*(1), 29-51.

Donaldson, M. E., Meng, S., Gagarinova, A., Babu, M., Lambie, S. C., Swiadek, A. A., & Saville, B. J. (2013). Investigating the *Ustilago maydis/Zea mays* pathosystem: Transcriptional responses and novel functional aspects of a fungal calcineurin regulatory B subunit. *Fungal Genetics and Biology*, *58*, 91-104.

Drakulic, J., Gorton, C., Perez-Sierra, A., Clover, G., & Beal, L. (2017). Associations between *Armillaria* species and host plants in UK gardens. *Plant Disease*, *101*(11), 1903-1909.

Duarte-Mata, E., Elías-Román, R. D., Klopfenstein, N. B., Hanna, J. W., & Kim, M. S. (2021). First report of the Armillaria root-disease pathogen, *Armillaria gallica*, associated

with several woody hosts in three states of central Mexico (Guanajuato, Jalisco, and Michoacan). *Plant Disease*, *105*(1), 222.

Dubey, M., Vélëz, H., Broberg, M., Jensen, D. F., & Karlsson, M. (2020). LysM proteins regulate fungal development and contribute to hyphal protection and biocontrol traits in Clonostachys rosea. *Frontiers in Microbiology*, 11, 679.

Dumas, M. T., & Boyonoski, N. W. (1992). Scanning electron microscopy of mycoparasitism of *Armillaria* rhizomorphs by species of *Trichoderma*. *European Journal of Forest Pathology*, *22*(6‐7), 379-383.

Eisenhaber, B., Schneider, G., Wildpaner, M., & Eisenhaber, F. (2004). A sensitive predictor for potential GPI lipid modification sites in fungal protein sequences and its application to genome-wide studies for *Aspergillus nidulans*, *Candida albicans Neurospora crassa*, *Saccharomyces cerevisiae* and *Schizosaccharomyces pombe*. *Journal of Molecular Biology*, *337*(2), 243-253.

Ekstrom, A., & Yin, Y. (2016). ORFanFinder: automated identification of taxonomically restricted orphan genes. *Bioinformatics*, *32*(13), 2053-2055.

Elad, Y., Barak, R., Chet, I., & Henis, Y. (1983). Ultrastructural studies of the interaction between *Trichoderma* spp. and plant pathogenic fungi. *Journal of Phytopathology*, *107*(2), 168-175.

Elías‐Román, R. D., Guzmán‐Plazola, R. A., Klopfenstein, N. B., Alvarado‐Rosales, D., Calderón‐Zavala, G., Mora‐Aguilera, J. A., ... & García‐Espinosa, R. (2013). Incidence and phylogenetic analyses of *Armillaria* spp. associated with root disease in peach orchards in the State of Mexico, Mexico. *Forest Pathology*, *43*(5), 390-401.

Ellis, L. B., Roe, D., & Wackett, L. P. (2006). The University of Minnesota biocatalysis/biodegradation database: the first decade. *Nucleic Acids Research*, *34*, D517-D521.

Emms, D. M., & Kelly, S. (2019). OrthoFinder: phylogenetic orthology inference for comparative genomics. *Genome Biology*, *20*, 1-14.

Engreitz, J. M., Haines, J. E., Perez, E. M., Munson, G., Chen, J., Kane, M., ... & Lander, E. S. (2016). Local regulation of gene expression by lncRNA promoters, transcription and splicing. *Nature*, 539(7629), 452-455.

Fanelli, F., Liuzzi, V. C., Logrieco, A. F., & Altomare, C. (2018). Genomic characterization of *Trichoderma atrobrunneum* (*T. harzianum* species complex) ITEM 908: insight into the genetic endowment of a multi-target biocontrol strain. *BMC Genomics*, *19*, 1-18.

Fiorin, G. L., Sanchéz-Vallet, A., de Toledo Thomazella, D. P., do Prado, P. F. V., do Nascimento, L. C., de Oliveira Figueira, A. V., ... & Teixeira, P. J. P. L. (2018). Suppression of plant immunity by fungal chitinase-like effectors. *Current Biology*, *28*(18), 3023-3030.

Fischer, M., & Pleiss, J. (2003). The Lipase Engineering Database: a navigation and analysis tool for protein families. *Nucleic Acids Research*, *31*, 319-321.

Flores, A., Chet, I., & Herrera-Estrella, A. (1997). Improved biocontrol activity of *Trichoderma harzianum* by over-expression of the proteinase-encoding gene prb1. *Current Genetics*, *31*, 30-37.

Franceschetti, M., Maqbool, A., Jiménez-Dalmaroni, M. J., Pennington, H. G., Kamoun, S., & Banfield, M. J. (2017). Effectors of filamentous plant pathogens: commonalities amid diversity. *Microbiology and Molecular Biology Reviews*, *81*(2), e00066-16.

Fuchs, G., Boll, M., & Heider, J. (2011). Microbial degradation of aromatic compounds—from one strategy to four. *Nature Reviews Microbiology*, *9*(11), 803-816.

Gawade, D. B., Perane, R. R., Suryawanshi, A. P., & Deokar, C. D. (2017). Extracellular enzymes activity determining the virulence of *Rhizoctonia bataticola*, causing root rot in soybean. *Physiological and Molecular Plant Pathology*, *100*, 49-56.

Gene Ontology Consortium. (2004). The Gene Ontology (GO) database and informatics resource. *Nucleic Acids Research*, 32, D258-D261.

Girard, V., Dieryckx, C., Job, C., & Job, D. (2013). Secretomes: the fungal strike force. *Proteomics*, *13*(3-4), 597-608.

Gkarmiri, K., Finlay, R. D., Alström, S., Thomas, E., Cubeta, M. A., & Högberg, N. (2015). Transcriptomic changes in the plant pathogenic fungus *Rhizoctonia solani* AG-3 in response

to the antagonistic bacteria *Serratia proteamaculans* and *Serratia plymuthica*. *BMC Genomics*, *16*(1), 1-17.

Gleason, J. E., Galaleldeen, A., Peterson, R. L., Taylor, A. B., Holloway, S. P., Waninger-Saroni, J., ... & Culotta, V. C. (2014). *Candida albicans* SOD5 represents the prototype of an unprecedented class of Cu-only superoxide dismutases required for pathogen defense. *Proceedings of the National Academy of Sciences*, 111(16), 5866-5871.

Goulet, K. M., Storfie, E. R., & Saville, B. J. (2020). Exploring links between antisense RNAs and pathogenesis in *Ustilago maydis* through transcript and gene characterization. *Fungal Genetics and Biology*, *134*, 103283.

Grabherr, M. G., Haas, B. J., Yassour, M., Levin, J. Z., Thompson, D. A., Amit, I., ... & Regev, A. (2011). Trinity: reconstructing a full-length transcriptome without a genome from RNA-Seq data. *Nature Biotechnology*, *29*(7), 644.

Gregori, R., Guidarelli, M., & Mari, M. (2010). Preliminary studies on partial reduction of *Colletotrichum acutatum* infection by proteinase inhibitors extracted from apple skin. *Physiological and Molecular Plant Pathology*, *74*(5-6), 303-308.

Grillo, R., Tirró, A., Pennisi, A. M., & Agosteo, G. E. (1996). *Armillaria* species in Calabria. *Micol. Ital*, *25*, 92-100.

Gui, Y. J., Chen, J. Y., Zhang, D. D., Li, N. Y., Li, T. G., Zhang, W. Q., ... & Dai, X. F. (2017). *Verticillium dahliae* manipulates plant immunity by glycoside hydrolase 12 proteins in conjunction with carbohydrate‐binding module 1. *Environmental Microbiology*, *19*(5), 1914-1932.

Guillaumin, J. J., Anderson, J. B., & Korhonen, K. (1991). Life cycle, interfertility and biological species. *Mycologia*, 10-20.

Guillaumin, J. J., Lung, B., Romagnesi, H., Marxmuller, H., Lamoure, D., Durrieu, G., ... & Mohammed, C. (1985). Sustématique des Armilaires du groupe Mellea. Conséquenmces phytopathologiques. *European Journal of Forest Pathology*, *15*(5‐6), 268-277.

Guillaumin, J. J., Mohammed, C., Anselmi, N., Courtecuisse, R., Gregory, S. C., Holdenrieder, O., ... & van Dam, B. (1993). Geographical distribution and ecology of the

Armillaria species in western Europe. *European Journal of Forest Pathology*, *23*(6‐7), 321-341.

Harold, E. T. (1934). Studies on *Armillaria mellea* (Vahl) Quel., infection, parasitism, and host resistance. *Journal of Agricultural Research*, *48*, 187.

Hanna J.W. (2005) *Master's Thesis.* University of Idaho; Moscow, ID, USA:. *Armillaria ostoyae*: Genetic Characterization and Distribution in the Western United States

Hastie, T., Tibshirani, R., Friedman, J., Hastie, T., Tibshirani, R., & Friedman, J. (2009). Unsupervised learning. The elements of statistical learning: Data mining. Inference, and Prediction, *Taylor & Francis*, 485-585.

Hauptmann, P., & Lehle, L. (2008). Kex1 protease is involved in yeast cell death induced by defective N-glycosylation, acetic acid, and chronological aging. *Journal of Biological Chemistry*, *283*(27), 19151-19163.

Healy, V., O'Connell, J., McCarthy, T. V., & Doonan, S. (1999). The lysine-specific proteinase from *Armillaria mellea* is a member of a novel class of metalloendopeptidases located in Basidiomycetes. *Biochemical and Biophysical Research Communications*, *262*(1), 60-63.

Hefnawy, M. A., Gharieb, M. M., Shaaban, M. T., & Soliman, A. M. (2017). Optimization of culture condition for enhanced decolorization of direct blue dye by *Aspergillus flavus* and *Penicillium canescens*. *Journal of Applied Pharmaceutical Science*, *7*(2), 083-092.

Heinzelmann, R., Prospero, S., & Rigling, D. (2018). Frequent diploidisation of haploid *Armillaria ostoyae* strains in an outdoor inoculation experiment. *Fungal Biology*, *122*(2-3), 147-155.

Hess, J., Skrede, I., Chaib De Mares, M., Hainaut, M., Henrissat, B., & Pringle, A. (2018). Rapid divergence of genome architectures following the origin of an ectomycorrhizal symbiosis in the genus *Amanita*. *Molecular Biology and Evolution*, *35*(11), 2786-2804.

Horton, P., Park, K. J., Obayashi, T., Fujita, N., Harada, H., Adams-Collier, C. J., & Nakai, K. (2007). WoLF PSORT: protein localization predictor. *Nucleic Acids Research*, *35*, W585-W587.

Howard, R. J., & Ferrari, M. A. (1989). Role of melanin in appressorium function. *Experimental Mycology*, *13*(4), 403-418.

Huang, J., Liu, T., Shang, C., Zhao, Y., Wang, W., Liang, Y., ... & Yao, S. (2018). Identification of lncRNAs by microarray analysis reveals the potential role of lncRNAs in cervical cancer pathogenesis. *Oncology Letters*, *15*(4), 5584-5592.

Jashni, M. K., Dols, I. H., Iida, Y., Boeren, S., Beenen, H. G., Mehrabi, R., ... & de Wit, P. J. (2015). Synergistic action of a metalloprotease and a serine protease from *Fusarium oxysporum* f. sp. *lycopersici* cleaves chitin-binding tomato chitinases, reduces their antifungal activity, and enhances fungal virulence. *Molecular Plant-Microbe Interactions*, *28*(9), 996-1008.

Jashni, M. K., Mehrabi, R., Collemare, J., Mesarich, C. H., & de Wit, P. J. (2015). The battle in the apoplast: further insights into the roles of proteases and their inhibitors in plant–pathogen interactions. *Frontiers in Plant Science*, *6*, 584.

Jombart, T., Balloux, F., & Dray, S. (2010). Adephylo: new tools for investigating the phylogenetic signal in biological traits. *Bioinformatics*, *26*(15), 1907-1909.

Jones, P., Binns, D., Chang, H. Y., Fraser, M., Li, W., McAnulla, C., ... & Hunter, S. (2014). InterProScan 5: genome-scale protein function classification. *Bioinformatics*, *30*(9), 1236-1240.

Joshi, R. K., Megha, S., Basu, U., Rahman, M. H., & Kav, N. N. (2016). Genome wide identification and functional prediction of long non-coding RNAs responsive to *Sclerotinia sclerotiorum* infection in Brassica napus. *PLoS One*, *11*(7), e0158784.

Kalvari, I., Nawrocki, E. P., Ontiveros-Palacios, N., Argasinska, J., Lamkiewicz, K., Marz, M., ... & Petrov, A. I. (2021). Rfam 14: expanded coverage of metagenomic, viral and microRNA families. *Nucleic Acids Research*, *49*(D1), D192-D200.

Kanehisa, M., & Goto, S. (2000). KEGG: kyoto encyclopedia of genes and genomes. *Nucleic Acids Research*, *28*(1), 27-30.

Kang, Y. J., Yang, D. C., Kong, L., Hou, M., Meng, Y. Q., Wei, L., & Gao, G. (2017). CPC2: a fast and accurate coding potential calculator based on sequence intrinsic features. *Nucleic Acids Research*, 45(W1), W12-W16.

Kang, Z., & Buchenauer, H. (2000). Ultrastructural and cytochemical studies on cellulose, xylan and pectin degradation in wheat spikes infected by *Fusarium culmorum*. *Journal of Phytopathology*, *148*(5), 263-275.

Kappel, L., Münsterkötter, M., Sipos, G., Escobar Rodriguez, C., & Gruber, S. (2020). Chitin and chitosan remodeling defines vegetative development and *Trichoderma* biocontrol. *PLoS Pathogens*, *16*(2), e1008320.

Katoh, K., & Standley, D. M. (2013). MAFFT multiple sequence alignment software version 7: improvements in performance and usability. *Molecular Biology and Evolution*, *30*(4), 772-780.

Keča, N., Bodles, W. J. A., Woodward, S., Karadžić, D., & Bojović, S. (2006). Molecular‐based identification and phylogeny of *Armillaria* species from Serbia and Montenegro. *Forest Pathology*, *36*(1), 41-57.

Keča, N., Karadžić, D., & Woodward, S. (2009). Ecology of *Armillaria* species in managed forests and plantations in Serbia. *Forest Pathology*, *39*(4), 217-231.

Kedves, O., Shahab, D., Champramary, S., Chen, L., Indic, B., Bóka, B., ... & Sipos, G. (2021). Epidemiology, biotic interactions and biological bicontrol of Armillarioids in the northern hemisphere. *Pathogens*, *10*(1), 76.

Kile, G. A. (1983). Identification of genotypes and the clonal development of *Armillaria luteobubalina* Watling & Kile in eucalypt forests. *Australian Journal of Botany*, *31*(6), 657-671.

Kim, D., Langmead, B., & Salzberg, S. L. (2015). HISAT: a fast spliced aligner with low memory requirements. *Nature Methods*, *12*(4), 357-360.

King, B. C., Waxman, K. D., Nenni, N. V., Walker, L. P., Bergstrom, G. C., & Gibson, D. M. (2011). Arsenal of plant cell wall degrading enzymes reflects host preference among plant pathogenic fungi. *Biotechnology for Biofuels*, *4*(1), 1-14.

Kini, K., Agnimonhan, R., Dossa, R., Soglonou, B., Gbogbo, V., Ouedraogo, I., ... & Silue, D. (2017). First report of *Sphingomonas* sp. causing bacterial leaf blight of rice in Benin, Burkina Faso, The Gambia, Ivory Coast, Mali, Nigeria, Tanzania and Togo. *New Disease Reports*, *35*, 32-32.

Klopfenstein, N. B., Hanna, J. W., Cannon, P. G., Medel-Ortiz, R., Alvarado-Rosales, D., Lorea-Hernández, F., ... & Kim, M. S. (2014). First report of the Armillaria root-disease pathogen, *Armillaria gallica*, associated with several woody hosts in three states of Mexico. *Plant Disease*, *98*(9), 1280.

Klopfenstein, N. B., Lundquist, J. E., Hanna, J. W., Kim, M. S., & McDonald, G. I. (2009). First report of *Armillaria sinapina*, a cause of Armillaria root disease, associated with a variety of forest tree hosts on sites with diverse climates in Alaska. *Plant Disease*, *93*(1), 111.

Klopfenstein, N. B., Stewart, J. E., Ota, Y., Hanna, J. W., Richardson, B. A., Ross-Davis, A. L., ... & Kim, M. S. (2017). Insights into the phylogeny of Northern Hemisphere *Armillaria*: Neighbor-net and Bayesian analyses of translation elongation factor 1-α gene sequences. *Mycologia*, *109*(1), 75-91.

Kloppholz, S., Kuhn, H., & Requena, N. (2011). A secreted fungal effector of *Glomus intraradices* promotes symbiotic biotrophy. *Current Biology*, *21*(14), 1204-1209.

Koch, R. A., & Herr, J. R. (2021). Global distribution and richness of *Armillaria* and related species inferred from public databases and amplicon sequencing datasets. *Frontiers in Microbiology*, 12, 3395.

Koch, R. A., & Herr, J. R. (2021). Transcriptomics reveals the putative mycoparasitic strategy of the mushroom *Entoloma abortivum* on species of the mushroom genus *Armillaria*. *Msystems*, *6*(5), e00544-21.

Koch, R. A., Wilson, A. W., Séné, O., Henkel, T. W., & Aime, M. C. (2017). Resolved phylogeny and biogeography of the root pathogen *Armillaria* and its gasteroid relative, Guyanagaster. *BMC Evolutionary Biology*, *17*(1), 1-16.

Kopp, F., & Mendell, J. T. (2018). Functional classification and experimental dissection of long noncoding RNAs. *Cell*, *172*(3), 393-407.

Krassowski, M. (2020). ComplexUpset: Create complex UpSet plots using ggplot2 components. *R Package Version* 0.5, 18.

Krause, C., Richter, S., Knöll, C., & Jürgens, G. (2013). Plant secretome—from cellular process to biological activity. *Biochimica et Biophysica Acta (BBA)-Proteins and Proteomics*, *1834*(11), 2429-2441.

Krijger, J. J., Thon, M. R., Deising, H. B., & Wirsel, S. G. (2014). Compositions of fungal secretomes indicate a greater impact of phylogenetic history than lifestyle adaptation. *BMC Genomics*, *15*(1), 1-19.

Krijger, J. J., Thon, M. R., Deising, H. B., & Wirsel, S. G. (2014). Compositions of fungal secretomes indicate a greater impact of phylogenetic history than lifestyle adaptation. *BMC Genomics*, *15*(1), 1-19.

Krishnan, P., Ma, X., McDonald, B. A., & Brunner, P. C. (2018). Widespread signatures of selection for secreted peptidases in a fungal plant pathogen.*BMC Evolutionary Biology*,*18*(1), 1-10.

Kubicek, C. P., Starr, T. L., & Glass, N. L. (2014). Plant cell wall-degrading enzymes and their secretion in plant-pathogenic fungi. *Annual Reviews in Phytopathology*, *52*(1), 427-451.

Kullnig, C., Mach, R. L., Lorito, M., & Kubicek, C. P. (2000). Enzyme diffusion from *Trichoderma atroviride* (= *T. harzianum* P1) to *Rhizoctonia solani* is a prerequisite for triggering of *Trichoderma* ech42 gene expression before mycoparasitic contact. *Applied and Environmental Microbiology*, *66*(5), 2232-2234.

Kulshreshtha, S., Mathur, N., & Bhatnagar, P. (2014). Mushroom as a product and their role in mycoremediation. AMB Express, 4, 29–36.

Kuo, H. C., Détry, N., Choi, J., & Lee, Y. H. (2015). Potential roles of laccases on virulence of *Heterobasidion annosum* ss. *Microbial Pathogenesis*, *81*, 16-21.

Kursa, M. B., & Rudnicki, W. R. (2010). Feature selection with the Boruta package. *Journal of Statistical Software*, *36*, 1-13.

Kyriakou, D., Stavrou, E., Demosthenous, P., Angelidou, G., San Luis, B. J., Boone, C., ... & Kirmizis, A. (2016). Functional characterisation of long intergenic non-coding RNAs through genetic interaction profiling in *Saccharomyces cerevisiae*. *BMC Biology*, *14*(1), 1-16.

Lalande, B., Abdo, Z., Hanna, J. W., Page-Dumroese, D. S., Warwell, M. V., Tirocke, J. M., ... & Stewart, J. E. (2019). Metagenomic approaches to determine soil microbial communities associated with *Armillaria* root disease. *Proceedings of the 65th annual Western International Forest Disease Work Conference; 2-6 October 2017; Parksville, BC, Canada. WIFDWC. p. 123-126*.

Lamoth, F., Juvvadi, P. R., & Steinbach, W. J. (2015). Histone deacetylase inhibition as an alternative strategy against invasive aspergillosis. *Frontiers in Microbiology*, *6*, 96.

Langmead, B., & Salzberg, S. L. (2012). Fast gapped-read alignment with Bowtie 2. *Nature Methods*, *9*(4), 357-359.

Li, B., & Dewey, C. N. (2011). RSEM: accurate transcript quantification from RNA-Seq data with or without a reference genome. *BMC Bioinformatics*, *12*, 1-16.

Li, J., Liu, X., Yin, Z., Hu, Z., & Zhang, K. Q. (2021). An overview on identification and regulatory mechanisms of long non-coding RNAs in fungi. *Frontiers in Microbiology*, *12*, 638617.

Liang, X., Moomaw, E. W., & Rollins, J. A. (2015). Fungal oxalate decarboxylase activity contributes to *Sclerotinia sclerotiorum* early infection by affecting both compound appressoria development and function. *Molecular Plant Pathology*, *16*(8), 825-836.

Lienemann, M., Boer, H., Paananen, A., Cottaz, S., & Koivula, A. (2009). Toward understanding of carbohydrate binding and substrate specificity of a glycosyl hydrolase 18 family (GH-18) chitinase from *Trichoderma harzianum*. *Glycobiology*, *19*(10), 1116-1126.

Lin, R., Qin, F., Shen, B., Shi, Q., Liu, C., Zhang, X., ... & Xie, B. (2018). Genome and secretome analysis of *Pochonia chlamydosporia* provide new insight into egg-parasitic mechanisms. *Scientific Reports*, *8*(1), 1123.

Lin, X., Jackson, J. C., Feretzaki, M., Xue, C., & Heitman, J. (2010). Transcription factors Mat2 and Znf2 operate cellular circuits orchestrating opposite-and same-sex mating in *Cryptococcus neoformans*. *PLoS Genetics*, *6*(5), e1000953.

Liu, N., Wang, P., Li, X., Pei, Y., Sun, Y., Ma, X., ... & Hou, Y. (2022). Long Non-Coding RNAs profiling in pathogenesis of *Verticillium dahliae*: New insights in the host-pathogen interaction. *Plant Science*, *314*, 111098.

Lo Presti, L., Lanver, D., Schweizer, G., Tanaka, S., Liang, L., Tollot, M., ... & Kahmann, R. (2015). Fungal effectors and plant susceptibility. *Annual Review of Plant Biology*, *66*, 513-545.

Lo Presti, L., Lanver, D., Schweizer, G., Tanaka, S., Liang, L., Tollot, M., ... & Kahmann, R. (2015). Fungal effectors and plant susceptibility. *Annual Review of Plant Biology*, *66*, 513-545.

Lushaj, B. M., Woodward, S., Keča, N., & Intini, M. (2010). Distribution, ecology and host range of *Armillaria* species in Albania. *Forest Pathology*, 40(6), 485-499.

Lyu, X., Shen, C., Fu, Y., Xie, J., Jiang, D., Li, G., & Cheng, J. (2015). Comparative genomic and transcriptional analyses of the carbohydrate-active enzymes and secretomes of phytopathogenic fungi reveal their significant roles during infection and development. *Scientific Reports*, *5*(1), 1-16.

M'Barek, S. B., Cordewener, J. H., Ghaffary, S. M. T., van der Lee, T. A., Liu, Z., Gohari, A. M., ... & Kema, G. H. (2015). FPLC and liquid-chromatography mass spectrometry identify candidate necrosis-inducing proteins from culture filtrates of the fungal wheat pathogen *Zymoseptoria tritici*. *Fungal Genetics and Biology*, *79*, 54-62.

Maere, S., Heymans, K., & Kuiper, M. (2005). BiNGO: a Cytoscape plugin to assess overrepresentation of gene ontology categories in biological networks. *Bioinformatics*, *21*(16), 3448-3449.

Mallett, K. I., & Colotelo, N. (1984). Rhizomorph exudate of *Armillaria mellea*. *Canadian Journal of Microbiology*, *30*(10), 1247-1252.

Marcelino, V. R., Clausen, P. T., Buchmann, J. P., Wille, M., Iredell, J. R., Meyer, W., ... & Holmes, E. C. (2020). CCMetagen: comprehensive and accurate identification of eukaryotes and prokaryotes in metagenomic data. *Genome Biology*, 21(1), 1-15.

Martens, J. A., Wu, P. Y. J., & Winston, F. (2005). Regulation of an intergenic transcript controls adjacent gene transcription in *Saccharomyces cerevisiae*. *Genes & Development*, *19*(22), 2695-2704.

Martin, F., Kohler, A., Murat, C., Veneault-Fourrey, C., & Hibbett, D. S. (2016). Unearthing the roots of ectomycorrhizal symbioses. *Nature Reviews Microbiology*, *14*(12), 760-773.

Martins, T. M., Hartmann, D. O., Planchon, S., Martins, I., Renaut, J., & Pereira, C. S. (2015). The old 3-oxoadipate pathway revisited: new insights in the catabolism of aromatics in the saprophytic fungus *Aspergillus nidulans*. *Fungal Genetics and Biology*, *74*, 32-44.

Mary Wanjiru, W., Zhensheng, K., & Buchenauer, H. (2002). Importance of cell wall degrading enzymes produced by *Fusarium graminearum* during infection of wheat heads. *European Journal of Plant Pathology*, *108*(8), 803-810.

Mercado-Blanco, J., Abrantes, I., Barra Caracciolo, A., Bevivino, A., Ciancio, A., Grenni, P., ... & Proença, D. N. (2018). Belowground microbiota and the health of tree crops. *Frontiers in Microbiology*, *9*, 1006.

Merico, D., Isserlin, R., Stueker, O., Emili, A., & Bader, G. D. (2010). Enrichment map: a network-based method for gene-set enrichment visualization and interpretation. *PloS One*, *5*(11), e13984.

Moffat, C. S., See, P. T., & Oliver, R. P. (2014). Generation of a *ToxA* knockout strain of the wheat tan spot pathogen *Pyrenophora tritici‐repentis*. *Molecular Plant Pathology*, *15*(9), 918-926.

Moreno-Forero, S. K., & Van Der Meer, J. R. (2015). Genome-wide analysis of *Sphingomonas wittichii* RW1 behaviour during inoculation and growth in contaminated sand. *The ISME Journal*, *9*(1), 150-165.

Morrison, D. J., & Pellow, K. W. (2002). Variation in virulence among isolates of *Armillaria ostoyae*. *Forest Pathology*, 32(2), 99-107.

Morrison, D. J., Chu, D., & Johnson, A. L. S. (1985). Species of *Armillaria* in British Columbia. *Canadian Journal of Plant Pathology*, *7*(3), 242-246.

Morrison, E. N., Donaldson, M. E., & Saville, B. J. (2012). Identification and analysis of genes expressed in the *Ustilago maydis* dikaryon: uncovering a novel class of pathogenesis genes. *Canadian Journal of Plant Pathology*, 34(3), 417-435.

Movahedi, S., & Heale, J. B. (1990). Purification and characterization of an aspartic proteinase secreted by *Botrytis cinerea* Pers ex. Pers in culture and in infected carrots. *Physiological and Molecular Plant Pathology*, *36*(4), 289-302.

Mueller, A. N., Ziemann, S., Treitschke, S., Aßmann, D., & Doehlemann, G. (2013). Compatibility in the *Ustilago maydis*–maize interaction requires inhibition of host cysteine proteases by the fungal effector Pit2. *PLoS Pathogens*, *9*(2), e1003177.

Mulholland, V., MacAskill, G. A., Laue, B. E., Steele, H., Kenyon, D., & Green, S. (2012). Development and verification of a diagnostic assay based on EF‐1 α for the identification of *Armillaria* species in Northern Europe. *Forest Pathology*, *42*(3), 229-238.

Myszczynska, M. A., Ojamies, P. N., Lacoste, A., Neil, D., Saffari, A., Mead, R., ... & Ferraiuolo, L. (2020). Applications of machine learning to diagnosis and treatment of neurodegenerative diseases. *Nature Reviews Neurology*, *16*(8), 440-456.

Nadal-Ribelles, M., Solé, C., Xu, Z., Steinmetz, L. M., de Nadal, E., & Posas, F. (2014). Control of Cdc28 CDK1 by a stress-induced lncRNA. *Molecular Cell*, 53(4), 549-561.

O'Connell, R. J., Thon, M. R., Hacquard, S., Amyotte, S. G., Kleemann, J., Torres, M. F., ... & Vaillancourt, L. J. (2012). Lifestyle transitions in plant pathogenic *Colletotrichum* fungi deciphered by genome and transcriptome analyses. *Nature Genetics*, *44*(9), 1060-1065.

Oehme, D. P., Shafee, T., Downton, M. T., Bacic, A., & Doblin, M. S. (2019). Differences in protein structural regions that impact functional specificity in GT2 family β-glucan synthases. *PLoS One*, *14*(10), e0224442.

Ökmen, B., Bachmann, D., & De Wit, P. J. (2019). A conserved GH17 glycosyl hydrolase from plant pathogenic Dothideomycetes releases a DAMP causing cell death in tomato. *Molecular Plant Pathology*, *20*(12), 1710-1721.

Omdal, D. W., Shaw III, C. G., Jacobi, W. R., & Wager, T. C. (1995). Variation of pathogenicity and virulence of isolates of *Armillaria ostoyae* on eight tree species. *Plant Disease*, *79*(9), 939-944.

Onsando, J. M., & Waudo, S. W. (1994). Interaction between *Trichoderma* species and *Armillaria* root rot fungus of tea in Kenya. *International Journal of Pest Management*, *40*(1), 69-74.

Pal, N., & Christodoulatos, C. (1995). Fungal degradation of 2, 4-dinitrotoluene and nitroglycerin in batch and fixed-film bioreactors. *Journal of Energetic Materials*, *13*(3-4), 259-282.

PAN, L. J., Lin, L. U., LIU, Y. P., WEN, S. X., & ZHANG, Z. Y. (2020). The M43 domain-containing metalloprotease RcMEP1 in *Rhizoctonia cerealis* is a pathogenicity factor during the fungus infection to wheat. *Journal of Integrative Agriculture*, *19*(8), 2044-2055.

Park, H. J., Wang, W., Curlango-Rivera, G., Xiong, Z., Lin, Z., Huskey, D. A., ... & Turgeon, B. G. (2019). A DNase from a fungal phytopathogen is a virulence factor likely deployed as counter defense against host-secreted extracellular DNA. *MBio*, *10*(2), e02805-18.

Park, K. H., Oh, S. Y., Park, M. S., Kim, M. S., Klopfenstein, N. B., Kim, N. K., ... & Lim, Y. W. (2018). Re‐evaluation of *Armillaria* and *Desarmillaria* in South Korea based on ITS/*tef1* sequences and morphological characteristics. *Forest Pathology*, *48*(6), e12447.

Patro, R., Duggal, G., Love, M. I., Irizarry, R. A., & Kingsford, C. (2017). Salmon provides fast and bias-aware quantification of transcript expression. *Nature Methods*, 14(4), 417-419.

Pellegrin, C., Morin, E., Martin, F. M., & Veneault-Fourrey, C. (2015). Comparative analysis of secretomes from ectomycorrhizal fungi with an emphasis on small-secreted proteins. *Frontiers in Microbiology*, *6*, 1278.

Pellegrini, A., Prodorutti, D., & Pertot, I. (2014). Use of bark mulch pre-inoculated with *Trichoderma atroviride* to control *Armillaria* root rot. *Crop Protection*, *64*, 104-109.

Pennington, H. G., Jones, R., Kwon, S., Bonciani, G., Thieron, H., Chandler, T., ... & Spanu, P. D. (2019). The fungal ribonuclease-like effector protein CSEP0064/BEC1054 represses

plant immunity and interferes with degradation of host ribosomal RNA. *PLoS Pathogens*, *15*(3), e1007620.

Perazzolli, Michele, *et al.,* "*Armillaria mellea* induces a set of defense genes in grapevine roots and one of them codifies a protein with antifungal activity." *Molecular Plant-Microbe Interactions* 23.4 (2010): 485-496.

Percival, G. C., Smiley, E. T., & Fox, R. T. (2011). Root collar excavation with *Trichoderma* inoculations as a potential management strategy for honey fungus (*Armillaria mellea*). *Arboricultural Journal*, *33*(4), 267-280.

Pérez-Nadales, E., & Di Pietro, A. (2011). The membrane mucin Msb2 regulates invasive growth and plant infection in *Fusarium oxysporum*. *The Plant Cell*, *23*(3), 1171-1185.

Pertea, G., & Pertea, M. (2020). GFF utilities: GffRead and GffCompare. *F1000Research*, 9.

Pertea, M., Pertea, G. M., Antonescu, C. M., Chang, T. C., Mendell, J. T., & Salzberg, S. L. (2015). StringTie enables improved reconstruction of a transcriptome from RNA-seq reads. *Nature Biotechnology*, *33*(3), 290-295.

Plett, J. M., Kemppainen, M., Kale, S. D., Kohler, A., Legué, V., Brun, A., ... & Martin, F. (2011). A secreted effector protein of *Laccaria bicolor* is required for symbiosis development. *Current Biology*, *21*(14), 1197-1203.

Presti, L. L., & Kahmann, R. (2017). How filamentous plant pathogen effectors are translocated to host cells. *Current Opinion in Plant Biology*, *38*, 19-24.

Price, M. N., Dehal, P. S., & Arkin, A. P. (2010). FastTree 2–approximately maximum-likelihood trees for large alignments. *PloS One*, *5*(3), e9490.

Prospero, S., Holdenrieder, O., & Rigling, D. (2004). Comparison of the virulence of *Armillaria cepistipes* and *Armillaria ostoyae* on four Norway spruce provenances. *Forest Pathology*, *34*(1), 1-14.

Przemieniecki, S. W., Damszel, M., Ciesielski, S., Kubiak, K., Mastalerz, J., Sierota, Z., & Gorczyca, A. (2021). Bacterial microbiome in *Armillaria ostoyae* rhizomorphs inhabiting the root zone during progressively dying Scots pine. *Applied Soil Ecology*, *164*, 103929.

Purahong, W., Tanunchai, B., Muszynski, S., Maurer, F., Wahdan, S. F. M., Malter, J., ... & Noll, M. (2022). Cross-kingdom interactions and functional patterns of active microbiota matter in governing deadwood decay. *Proceedings of the Royal Society B*, *289*(1974), 20220130.

Rabouille, C. (2017). Pathways of unconventional protein secretion. *Trends in Cell Biology*, *27*(3), 230-240.

Rawlings, N. D., Barrett, A. J., & Bateman, A. (2010). MEROPS: the peptidase database. *Nucleic Acids Research*, *38*, D227-D233.

Rawlings, N. D., Barrett, A. J., Thomas, P. D., Huang, X., Bateman, A., & Finn, R. D. (2018). The MEROPS database of proteolytic enzymes, their substrates and inhibitors in 2017 and a comparison with peptidases in the PANTHER database. *Nucleic Acids Research*, 46(D1), D624-D632.

Redfern, D. B. (1973). Growth and behaviour of *Armillaria mellea* rhizomorphs in soil. *Transactions of the British Mycological Society*, *61*(3), 569-IN16.

Redman, R. S., & Rodriguez, R. J. (2002). Characterization and isolation of an extracellular serine protease from the tomato pathogen *Colletotrichum coccodes*, and it's role in pathogenicity. *Mycological Research*, *106*(12), 1427-1434.

Rigling, D., Günthardt-Goerg, M. S., Blauenstein, H., & Frey, B. (2006). Accumulation of heavy metals into *Armillaria* rhizomorphs from contaminated soils. *Forest Snow and Landscape Research*, *80*(2), 213-220.

Rigling, D., Lawrenz, P., Blauenstein, H., & Heiniger, U. (2003). An experimental study of the effects of ozone on tree–*Armillaria* interactions. In *Root and Butt Rots of Forest Trees. Proceedings of the IUFRO Working Party*, 7, 16-22.

Robinson D, Storey JD, Bass wcfAJ (2023). subSeq: Subsampling of high-throughput sequencing count data. doi:10.18129/B9.bioc.subSeq, R package version 1.32.0, https://bioconductor.org/packages/subSeq.

Robinson, D. G., Ding, Y., & Jiang, L. (2016). Unconventional protein secretion in plants: a critical assessment. *Protoplasma*, *253*(1), 31-43.

Robinson, M. D., McCarthy, D. J., & Smyth, G. K. (2010). edgeR: a Bioconductor package for differential expression analysis of digital gene expression data. *Bioinformatics*, *26*(1), 139-140.

Roll‐Hansen, F. (1985). The *Armillaria* species in Europe: a literature review. *European Journal of Forest Pathology*, *15*(1), 22-31.

Ruocco, M., Lanzuise, S., Lombardi, N., Woo, S. L., Vinale, F., Marra, R., ... & Lorito, M. (2015). Multiple roles and effects of a novel *Trichoderma* hydrophobin. *Molecular Plant-Microbe Interactions*, *28*(2), 167-179.

Sagt, C. M., ten Haaft, P. J., Minneboo, I. M., Hartog, M. P., Damveld, R. A., Metske van der Laan, J., ... & de Winde, J. H. (2009). Peroxicretion: a novel secretion pathway in the eukaryotic cell. *BMC Biotechnology*, *9*(1), 1-11.

Sahu, N., Indic, B., Wong-Bajracharya, J., Merényi, Z., Ke, H. M., Ahrendt, S., ... & Nagy, L. G. (2023). Vertical and horizontal gene transfer shaped plant colonization and biomass degradation in the fungal genus *Armillaria*. *Nature Microbiology*, 8(9), 1668-1681.

Sahu, N., Merényi, Z., Bálint, B., Kiss, B., Sipos, G., Owens, R. A., & Nagy, L. G. (2021). Hallmarks of Basidiomycete soft-and white-rot in wood-decay-Omics data of two *Armillaria* species. *Microorganisms*, *9*(1), 149.

Saitoh, H., Fujisawa, S., Ito, A., Mitsuoka, C., Berberich, T., Tosa, Y., ... & Terauchi, R. (2009). SPM1 encoding a vacuole-localized protease is required for infection-related autophagy of the rice blast fungus *Magnaporthe oryzae*. *FEMS Microbiology Letters*, *300*(1), 115-121.

Sariaslani, F. S., & Dalton, H. (1989). Microbial enzymes for oxidation of organic molecules. *Critical Reviews in Biotechnology*, *9*(3), 171-257.

Savazzini, F., Longa, C. M. O., & Pertot, I. (2009). Impact of the biocontrol agent *Trichoderma atroviride* SC1 on soil microbial communities of a vineyard in northern Italy. *Soil Biology and Biochemistry*, *41*(7), 1457-1465.

Schaefer, K., Wagener, J., Ames, R. M., Christou, S., MacCallum, D. M., Bates, S., & Gow, N. A. (2020). Three related enzymes in *Candida albicans* achieve arginine-and

agmatine-dependent metabolism that is essential for growth and fungal virulence. *Mbio*, *11*(4), e01845-20.

Schlömann, M., Ngai, K. L., Ornston, L. N., & Knackmuss, H. J. (1993). Dienelactone hydrolase from *Pseudomonas cepacia*. *Journal of Bacteriology*, *175*(10), 2994-3001.

Seibert, V., Stadler-Fritzsche, K., & Schlömann, M. (1993). Purification and characterization of maleylacetate reductase from *Alcaligenes eutrophus* JMP134 (pJP4). *Journal of Bacteriology*, *175*(21), 6745-6754.

Semana, P., & Powlowski, J. (2019). Four aromatic intradiol ring cleavage dioxygenases from *Aspergillus niger*. *Applied and Environmental Microbiology*, 85(23), e01786-19.

Senthilkumar, S., Perumalsamy, M., and Janardhana Prabhu, H. (2014). Decolourization potential of white-rot fungus *Phanerochaete chrysosporium* on synthetic dye bath effluent containing amido black 10B. *Journal of Saudi Chemical Society,* 18 (6), 845–853.

Sesma, A., & Osbourn, A. E. (2004). The rice leaf blast pathogen undergoes developmental processes typical of root-infecting fungi. *Nature*, *431*(7008), 582-586.

Shannon, P., Markiel, A., Ozier, O., Baliga, N. S., Wang, J. T., Ramage, D., ... & Ideker, T. (2003). Cytoscape: a software environment for integrated models of biomolecular interaction networks. *Genome Research*, *13*(11), 2498-2504.

Sipos, G., Prasanna, A. N., Walter, M. C., O'Connor, E., Bálint, B., Krizsán, K., ... & Nagy, L. G. (2017). Genome expansion and lineage-specific genetic innovations in the forest pathogenic fungi *Armillaria*. *Nature Ecology & Evolution*, *1*(12), 1931-1941.

Soanes, D. M., Alam, I., Cornell, M., Wong, H. M., Hedeler, C., Paton, N. W., ... & Talbot, N. J. (2008). Comparative genome analysis of filamentous fungi reveals gene family expansions associated with fungal pathogenesis. *PLoS One*, *3*(6), e2300.

Solla, A., Tomlinson, F., & Woodward, S. (2002). Penetration of *Picea sitchensis* root bark by *Armillaria mellea*, *Armillaria ostoyae* and *Heterobasidion annosum*. *Forest Pathology*, *32*(1), 55-70.

Somai-Jemmali, L., Randoux, B., Siah, A., Magnin-Robert, M., Halama, P., Reignault, P., & Hamada, W. (2017). Similar infection process and induced defense patterns during

compatible interactions between *Zymoseptoria tritici* and both bread and durum wheat species. *European Journal of Plant Pathology*, *147*(4), 787-801.

Song, C., Zhu, F., Carrión, V. J., & Cordovez, V. (2020). Beyond plant microbiome composition: Exploiting microbial functions and plant traits via integrated approaches. *Frontiers in Bioengineering and Biotechnology*, *8*, 896.

Souza, C. D. A., Li, S., Lin, A. Z., Boutrot, F., Grossmann, G., Zipfel, C., & Somerville, S. C. (2017). Cellulose-derived oligomers act as damage-associated molecular patterns and trigger defense-like responses. *Plant Physiology*, 173(4), 2383-2398.

Stevens, R., Reyes, G., & Kanavillil, N. (2020). Examining the impact of winter and spring soil temperatures on the growth of *Hypholoma fasciculare*, a potential biocontrol agent against *Armillaria ostoyae*, in pine plantations. *Frontiers in Forests and Global Change*, *3*, 598527.

Storozhenko, D. S. V., & Krutov, V. I. (2004). Fungal communities in forest ecosystems. Materials of Coordination Investigations,2, 40-51

Szabó, M., Urbán, P., Virányi, F., Kredics, L., & Fekete, C. (2013). Comparative gene expression profiles of *Trichoderma harzianum* proteases during in vitro nematode egg-parasitism. *Biological Control*, *67*(3), 337-343.

Tereshina, V. M. (2005). Thermotolerance in fungi: the role of heat shock proteins and trehalose. *Microbiology*, 74, 247-257.

Thomidis, T., & Exadaktylou, E. (2012). Effectiveness of cyproconazole to control Armillaria root rot of apple, walnut and kiwifruit. *Crop Protection*, *36*, 49-51.

Till, P., Mach, R. L., & Mach-Aigner, A. R. (2018). A current view on long noncoding RNAs in yeast and filamentous fungi. *Applied Microbiology and Biotechnology*, 102, 7319-7331.

Tong, X., & Liu, S. (2019). CPPred: coding potential prediction based on the global description of RNA sequence. *Nucleic Acids Research*, *47*(8), e43-e43.

Tsykun, T., Rigling, D., Nikolaychuk, V., & Prospero, S. (2012). Diversity and ecology of *Armillaria* species in virgin forests in the Ukrainian Carpathians. *Mycological Progress*, *11*(2), 403-414.

Tucker, A. R., Salazar, N. A., Ayoola, A. O., Memili, E., Thomas, B. N., & Morenikeji, O. B. (2021). Regulatory network of miRNA, lncRNA, transcription factor and target immune response genes in bovine mastitis. *Scientific Reports*, *11*(1), 1-18.

Urban, M., Cuzick, A., Seager, J., Wood, V., Rutherford, K., Venkatesh, S. Y., ... & Hammond-Kosack, K. E. (2020). PHI-base: the pathogen–host interactions database. *Nucleic Acids Research*, *48*, D613-D620.

Varden, F. A., De la Concepcion, J. C., Maidment, J. H., & Banfield, M. J. (2017). Taking the stage: effectors in the spotlight. *Current Opinion in Plant Biology*, *38*, 25-33.

Viterbo, A., Harel, M., & Chet, I. (2004). Isolation of two aspartyl proteases from *Trichoderma asperellum* expressed during colonization of cucumber roots. *FEMS Microbiology Letters*, *238*(1), 151-158.

Volk, T. J., Burdsall Jr, H. H., & Banik, M. T. (1996). *Armillaria nabsnona*, a new species from western North America. *Mycologia*, *88*(3), 484-491.

Wang, F., Wei, Y., Yan, T., Wang, C., Chao, Y., Jia, M., ... & Sheng, H. (2022). *Sphingomonas* sp. Hbc-6 alters physiological metabolism and recruits beneficial rhizosphere bacteria to improve plant growth and drought tolerance. *Frontiers in Plant Science*, *13*.

Wang, Y., Ye, W., & Wang, Y. (2018). Genome‐wide identification of long non‐coding RNAs suggests a potential association with effector gene transcription in *Phytophthora sojae*. *Molecular Plant Pathology*, *19*(9), 2177-2186.

Wang, Z., Jiang, Y., Wu, H., Xie, X., & Huang, B. (2019). Genome-wide identification and functional prediction of long non-coding RNAs involved in the heat stress response in *Metarhizium robertsii*. *Frontiers in Microbiology*, *10*, 2336.

Wang, Z., Zhu, T., Ma, W., Wang, N., Qu, G., Zhang, S., & Wang, J. (2018). Genome-wide analysis of long non-coding RNAs in *Catalpa bungei* and their potential function in floral transition using high-throughput sequencing. *BMC Genetics*, *19*(1), 1-16.

Wargo, P. M., & Kile, G. A. (1992). *Armillaria* root disease. *Plant Diseases of International Importance*, *4*, 311-345.

Warwell, M. V., McDonald, G. I., Hanna, J. W., Kim, M. S., Lalande, B. M., Stewart, J. E., ... & Klopfenstein, N. B. (2019). *Armillaria altimontana* is associated with healthy western white pine (*Pinus monticola*): Potential in situ biological control of the *Armillaria* root disease pathogen, *A. solidipes*. *Forests*, *10*(4), 294.

Wenzel, A., Akbaşli, E., & Gorodkin, J. (2012). RIsearch: fast RNA–RNA interaction search using a simplified nearest-neighbor energy model. *Bioinformatics*, *28*(21), 2738-2746.

Wilhelm, R. C., Singh, R., Eltis, L. D., & Mohn, W. W. (2019). Bacterial contributions to delignification and lignocellulose degradation in forest soils with metagenomic and quantitative stable isotope probing. *The ISME Journal*, 13(2), 413-429.

Wolf, T., Shelest, V., Nath, N., & Shelest, E. (2016). CASSIS and SMIPS: promoter-based prediction of secondary metabolite gene clusters in eukaryotic genomes. *Bioinformatics*, *32*(8), 1138-1143.

Wrzosek, M., Ruszkiewicz-Michalska, M., Sikora, K., Damszel, M., & Sierota, Z. (2017). The plasticity of fungal interactions. *Mycological Progress*, *16*(2), 101-108.

Wucher, V., Legeai, F., Hédan, B., Rizk, G., Lagoutte, L., Leeb, T., ... & Derrien, T. (2017). FEELnc: a tool for long non-coding RNA annotation and its application to the dog transcriptome. *Nucleic Acids Research*, *45*(8), e57-e57.

Xiao, F., Xu, W., Hong, N., Wang, L., Zhang, Y., & Wang, G. (2022). A secreted lignin peroxidase required for fungal growth and virulence and related to plant immune response. *International Journal of Molecular Sciences*, *23*(11), 6066.

Xu, J., Bai, J., Zhang, X., Lv, Y., Gong, Y., Liu, L., ... & Li, X. (2017). A comprehensive overview of lncRNA annotation resources. *Briefings in Bioinformatics*, *18*(2), 236-249.

Xu, Y. H., Brandl, H., Osterwalder, S., Elzinga, E. J., & Huang, J. H. (2019). Vanadium-basidiomycete fungi interaction and its impact on vanadium biogeochemistry. *Environment International*, *130*, 104891.

Yafetto, L., Davis, D. J., & Money, N. P. (2009). Biomechanics of invasive growth by *Armillaria* rhizomorphs. *Fungal Genetics and Biology*, *46*(9), 688-694.

Yang, C., Liang, Y., Qiu, D., Zeng, H., Yuan, J., & Yang, X. (2018). Lignin metabolism involves *Botrytis cinerea* BcGs1-induced defense response in tomato. *BMC Plant biology*, *18*(1), 1-15.

Yildirim, N., Erguven, G. O., & Adar, E. (2018). The chemical and biochemical oxygen demand reduction by *Armillaria tabescens* in malathion supplemented culture medium. *Glob Nest J*, *20*, 529-533.

Yin, Y., Mao, X., Yang, J., Chen, X., Mao, F., & Xu, Y. (2012). dbCAN: a web resource for automated carbohydrate-active enzyme annotation. *Nucleic Acids Research*, 40(W1), W445-W451.

Yu, G., Wang, L. G., Han, Y., & He, Q. Y. (2012). clusterProfiler: an R package for comparing biological themes among gene clusters. *Omics: A Journal of Integrative Biology*, *16*(5), 284-287.

Yun, H. S., Sul, W. J., Chung, H. S., Lee, J. H., & Kwon, C. (2023). Secretory membrane traffic in plant–microbe interactions. *New Phytologist*, 237(1), 53-59.

Zahran, H. H. (1999). Rhizobium-legume symbiosis and nitrogen fixation under severe conditions and in an arid climate. *Microbiology and Molecular Biology Reviews*, *63*(4), 968-989.

Zhang, H., Yohe, T., Huang, L., Entwistle, S., Wu, P., Yang, Z., ... & Yin, Y. (2018). dbCAN2: a meta server for automated carbohydrate-active enzyme annotation. *Nucleic Acids Research*, *46*(W1), W95-W101.

Zhang, J., Bruton, B. D., & Biles, C. L. (2014). Cell wall-degrading enzymes of *Didymella bryoniae* in relation to fungal growth and virulence in cantaloupe fruit. *European Journal of Plant Pathology*, *139*(4), 749-761.

Zhang, X., Huang, H., Wu, B., Xie, J., Viljoen, A., Wang, W., ... & Li, C. (2021). The M35 metalloprotease effector FocM35_1 is required for full virulence of *Fusarium oxysporum* f. sp. cubense tropical race 4. *Pathogens*, *10*(6), 670.

Zhang, Y., Wu, L., Wang, X., Chen, B., Zhao, J., Cui, J., ... & Ma, Z. (2019). The cotton laccase gene GhLAC15 enhances *Verticillium* wilt resistance via an increase in

defence‐induced lignification and lignin components in the cell walls of plants. *Molecular Plant Pathology*, *20*(3), 309-322.

Zhang, Y., Zhang, Y., Qiu, D., Zeng, H., Guo, L., & Yang, X. (2015). BcGs1, a glycoprotein from *Botrytis cinerea*, elicits defence response and improves disease resistance in host plants. *Biochemical and Biophysical Research Communications*, *457*(4), 627-634.

Zhao, Z., Liu, H., Wang, C., & Xu, J. R. (2014). Erratum to: comparative analysis of fungal genomes reveals different plant cell wall degrading capacity in fungi. *BMC Genomics*, *15*(1), 1-15.

LIST OF PUBLICATIONS

MTMT Author ID: 10072893

Mandatory peer-reviewed publications for the fulfilment of the doctoral process:

1. **Champramary, S***., Indic, B., Szűcs, A., Languar, O., Hasan, F. K., Szekeres, A., ... & Sipos, G. The mycoremediation potential of the Armillarioids: a comparative genomics analysis. Frontiers in Bioengineering and Biotechnology, 11, 1189640. (IF 2023 : 6.1)

2. Chen, L*., **Champramary, S***., Sahu, N., Indic, B., Szűcs, A., Nagy, G., ... & Sipos, G. (2023). Dual RNA-Seq profiling unveils mycoparasitic activities of Trichoderma atroviride against haploid Armillaria ostoyae in antagonistic interaction assays. Microbiology Spectrum, e04626-22. (IF 2023: 9.0)

Other Publications:

Sahu, N., Indic, B., Wong-Bajracharya, J., Merényi, Z., Ke, H. M., Ahrendt,….., **Champramary S**.,….. & Nagy, L. G. (2023). Vertical and horizontal gene transfer shaped plant colonization and biomass degradation in the fungal genus Armillaria. Nature Microbiology, 1-14. (IF 2023 : 31.0)

Bhattacharya, A., **Champramary, S**., Tripathi, T., Thakur, D., Ioshikhes, I., Singh, S. K., & Nandi, S. (2021). Identification of the conserved long non-coding RNAs in myogenesis. BMC genomics, 22(1), 336. (IF 2021: 4.6)

Kedves, O., Shahab, D., **Champramary, S**., Chen, L., Indic, B., Bóka, B., ... & Sipos, G. (2021). Epidemiology, Biotic Interactions and Biological Control of Armillarioids in the Northern Hemisphere. Pathogens, 10(1), 76. (IF 2021: 3.5)

Chen, L., Bóka, B., Kedves, O., Nagy, V. D., Szűcs, A., **Champramary, S**., ... & Kredics, L. (2019). Towards the biological control of devastating forest pathogens from the genus Armillaria. Forests, 10(11), 1013. (IF 2019: 2.2)

Conference paper:

Simang, Champramary ; Boris, Indic ; László, Kredics ; György, Sipos. A comparison of the wood decay abilities of common white-rot fungi from the Carpathian Basin. 10TH HARDWOOD CONFERENCE PROCEEDINGS: University of Sopron Press (2022) 323 p. pp. 188-193.

Liqiong, Chen ; Danish, Shahab ; Orsolya, Kedves ; **Simang, Champramary**; Boris, Indic ; Viktor, Dávid Nagy ; Csaba, Vágvölgyi ; László, Kredics ; György, Sipos. Armillarioid root rot invasion: possibilities of silvicultural and chemical control. Hardwood Conference Proceedings 9TH HARDWOOD PROCEEDINGS: PART II pp. 90-97. , 8 p. (2021)

Conference abstracts:

Boris, Indic ; **Simang, Champramary** ; Liqiong, Chen ; Huynh, Thu ; Orsolya, Kedves ; Ferenc, Lakatos ; Csaba, Vágvölgyi ; László, Kredics ; György, Sipos. Phylogenetic analysis shows contrasting genetic diversity among various Armillarioid species in Pannonian forests. 10TH HARDWOOD CONFERENCE PROCEEDINGS: University of Sopron Press (2022) 323 p. p. 203

Chen L ; **Champramary S**; Sahu N; Indic B ; Csaba, Vágvölgyi ; László, Kredics ; György, Sipos et al., In vitro transcriptome level interactions between mycoparasitic Trichoderma atroviride and haploid Armillaria ostoyae uncovered by dual RNA-Seq profiling: (2022) 54 p. p. 12 , 1 p.

Bencsik-Bóka, B ; Sahu, N ; Huynh, T ; Kedves, O ; Merényi, Z ; Kovács, G ; Chen, L ; **Champramary, S** ; Patocskai, Z ; Münsterkötter, M et al., Classical and 'omics' approaches towards the biological control of devastating forest pathogens from the genus Armillaria. Hungarian Society for Microbiology (2018) 70 p. p. 6

Champramary, S, Münsterkötter M, György, S. Rhizomorph formation in Armillaria ostoyae: the contribution of rhizomorph-specific genes (2019), Zürich Mycology Symposium 2019, 2019.01.18.,

Indjic, B ; **Champramary, S** ; Münsterkötter, M ; Kredics, L ; Sipos, G. The Genome Of The Pathogenic White Rot Fungus Armillaria Ostoyae Encodes A Distinctive Genetic Potential To Degrade Aromatic Compounds. HASAT INTERNATIONAL AGRICULTURE AND FOREST CONGRESS:Adnan Menderes University (2019) p. 267 , 1 p.

Other publication not related to thesis:

Hasan, K. F., **Champramary, S**., Al Hasan, K. N., Indic, B., Ahmed, T., Pervez, M. N., ... & Bejó, L. (2023). Eco-friendly production of cellulosic fibers from Scots pine wood and sustainable nanosilver modification: A path toward sustainability. Results in Engineering, 101244. (IF 2023: 5.1)

Cumulative impact factor (IF) of the publications directly related to the thesis: 61.5

SUPPLEMENTARY MATERIALS

Supplementary material 1. List of organisms used for biodegradation prospect comparisons

Organism	ShortName	Number of Proteins	Phylum	JGI Collection Name
Trichoderma citrinoviride	Trici4	9737	Ascomycota	*Trichoderma citrinoviride* TUCIM 6016 v4.0
Aspergillus flavus	Aspfl2_3	13715	Ascomycota	*Aspergillus flavus* NRRL3357
Aspergillus glaucus	Aspgl1	11277	Ascomycota	*Aspergillus glaucus* v1.0
Botryosphaeria dothidea	Botdo1_1	14998	Ascomycota	*Botryosphaeria dothidea*
Cladosporium sphaerospermum	Clasph1	8807	Ascomycota	*Cladosporium sphaerospermum* UM 843
Cochliobolus lunatus	Coclu2	12131	Ascomycota	*Cochliobolus lunatus* m118 v2.0
Dentipellis sp. (KUC8613)	Densp1	14320	Ascomycota	*Dentipellis* sp. KUC8613
Fusarium oxysporum	FoxFo5176	19130	Ascomycota	*Fusarium oxysporum* Fo5176
Geotrichum candidum	Galgeo1	6826	Ascomycota	*Galactomyces geotrichum* Phaff 72-186
Penicillium arizonense	Penar1	12253	Ascomycota	*Penicillium arizonense* CBS 141311
Penicillium chrysogenum	PenchWisc1_1	13671	Ascomycota	*Penicillium chrysogenum* Wisconsin 54-1255
Purpureocillium lilacinum	Purli1	11763	Ascomycota	*Purpureocillium lilacinum* PLFJ-1
Trichoderma harzianum	Trihar1	13932	Ascomycota	*Trichoderma harzianum* TR274 v1.0
Armillaria borealis	Armbor1	19984	Basidiomycota	*Armillaria borealis*
Armillaria cepistipes	Armcep1	23460	Basidiomycota	*Armillaria cepistipes* B5
Desrmillaria ectypa	Armect1	12228	Basidiomycota	*Armillaria ectypa* FPL83.16 v1.0
Armillaria gallica	Armga1	25704	Basidiomycota	*Armillaria gallica* 21-2 v1.0
Armillaria luteobubalina	Armlut1	20318	Basidiomycota	*Armillaria luteobubalina* HWK02 v1.0
Armillaria mellea	Armmel1	15646	Basidiomycota	*Armillaria mellea*
Armillaria solidipes	Armost1	20811	Basidiomycota	*Armillaria solidipes* 28-4 v1.0
Armillaria ostoyae	Armosto1	22705	Basidiomycota	*Armillaria ostoyae C18/9*
Desarmillaria tabescens	Armtab1	19032	Basidiomycota	*Armillaria tabescens* CCBAS 213 v1.0
Guyanagaster necrorhizus	Guyne1	14276	Basidiomycota	*Guyanagaster necrorhizus* MCA 3950 v1.0
Heterobasidion annosum	Hetan2	13405	Basidiomycota	*Heterobasidion annosum* v2.0
Polyporus squamosus	Polsqu1	15283	Basidiomycota	*Polyporus squamosus* CCBS 676 v1.0
Schizophyllum commune	Schco3	16319	Basidiomycota	*Schizophyllum commune* H4-8 v3.0
Bjerkandera adusta	Bjead1_1	15473	Basidiomycota	*Bjerkandera adusta* v1.0
Irpex lacteus	Irplac1	15319	Basidiomycota	*Irpex lacteus* CCBAS Fr. 238 617/93 v1.0

Lentinula edodes	Lenedo1	14079	Basidiomycota	*Lentinula edodes* Le(Bin) 0899 ss11 v1.0
Marasmius fiardii	Marfi1	17098	Basidiomycota	*Marasmius fiardii* PR-910 v1.0
Phanerochaete chrysosporium	Phchr2	13602	Basidiomycota	*Phanerochaete chrysosporium RP-78 v2.2*
Phlebia radiata	Phlrad1	14629	Basidiomycota	*Phlebia radiata* Fr. (isolate 79, FBCC0043)
Pleurotus eryngii	Pleery1	15960	Basidiomycota	*Pleurotus eryngii* ATCC 90797 v1.0
Pleurotus ostreatus	PleosPC9_1	12206	Basidiomycota	*Pleurotus ostreatus* PC9 v1.0
Trametes betulina	Trabet1	13239	Basidiomycota	*Trametes betulina* CIRM-BRFM 1801 v1.0
Trametes versicolor	Trave1	14296	Basidiomycota	*Trametes versicolor* v1.0
Mucor lusitanicus	Muccir1_3	11843	Mucoromycota	*Mucor lusitanicus (circinelloides)* MU402 v1.0

Supplementary material 2. Orthologs based phylogenetic tree

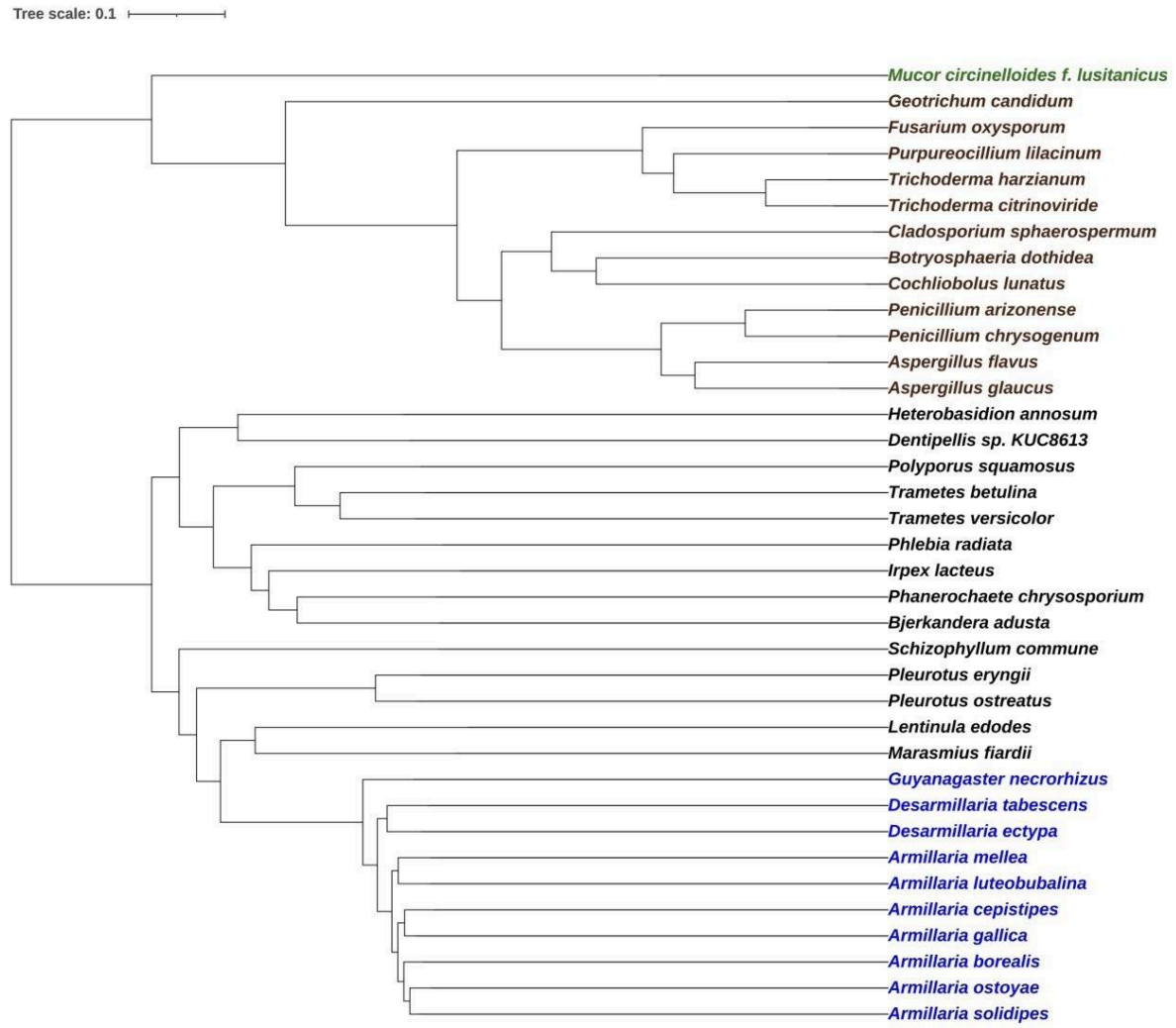

Orthologs-based phylogenetic tree

Supplementary material 3. List of fungal species used for comparative secretomics and machine learning.

Scientific Name	jgi_name	short_name	Phylum
Chaetomium thermophilum	*Chaetoium thermophilum var thermophilum* DSM 1495	Chathe1	*Ascomycota*
Coniochaeta (Lecythophora) sp.	*Coniochaeta* sp. 2T2.1 v1.0	Conioc1	*Ascomycota*
Thielavia terrestris	*Thielavia terrestris* v2.0	Thite2	*Ascomycota*
Trichoderma reesei	*Trichoderma reesei* QM6a	Trire_Chr	*Ascomycota*
Rhizopus delemar	*Rhizopus delemar* 99-880 from Broad	Rhior3	*Mucoromycota*
Aspergillus wentii	*Aspergillus wentii* v1.0	Aspwe1	*Ascomycota*
Penicillium chrysogenum	*Penicillium chrysogenum* Wisconsin 54-1255	PenchWisc1_1	*Ascomycota*
Daldinia eschscholtzii	*Daldinia eschscholtzii* EC12 v1.0	DalEC12_1	*Ascomycota*
Hypoxylon sp.	*Hypoxylon* sp. EC38 v3.0	HypEC38_3	*Ascomycota*
Neurospora crassa	*Neurospora crassa* OR74A v2.0	Neucr2	*Ascomycota*
Botryosphaeria dothidea	*Botryosphaeria dothidea*	Botdo1_1	*Ascomycota*
Fusarium oxysporum	*Fusarium oxysporum f. sp. lycopersici* MN25 (FoMN25) NRRL 54003	Fusoxlyc1	*Ascomycota*
Mucor circinelloides	*Mucor circinelloides* CBS277.49 v2.0	Mucci2	*Mucoromycota*
Paecilomyces variotii	*Paecilomyces variotii* CBS 101075 v1.0	Paevar1	*Ascomycota*
Aspergillus niger	*Aspergillus niger* ATCC 1015 v4.0	Aspni7	*Ascomycota*
Coniophora olivacea	*Coniophora olivacea* MUCL 20566 v1.0	Conol1	*Basidiomycota*
Daedalea quercina	*Daedalea quercina* v1.0	Daequ1	*Basidiomycota*
Fomitopsis pinicola	*Fomitopsis pinicola* FP-58527 SS1 v3.0	Fompi3	*Basidiomycota*
Laetiporus sulphureus	*Laetiporus sulphureus var. sulphureus* v1.0	Laesu1	*Basidiomycota*
Wolfiporia cocos	*Wolfiporia cocos* MD-104 SS10 v1.0	Wolco1	*Basidiomycota*
Fomitopsis betulina	*Fomitopsis betulina* CIRM-BRFM 1772 v1.1	Pipbet1_1	*Basidiomycota*
Sparassis latifolia	*Sparassis latifolia* CCMJ1100 v1.0	Spalat1	*Basidiomycota*
Postia stiptica	*Postia stiptica* OMC1664 v1.0	Possti1	*Basidiomycota*
Gloeophyllum trabeum	*Gloeophyllum trabeum* v1.0	Glotr1_1	*Basidiomycota*
Neolentinus lepideus	*Neolentinus lepideus* v1.0	Neole1	*Basidiomycota*
Fibroporia radiculosa	*Fibroporia radiculosa* TFFH 294	Fibra1	*Basidiomycota*
Dacryopinax primogenitus	*Dacryopinax primogenitus* DJM 731 SSP1 v1.0	Dacsp1	*Basidiomycota*
Serpula lacrymans	*Serpula lacrymans* S7.9 v2.0	SerlaS7_9_2	*Basidiomycota*
Calocera cornea	*Calocera cornea* v1.0	Calco1	*Basidiomycota*
Fistulina hepatica	*Fistulina hepatica* v1.0	Fishe1	*Basidiomycota*
Armillaria ostoyae	*Armillaria* ostoyae C18/9	Armosto1	*Basidiomycota*
Armillaria borealis	*Armillaria* borealis FPL87.14 v1.0	Armbor1	*Basidiomycota*
Armillaria mellea	*Armillaria* mellea ELDO17 v1.0	Armmel1	*Basidiomycota*
Armillaria tabescens	*Armillaria* tabescens CCBAS 213 v1.0	Armtab1	*Basidiomycota*
Armillaria luteobubalina	*Armillaria* luteobubalina HWK02 v1.0	Armlut1	*Basidiomycota*
Armillaria ectypa	*Armillaria* ectypa FPL83.16 v1.0	Armect1	*Basidiomycota*
Armillaria nabsnona	*Armillaria* nabsnona CMW6904 v1.0	Armnab1	*Basidiomycota*
Armillaria cepistipes	*Armillaria* cepistipes B5	Armcep1	*Basidiomycota*
Armillaria solidipes	*Armillaria* solidipes 28-4 v1.0	Armost1	*Basidiomycota*
Armillaria gallica	*Armillaria gallica* 21-2 v1.0	Armga1	*Basidiomycota*
Armillaria mellea (Fractionated)	*Armillaria* mellea DSM 3731	Armme1_1	*Basidiomycota*
Guyanagaster necrorhiza	*Guyanagaster necrorhiza* MCA 3950 v1.0	Guyne1	*Basidiomycota*

Oudemansiella mucida	*Oudemansiella mucida* CBS 558.79 v1.0	Oudmuc1	*Basidiomycota*
Amylostereum chailletii	*Amylostereum chailletii* DWAch2 v1.0	Amycha1	*Basidiomycota*
Cylindrobasidium torrendii	*Cylindrobasidium torrendii* FP15055 v1.0	Cylto1	*Basidiomycota*
Fomitiporia mediterranea	*Fomitiporia mediterranea* v1.0	Fomme1	*Basidiomycota*
Dichomitus squalens	*Dichomitus squalens* CBS464.89 v1.0	Dicsqu464_1	*Basidiomycota*
Earliella scabrosa	*Earliella scabrosa* CIRM-BRFM 1817 v1.0	Earsca1	*Basidiomycota*
Heterobasidion annosum	*Heterobasidion annosum* v2.0	Hetan2	*Basidiomycota*
Peniophora sp.	*Peniophora sp.* CONTA v1.0	Lopni1	*Basidiomycota*
Meripilus sumstinei	*Meripilus sumstinei* FP 105329 v1.0	Mersum1	*Basidiomycota*
Rhizina undulata	*Rhizina undulata* CBS 300.56 v1.0	Rhiund1	*Ascomycota*
Kretzschmaria deusta	*Kretzschmaria deusta* IL1129 v1.0	Kredeu1	*Ascomycota*
Bjerkandera adusta	*Bjerkandera adusta* v1.0	Bjead1_1	*Basidiomycota*
Climacocystis borealis	*Climacocystis borealis* CliBor001 v1.0	Clibor1	*Basidiomycota*
Moniliophthora perniciosa	*Moniliophthora perniciosa* FA553	Monpe1_1	*Basidiomycota*
Phanerochaete chrysosporium	*Phanerochaete chrysosporium* RP-78 v2.2	Phchr2	*Basidiomycota*
***Ganoderma* sp.**	*Ganoderma sp.* 10597 SS1 v1.0	Gansp1	*Basidiomycota*
Fomes fomentarius	*Fomes fomentarius* CIRM-BRFM 1821 v1.0	Fomfom1	*Basidiomycota*

Supplementary material 4. Rarefaction Curve Analysis of Microbiome Diversity. Reads in X-axis and Species in Y-axis.

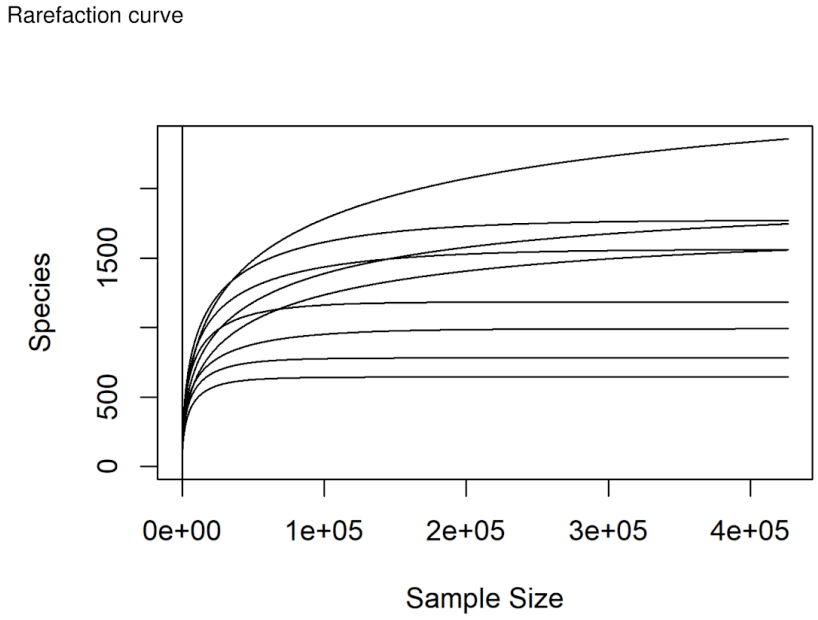

Supplementary material 5. Differentially expressed SSPs in *A. ostoyae* during *in vitro* interaction with *T. atroviride*

IPR_Description	Cysteine Percentage	ProtID	0th Hour	53rd Hour	62nd Hour	Upreg_in
Alpha/Beta hydrolase fold|Fungal lipase-like domain	2.00	ARMOST_17207	4.43	2.63	2.92	0th Hour
Alpha/Beta hydrolase fold|Peptidase S10, serine carboxypeptidase	2.22	ARMOST_15388	3.03	2.22	1.72	0th Hour
Cell wall mannoprotein 1	0.00	ARMOST_00746	5.13	2.95	4.14	0th Hour
Cerato-platanin|RlpA-like domain superfamily	2.94	ARMOST_11001	6.29	4.28	2.18	0th Hour
DUF1524	2.36	ARMOST_16736	6.04	3.21	3.10	0th Hour
Extracellular membrane protein, CFEM domain	4.94	ARMOST_16536	5.53	3.06	2.39	0th Hour
Extracellular membrane protein, CFEM domain	3.59	ARMOST_01639	7.47	5.74	5.73	0th Hour
Glycoside hydrolase, family 11/12	0.39	ARMOST_08301	3.89	2.80	2.81	0th Hour
Glycoside hydrolase, family 61	0.87	ARMOST_01648	1.25	0.74	0.14	0th Hour
Hydrophobin	7.55	ARMOST_09996	6.23	2.27	1.65	0th Hour
Hydrophobin	7.41	ARMOST_02721	2.23	0.91	0.93	0th Hour
Hydrophobin	7.27	ARMOST_17970	2.54	0.94	0.87	0th Hour
Hydrophobin	7.14	ARMOST_04909	4.16	1.49	0.86	0th Hour
Hydrophobin	7.14	ARMOST_00270	7.45	1.39	0.22	0th Hour
Hydrophobin	7.08	ARMOST_15834	4.73	1.99	1.46	0th Hour
Hydrophobin	7.08	ARMOST_22336	7.30	1.49	0.09	0th Hour
Hydrophobin	7.02	ARMOST_17951	8.55	5.98	6.23	0th Hour
Hydrophobin	6.84	ARMOST_17948	7.30	5.27	5.15	0th Hour
Hydrophobin	6.72	ARMOST_00265	0.87	0.13	0.00	0th Hour
Hydrophobin	6.72	ARMOST_00242	6.26	3.15	2.17	0th Hour
Hydrophobin	6.72	ARMOST_12464	4.81	1.20	0.55	0th Hour
Hydrophobin	6.72	ARMOST_00281	8.21	3.05	0.97	0th Hour
Hydrophobin	6.72	ARMOST_00279	7.69	1.49	0.22	0th Hour
Hydrophobin	5.03	ARMOST_17954	5.91	4.50	4.90	0th Hour
Hydrophobin	3.60	ARMOST_11483	7.54	4.16	3.13	0th Hour
Hydrophobin	7.14	ARMOST_17997	11.59	10.24	9.04	0th Hour
Hydrophobin	7.14	ARMOST_17965	8.94	6.21	4.25	0th Hour
Hydrophobin	6.96	ARMOST_17956	9.89	6.99	4.24	0th Hour
Hydrophobin	6.90	ARMOST_11435	2.84	1.41	1.38	0th Hour
Hydrophobin	6.90	ARMOST_17958	5.70	2.54	0.35	0th Hour
Hydrophobin	5.71	ARMOST_17946	3.08	1.51	1.22	0th Hour
Kre9/Knh1 family	0.00	ARMOST_00062	7.21	5.53	5.84	0th Hour
Kre9/Knh1 family	0.00	ARMOST_18327	6.12	4.38	4.50	0th Hour
Kre9/Knh1 family	0.00	ARMOST_06493	7.96	4.84	4.26	0th Hour
Kre9/Knh1 family	0.41	ARMOST_13703	3.12	1.95	2.39	0th Hour
Kre9/Knh1 family	0.00	ARMOST_10946	5.10	4.24	4.12	0th Hour
LysM domain	3.49	ARMOST_12714	8.29	7.09	7.66	0th Hour
Peptidase M43	1.75	ARMOST_05523	8.68	5.58	5.36	0th Hour
Multicopper oxidase, type 3|Cupredoxin	0.62	ARMOST_22340	0.73	0.53	0.06	0th Hour
Pectate lyase PlyH	3.07	ARMOST_10011	2.93	2.45	2.10	0th Hour
Peptidase M43	1.73	ARMOST_11008	5.23	2.00	2.08	0th Hour

Ribonuclease/ribotoxin|Guanine-specific ribonuclease N1/T1/U2	3.05	ARMOST_13800	5.76	2.20	1.39	0th Hour
RlpA-like domain superfamily	3.10	ARMOST_05275	2.33	2.06	1.50	0th Hour
RlpA-like domain superfamily	3.55	ARMOST_08316	6.67	3.29	1.23	0th Hour
SGNH hydrolase superfamily	0.00	ARMOST_17433	2.41	1.06	1.56	0th Hour
SGNH hydrolase superfamily	1.17	ARMOST_13145	1.70	0.67	0.76	0th Hour
SGNH hydrolase superfamily	1.17	ARMOST_13144	5.02	1.59	1.92	0th Hour
START-like domain superfamily	0.49	ARMOST_14191	4.75	0.50	0.55	0th Hour
Superoxide dismutase-like, copper/zinc binding domain superfamily	1.12	ARMOST_18198	1.27	0.83	0.40	0th Hour
Survival protein SurE-like phosphatase	3.07	ARMOST_11826	2.99	2.68	2.15	0th Hour
	11.25	ARMOST_06331	0.71	0.05	0.15	0th Hour
	7.21	ARMOST_18002	6.22	3.21	1.43	0th Hour
	5.79	ARMOST_17962	4.03	0.47	0.00	0th Hour
	5.62	ARMOST_06329	6.31	4.80	5.32	0th Hour
	5.62	ARMOST_16093	5.30	3.00	1.88	0th Hour
	4.55	ARMOST_05497	5.84	3.04	3.06	0th Hour
	1.12	ARMOST_00167	2.24	1.47	0.86	0th Hour
	0.40	ARMOST_01789	8.05	6.44	5.82	0th Hour
	0.00	ARMOST_15979	4.87	3.60	2.49	0th Hour
	0.00	ARMOST_08808	8.46	6.80	7.35	0th Hour
	0.00	ARMOST_10828	2.92	1.55	1.57	0th Hour
	0.00	ARMOST_01431	3.17	1.64	2.08	0th Hour
	0.00	ARMOST_10399	6.28	3.32	3.59	0th Hour
	0.00	ARMOST_18451	8.87	5.51	3.73	0th Hour
	0.53	ARMOST_16962	5.62	4.56	4.71	0th Hour
	0.51	ARMOST_00524	3.62	1.37	2.39	0th Hour
	7.09	ARMOST_01386	0.93	0.70	0.20	0th Hour
	7.06	ARMOST_13609	3.35	2.03	1.01	0th Hour
	4.76	ARMOST_01736	3.55	2.23	1.53	0th Hour
	4.55	ARMOST_18027	1.73	1.23	0.90	0th Hour
	3.70	ARMOST_18600	1.33	1.01	0.52	0th Hour
	3.61	ARMOST_01486	1.73	2.00	1.09	0th Hour
	3.16	ARMOST_12045	9.43	9.20	7.85	0th Hour
	2.89	ARMOST_02739	1.89	1.78	1.23	0th Hour
	2.58	ARMOST_13434	10.16	8.55	4.56	0th Hour
	1.45	ARMOST_01923	3.92	3.66	2.92	0th Hour
	1.30	ARMOST_00441	8.68	7.76	6.55	0th Hour
	0.84	ARMOST_16259	6.37	5.45	3.48	0th Hour
	0.00	ARMOST_19545	9.09	8.22	7.36	0th Hour
LysM domain	4.35	ARMOST_10657	0.36	1.23	0.26	53rd Hour
RlpA-like domain superfamily	3.05	ARMOST_04534	1.09	3.23	2.56	53rd Hour
CAP domain, Cysteine-rich secretory protein-related	3.93	ARMOST_06352	0.70	7.83	7.63	53rd & 62nd Hour
CAP domain, Cysteine-rich secretory protein-related	1.93	ARMOST_08362	5.50	10.81	11.09	53rd & 62nd Hour
Cupredoxin	2.04	ARMOST_02562	2.15	5.32	5.36	53rd & 62nd Hour

Cupredoxin|DUF11	2.11	ARMOST_02583	1.73	3.64	3.52	53rd & 62nd Hour
FAD linked oxidase	1.74	ARMOST_16637	2.56	7.64	7.49	53rd & 62nd Hour
Glycoside hydrolase family 11/12	1.52	ARMOST_12600	4.04	6.25	6.03	53rd & 62nd Hour
Glycoside hydrolase superfamily	1.86	ARMOST_17020	7.53	10.42	9.77	53rd & 62nd Hour
Kre9/Knh1 family	0.00	ARMOST_07477	6.53	9.14	10.94	53rd & 62nd Hour
LysM domain	5.19	ARMOST_19347	0.00	2.08	1.77	53rd & 62nd Hour
LysM domain	5.19	ARMOST_15376	1.58	8.71	8.41	53rd & 62nd Hour
Osmotin/thaumatin-like superfamily	5.00	ARMOST_21555	2.06	3.52	4.24	53rd & 62nd Hour
Osmotin/thaumatin-like superfamily	4.28	ARMOST_11376	3.99	7.67	7.19	53rd & 62nd Hour
Pectate lyase PlyH	4.10	ARMOST_08479	2.86	5.02	6.09	53rd & 62nd Hour
Pectate lyase PlyH	3.33	ARMOST_08488	1.91	3.00	4.51	53rd & 62nd Hour
Pectate lyase PlyH	3.03	ARMOST_08483	1.21	4.01	6.45	53rd & 62nd Hour
DUF3455	2.16	ARMOST_01790	1.82	5.34	7.86	53rd & 62nd Hour
Ricin B, lectin	3.43	ARMOST_20051	4.28	8.54	10.16	53rd & 62nd Hour
RlpA-like domain superfamily	1.86	ARMOST_11949	1.88	6.73	6.95	53rd & 62nd Hour
RlpA-like domain superfamily	3.45	ARMOST_21105	0.04	1.55	0.58	53rd & 62nd Hour
Superoxide dismutase-like, copper/zinc binding domain superfamily	1.13	ARMOST_18251	2.61	3.73	4.77	53rd & 62nd Hour
	8.62	ARMOST_03990	0.08	4.43	3.24	53rd & 62nd Hour
	7.46	ARMOST_04025	0.39	4.57	2.67	53rd & 62nd Hour
	7.41	ARMOST_17491	0.35	5.03	3.02	53rd & 62nd Hour
	6.45	ARMOST_16748	0.12	1.28	1.04	53rd & 62nd Hour
	5.74	ARMOST_08158	0.75	9.24	9.50	53rd & 62nd Hour
	5.51	ARMOST_11587	6.63	8.16	8.92	53rd & 62nd Hour
	5.48	ARMOST_00100	7.60	8.96	9.10	53rd & 62nd Hour
	4.97	ARMOST_01715	2.59	7.30	7.76	53rd & 62nd Hour
	4.69	ARMOST_04001	0.07	2.72	1.25	53rd & 62nd Hour
	2.80	ARMOST_10523	0.38	1.58	2.51	53rd & 62nd Hour
	2.31	ARMOST_10529	0.69	2.98	3.06	53rd & 62nd Hour

	2.20	ARMOST_11172	7.22	8.35	8.70	53rd & 62nd Hour
	1.86	ARMOST_09271	0.31	2.08	1.27	53rd & 62nd Hour
	1.83	ARMOST_20679	2.23	3.10	3.83	53rd & 62nd Hour
	1.29	ARMOST_15005	5.68	7.66	8.97	53rd & 62nd Hour
	1.27	ARMOST_08350	6.65	9.02	8.88	53rd & 62nd Hour
	1.24	ARMOST_18408	1.49	3.00	2.60	53rd & 62nd Hour
	1.20	ARMOST_07358	0.96	2.76	3.39	53rd & 62nd Hour
	1.16	ARMOST_18417	2.10	3.29	3.40	53rd & 62nd Hour
	0.60	ARMOST_17031	4.64	10.00	11.15	53rd & 62nd Hour
	0.58	ARMOST_12428	5.48	10.00	10.98	53rd & 62nd Hour
	0.53	ARMOST_14068	0.42	2.27	3.07	53rd & 62nd Hour
	0.00	ARMOST_06445	5.51	11.98	13.02	53rd & 62nd Hour
	0.00	ARMOST_01492	3.31	8.30	9.95	53rd & 62nd Hour
	0.00	ARMOST_08863	7.81	9.93	11.29	53rd & 62nd Hour
	0.00	ARMOST_20570	1.53	2.85	4.62	53rd & 62nd Hour
Cell wall mannoprotein 1	3.95	ARMOST_19537	0.04	0.12	0.57	62nd Hour
Cellulose-binding domain, fungal	2.47	ARMOST_13810	2.87	3.74	3.90	62nd Hour
Cerato-platanin|RlpA-like domain superfamily	2.92	ARMOST_00895	2.01	4.09	6.54	62nd Hour
Glycoside hydrolase family 16	1.08	ARMOST_14905	2.49	5.11	4.97	62nd Hour
Glycoside hydrolase family 1	0.00	ARMOST_12473	0.71	1.65	1.38	62nd Hour
Glycoside hydrolase, family 61	0.90	ARMOST_18350	0.98	1.65	1.85	62nd Hour
Kre9/Knh1 family	0.00	ARMOST_07459	0.04	0.23	0.80	62nd Hour
NodB homology domain	1.23	ARMOST_13355	0.54	0.84	1.58	62nd Hour
Pectate lyase PlyH	3.03	ARMOST_22631	1.40	2.27	3.59	62nd Hour
RlpA-like domain superfamily	5.26	ARMOST_07341	0.89	1.51	2.18	62nd Hour
RlpA-like domain superfamily	1.80	ARMOST_09015	7.75	8.41	9.07	62nd Hour
Glycoside hydrolase superfamily	1.49	ARMOST_19254	2.06	2.03	3.15	62nd Hour
	5.98	ARMOST_02965	0.25	0.59	0.99	62nd Hour
	4.17	ARMOST_10029	6.91	7.88	9.02	62nd Hour
	4.15	ARMOST_10030	3.49	4.19	5.87	62nd Hour
	4.08	ARMOST_16746	0.00	0.48	0.31	62nd Hour
	3.70	ARMOST_21556	0.00	0.00	0.35	62nd Hour
	3.31	ARMOST_19961	0.08	0.22	1.00	62nd Hour
	2.79	ARMOST_19529	0.95	1.20	2.19	62nd Hour
	2.29	ARMOST_01760	1.33	1.58	2.20	62nd Hour
	2.11	ARMOST_07177	0.11	0.25	0.58	62nd Hour
	2.05	ARMOST_03405	2.62	6.87	7.24	62nd Hour
	1.82	ARMOST_12445	1.83	2.11	4.58	62nd Hour

	1.67	ARMOST_19197	0.74	1.41	3.06	62nd Hour
	1.33	ARMOST_11281	2.51	2.15	4.75	62nd Hour
	0.99	ARMOST_15587	6.29	7.00	7.98	62nd Hour
	0.61	ARMOST_11810	0.07	0.51	0.92	62nd Hour
	0.60	ARMOST_17028	2.34	5.88	7.50	62nd Hour
	0.51	ARMOST_08864	4.80	5.34	8.10	62nd Hour
	0.37	ARMOST_13279	3.14	3.77	5.58	62nd Hour
	0.00	ARMOST_19567	6.43	7.19	9.38	62nd Hour
	0.00	ARMOST_17604	0.77	0.72	2.19	62nd Hour

Supplementary material 6. Differentially expressed SSPs in *T. atroviride* in *in-vitro* interaction assay with *A. ostoyae*

IPR_Description	Cysteine Percentage	GeneID	0th Hour	53rd Hour	62nd Hour	Upreg_in
Alginate lyase 2	2.07	XM_014090223.1	4.74	4.40	3.56	0th Hour
Blastomyces yeast-phase-specific protein	2.60	XM_014085515.1	8.12	7.64	4.97	0th Hour
Cell wall mannoprotein 1	0.00	XM_014092475.1	4.32	4.16	1.67	0th Hour
Cellulose-binding domain, fungal, RlpA-like protein	6.48	XM_014093435.1	5.98	5.51	2.88	0th Hour
Cerato-platanin	2.90	XM_014082295.1	11.89	11.60	9.92	0th Hour
Cerato-ulmin hydrophobin family	8.16	XM_014085643.1	14.87	14.94	13.49	0th Hour
Cutinase/acetylxylan esterase	2.43	XM_014084747.1	5.98	5.24	1.70	0th Hour
Cutinase/acetylxylan esterase	4.73	XM_014084305.1	2.62	2.14	0.00	0th Hour
Cyanovirin-N	4.38	XM_014087217.1	2.78	2.67	0.00	0th Hour
Cysteine-rich secretory protein-related,CAP domain	2.74	XM_014089336.1	2.51	2.58	0.74	0th Hour
Extracellular membrane protein, CFEM domain	8.99	XM_014082836.1	9.47	9.55	6.11	0th Hour
Fungal chitosanase	4.33	XM_014093431.1	2.87	2.54	1.26	0th Hour
Kre9/Knh1 family	0.92	XM_014090798.1	6.35	6.70	4.18	0th Hour
Peptidase S51	0.00	XM_014092032.1	2.63	2.45	0.00	0th Hour
Phytocyanin domain	1.74	XM_014087932.1	3.72	4.01	1.29	0th Hour
DUF1349	0.43	XM_014083997.1	6.10	6.43	4.28	0th Hour
Ribonuclease T2-like, Ribonuclease T2-like	3.82	XM_014085210.1	3.08	3.15	1.61	0th Hour
glycosyl hydrolase catalytic domain	0.69	XM_014085194.1	2.70	1.92	0.00	0th Hour
	1.68	XM_014082335.1	3.46	1.69	0.00	0th Hour
	11.11	XM_014085288.1	7.75	5.42	1.92	0th Hour
	3.28	XM_014092705.1	3.04	1.88	0.00	0th Hour
	6.10	XM_014084402.1	7.71	7.58	5.77	0th Hour
	1.72	XM_014085863.1	3.67	3.62	1.93	0th Hour
	3.52	XM_014092910.1	5.85	5.98	4.23	0th Hour
	0.00	XM_014082486.1	6.92	7.22	4.59	0th Hour

	3.21	XM_014084415.1	5.88	5.00	4.83	0th Hour
	1.11	XM_014085324.1	2.41	1.75	0.00	0th Hour
	2.22	XM_014084278.1	7.99	7.73	6.94	0th Hour
	0.00	XM_014093236.1	7.22	7.09	5.32	0th Hour
	2.85	XM_014086304.1	3.37	3.12	0.00	0th Hour
	0.00	XM_014092092.1	5.15	4.07	1.67	0th Hour
	1.42	XM_014084522.1	7.81	8.01	4.88	0th Hour
	6.06	XM_014082483.1	9.14	9.11	7.72	0th Hour
	4.17	XM_014087751.1	7.47	8.04	4.83	0th Hour
	2.12	XM_014088892.1	5.93	5.93	4.57	0th Hour
	0.53	XM_014089177.1	6.56	6.81	4.73	0th Hour
	4.88	XM_014087391.1	3.66	3.78	0.76	0th Hour
	4.03	XM_014093093.1	2.05	1.73	0.00	0th Hour
	4.38	XM_014091433.1	3.45	3.08	1.31	0th Hour
	1.50	XM_014091234.1	7.70	7.52	5.77	0th Hour
	4.76	XM_014086173.1	11.95	10.91	9.07	0th Hour
	4.88	XM_014083455.1	8.93	8.24	7.47	0th Hour
	7.08	XM_014082462.1	2.50	2.26	0.00	0th Hour
	1.04	XM_014088199.1	8.96	8.68	6.82	0th Hour
	10.23	XM_014091132.1	12.38	11.32	7.32	0th Hour
	9.30	XM_014086172.1	12.97	12.06	8.61	0th Hour
	6.15	XM_014089404.1	8.16	8.34	6.68	0th Hour
	3.70	XM_014087113.1	3.93	3.61	0.74	0th Hour
	5.95	XM_014084778.1	1.61	0.72	0.83	0th Hour
Cell wall mannoprotein 1	0.80	XM_014087166.1	0.10	1.13	1.69	53rd & 62rd Hour
Cerato-platanin	2.76	XM_014088753.1	0.79	2.81	2.15	53rd & 62rd Hour
Cerato-ulmin hydrophobin family	8.00	XM_014084796.1	1.72	6.15	5.65	53rd & 62rd Hour
DUF1524	1.92	XM_014086354.1	0.95	3.10	3.17	53rd & 62rd Hour
	0.00	XM_014093592.1	0.76	3.57	3.41	53rd & 62rd Hour
	0.00	XM_014086595.1	0.71	3.62	3.00	53rd & 62rd Hour
	0.00	XM_014088329.1	5.03	7.50	6.76	53rd & 62rd Hour
Cerato-ulmin hydrophobin family	4.95	XM_014082751.1	4.95	7.27	4.26	53rd Hour
Cerato-ulmin hydrophobin family	8.49	XM_014088786.1	7.89	11.01	7.83	53rd Hour
Cerato-ulmin hydrophobin family	8.99	XM_014085757.1	9.71	12.60	10.23	53rd Hour
Cerato-ulmin hydrophobin family	9.30	XM_014082790.1	2.42	5.26	2.61	53rd Hour
Chloroperoxidase	0.38	XM_014092300.1	4.44	6.18	2.71	53rd Hour
Extracellular membrane protein, CFEM domain	9.64	XM_014083277.1	0.56	1.42	0.00	53rd Hour
	2.89	XM_014083267.1	3.08	6.09	2.41	53rd Hour
	3.33	XM_014091308.1	1.81	3.60	1.60	53rd Hour
	6.93	XM_014090385.1	0.86	3.93	1.60	53rd Hour
	2.93	XM_014085007.1	1.82	4.12	3.05	53rd Hour
	1.59	XM_014087171.1	3.23	4.22	1.97	53rd Hour
	12.08	XM_014092164.1	0.08	1.84	0.00	53rd Hour

	2.78	XM_014093461.1	0.17	1.23	0.00	53rd Hour
	1.65	XM_014083321.1	3.49	4.58	2.13	53rd Hour
Alternaria alternata allergen 1	3.03	XM_014091848.1	9.28	8.43	10.40	62rd Hour
Cerato-ulmin hydrophobin family	8.25	XM_014092471.1	0.76	0.12	3.19	62rd Hour
Extracellular membrane protein, CFEM domain	5.33	XM_014092222.1	10.28	10.33	11.57	62rd Hour
FAS1 domain-containing protein Mug57-like	0.46	XM_014082454.1	4.99	5.08	6.58	62rd Hour
Guanine-specific ribonuclease N1/T1/U2	3.05	XM_014085555.1	4.69	4.78	6.06	62rd Hour
Peptidase G1	0.75	XM_014091441.1	4.93	5.72	7.87	62rd Hour
Peptidase G1	2.73	XM_014088298.1	4.65	4.15	7.26	62rd Hour
Peptidase G1	1.65	XM_014093585.1	7.65	8.65	10.15	62rd Hour
Serine proteases, trypsin domain	2.35	XM_014090664.1	7.17	8.18	10.04	62rd Hour
	3.17	XM_014082072.1	0.54	0.40	1.97	62rd Hour
	0.00	XM_014093501.1	0.21	0.62	1.64	62rd Hour
	4.48	XM_014084029.1	0.60	1.04	2.15	62rd Hour
	3.50	XM_014091910.1	9.69	9.14	11.85	62rd Hour
	0.00	XM_014093780.1	0.28	0.14	1.36	62rd Hour
	1.75	XM_014086103.1	6.17	6.09	7.86	62rd Hour
	1.85	XM_014090948.1	4.93	4.86	7.14	62rd Hour
	0.97	XM_014092252.1	2.88	2.91	4.00	62rd Hour
	4.10	XM_014090766.1	10.05	10.23	12.31	62rd Hour
	2.72	XM_014082849.1	6.74	6.34	8.85	62rd Hour
	0.00	XM_014088729.1	9.13	8.22	10.93	62rd Hour
	4.52	XM_014091960.1	1.13	2.08	2.98	62rd Hour
	4.60	XM_014089490.1	1.21	1.03	3.23	62rd Hour
	1.20	XM_014090317.1	6.81	7.11	8.26	62rd Hour
	4.93	XM_014091521.1	1.28	1.56	5.59	62rd Hour
	0.78	XM_014082815.1	0.30	0.43	2.73	62rd Hour
	13.48	XM_014092520.1	0.35	0.18	1.61	62rd Hour
	7.14	XM_014090662.1	4.38	3.88	6.13	62rd Hour
	1.51	XM_014089100.1	3.94	2.51	6.70	62rd Hour
	6.12	XM_014088294.1	0.17	2.62	4.13	62rd Hour

Supplementary material 7. Differentially expressed CAZymes in *A. ostoyae* against *T. atroviride* in *in-vitro* interaction assay.

CAZYme	FCWDE	GeneID	0th Hour	53rd Hour	62nd Hour	Upreg_in
GH16	fcwde	ARMOST_07466	3.23	6.04	4.12	53rd Hour
GH128	fcwde	ARMOST_17020	7.53	10.42	9.77	53rd & 62nd Hour
GH16	fcwde	ARMOST_15647	2.98	4.15	4.79	53rd & 62nd Hour
GH16	fcwde	ARMOST_07364	3.27	5.66	5.72	53rd & 62nd Hour
GH18	fcwde	ARMOST_05720	7.02	8.10	9.23	53rd & 62nd Hour
GH76	fcwde	ARMOST_14007	5.44	6.89	7.37	53rd & 62nd Hour

GH76	fcwde	ARMOST_14068	0.42	2.27	3.07	53rd & 62nd Hour
GH128	fcwde	ARMOST_19254	2.06	2.03	3.15	62nd Hour
GH16	fcwde	ARMOST_10725	7.57	7.78	8.83	62nd Hour
GH16	fcwde	ARMOST_13508	3.61	5.19	4.82	62nd Hour
GH16	fcwde	ARMOST_10522	5.83	6.85	7.53	62nd Hour
GH16	fcwde	ARMOST_14905	2.49	5.11	4.97	62nd Hour
GH16	fcwde	ARMOST_06797	0.00	0.08	0.52	62nd Hour
GH17	fcwde	ARMOST_05378	4.47	5.46	6.17	62nd Hour
GH18	fcwde	ARMOST_00519	5.13	5.71	6.67	62nd Hour
GH5_9	fcwde	ARMOST_20692	5.30	6.18	6.96	62nd Hour
GH5_9	fcwde	ARMOST_11259	5.44	5.49	7.57	62nd Hour
GH76	fcwde	ARMOST_14067	0.51	1.41	2.31	62nd Hour
CBM5, GH18	fcwde	ARMOST_03314	8.59	5.93	5.54	0th Hour
CBM5, GH18	fcwde	ARMOST_03336	8.29	5.84	5.01	0th Hour
CBM5, GH18	fcwde	ARMOST_09226	6.43	4.37	4.43	0th Hour
GH16	fcwde	ARMOST_00680	6.27	3.86	3.73	0th Hour
GH16	fcwde	ARMOST_06206	6.96	5.06	5.50	0th Hour
GH16	fcwde	ARMOST_07475	1.61	0.66	0.19	0th Hour
GH16	fcwde	ARMOST_12141	4.12	3.14	3.13	0th Hour
GH17	fcwde	ARMOST_15439	7.03	5.44	4.47	0th Hour
GH20	fcwde	ARMOST_10552	5.75	3.72	3.62	0th Hour
GH30_3	fcwde	ARMOST_01723	3.98	2.84	2.94	0th Hour
GH5_15	fcwde	ARMOST_17208	7.54	5.11	4.95	0th Hour
GH55	fcwde	ARMOST_08127	9.73	8.37	6.88	0th Hour
GH71	fcwde	ARMOST_15821	4.60	1.04	0.13	0th Hour
GH76	fcwde	ARMOST_00450	6.40	5.18	4.33	0th Hour
GH92	fcwde	ARMOST_00458	9.33	7.00	6.19	0th Hour
GH125	fcwde	ARMOST_04824	7.21	6.26	5.91	0th Hour
GH128	fcwde	ARMOST_10948	4.68	3.74	3.28	0th Hour
GH16	fcwde	ARMOST_07352	8.67	7.84	7.23	0th Hour
GH16	fcwde	ARMOST_16276	6.98	7.00	5.68	0th Hour
GH16	fcwde	ARMOST_16317	2.39	1.87	1.52	0th Hour
GH16	fcwde	ARMOST_09678	7.73	7.20	6.74	0th Hour
GH18	fcwde	ARMOST_07163	4.97	2.67	1.49	0th Hour
GH18	fcwde	ARMOST_11301	2.12	2.06	0.87	0th Hour
GH18	fcwde	ARMOST_14295	8.18	7.29	6.41	0th Hour
GH18	fcwde	ARMOST_05121	2.52	1.93	1.61	0th Hour
GH30_3	fcwde	ARMOST_11841	8.47	7.79	7.33	0th Hour
GH5_9	fcwde	ARMOST_13007	5.62	4.82	3.96	0th Hour
GH5_9	fcwde	ARMOST_09471	7.16	6.46	5.69	0th Hour
GH71	fcwde	ARMOST_11029	1.56	1.03	0.43	0th Hour
GH16	fcwde	ARMOST_00501	5.40	4.00	4.39	0th Hour
GH16	fcwde	ARMOST_05464	5.11	4.00	4.87	0th Hour
GH18	fcwde	ARMOST_19697	4.60	3.39	3.90	0th Hour
GH20	fcwde	ARMOST_10495	4.63	2.58	3.67	0th Hour
GH5_15	fcwde	ARMOST_19572	1.86	1.15	1.36	0th Hour
GH92	fcwde	ARMOST_21599	5.86	4.81	5.05	0th Hour
AA3_2		ARMOST_12738	7.02	8.27	8.01	53rd Hour
AA3_2		ARMOST_16527	1.81	4.42	4.64	53rd Hour
AA8		ARMOST_17065	4.69	5.90	7.27	53rd Hour
CBM13		ARMOST_04411	4.84	6.17	4.63	53rd Hour

CBM50		ARMOST_10657	0.36	1.23	0.26	53rd Hour
CBM67		ARMOST_21228	3.73	4.90	3.99	53rd Hour
CE15		ARMOST_10694	2.93	3.84	3.60	53rd Hour
CE16		ARMOST_05781	1.46	3.13	3.42	53rd Hour
CE4		ARMOST_13812	5.07	6.47	5.83	53rd Hour
EXPN		ARMOST_04534	1.09	3.23	2.56	53rd Hour
GH152		ARMOST_06876	0.58	1.42	0.90	53rd Hour
GH3		ARMOST_01721	4.73	5.85	5.09	53rd Hour
GH79		ARMOST_02555	6.67	8.11	7.55	53rd Hour
PL1_7		ARMOST_04382	2.48	3.97	3.22	53rd Hour
PL14		ARMOST_08299	5.13	6.14	5.92	53rd Hour
AA1_1		ARMOST_18298	3.38	4.84	5.83	53rd & 62nd Hour
AA1_1		ARMOST_13438	1.55	2.73	2.82	53rd & 62nd Hour
AA1_1		ARMOST_06477	3.70	6.75	7.31	53rd & 62nd Hour
AA1_1		ARMOST_16700	1.89	6.45	7.44	53rd & 62nd Hour
AA16		ARMOST_13325	1.58	2.47	2.73	53rd & 62nd Hour
AA3_2		ARMOST_19175	5.65	7.84	7.77	53rd & 62nd Hour
AA3_2		ARMOST_13670	7.69	10.33	10.38	53rd & 62nd Hour
AA3_2		ARMOST_17615	1.84	4.21	4.36	53rd & 62nd Hour
AA3_2		ARMOST_16041	5.60	9.05	11.31	53rd & 62nd Hour
AA3_2		ARMOST_11606	4.65	8.97	10.70	53rd & 62nd Hour
AA3_2		ARMOST_17630	4.27	10.43	10.32	53rd & 62nd Hour
AA3_2		ARMOST_18416	4.55	10.79	10.64	53rd & 62nd Hour
AA3_2		ARMOST_11604	1.85	7.93	9.19	53rd & 62nd Hour
AA3_2		ARMOST_17629	3.48	10.92	10.72	53rd & 62nd Hour
AA3_3		ARMOST_13218	5.49	7.87	8.05	53rd & 62nd Hour
AA5_1		ARMOST_00390	2.59	3.74	3.96	53rd & 62nd Hour
AA6		ARMOST_20170	2.13	7.20	7.57	53rd & 62nd Hour
AA6		ARMOST_20160	0.82	5.60	5.13	53rd & 62nd Hour
AA7		ARMOST_05726	5.57	11.90	12.11	53rd & 62nd Hour
CBM50		ARMOST_19959	3.92	8.68	8.44	53rd & 62nd Hour
CBM50		ARMOST_00136	1.05	5.88	6.30	53rd & 62nd Hour
CBM50		ARMOST_15376	1.58	8.71	8.41	53rd & 62nd Hour
CBM50		ARMOST_19347	0.00	2.08	1.77	53rd & 62nd Hour
CBM67		ARMOST_05692	1.87	3.49	4.62	53rd & 62nd Hour
CE4		ARMOST_18526	5.52	6.93	7.59	53rd & 62nd Hour
CE4		ARMOST_13811	5.04	6.57	6.29	53rd & 62nd Hour
CE4		ARMOST_13329	8.10	11.89	11.41	53rd & 62nd Hour
EXPN		ARMOST_10945	2.86	4.55	6.78	53rd & 62nd Hour
EXPN		ARMOST_01114	2.24	4.55	6.53	53rd & 62nd Hour
EXPN		ARMOST_11949	1.88	6.73	6.95	53rd & 62nd Hour
EXPN		ARMOST_21105	0.04	1.55	0.58	53rd & 62nd Hour
GH12		ARMOST_12600	4.04	6.25	6.03	53rd & 62nd Hour
GH131		ARMOST_09365	1.19	3.12	3.08	53rd & 62nd Hour
GH15		ARMOST_21208	3.50	6.37	6.41	53rd & 62nd Hour
GH78		ARMOST_18332	0.35	3.59	2.61	53rd & 62nd Hour
GH79		ARMOST_04555	1.76	2.66	3.21	53rd & 62nd Hour

GT1		ARMOST_10761	7.07	8.19	9.58	53rd & 62nd Hour
GT39		ARMOST_15718	6.00	7.01	7.77	53rd & 62nd Hour
PL3_2		ARMOST_08488	1.91	3.00	4.51	53rd & 62nd Hour
PL3_2		ARMOST_08479	2.86	5.02	6.09	53rd & 62nd Hour
PL3_2		ARMOST_08483	1.21	4.01	6.45	53rd & 62nd Hour
AA1_1		ARMOST_07174	0.55	0.59	1.90	62nd Hour
AA1_1		ARMOST_18249	2.98	3.51	5.90	62nd Hour
AA1_1		ARMOST_04477	1.67	5.15	4.39	62nd Hour
AA14		ARMOST_11374	3.85	4.75	5.25	62nd Hour
AA2		ARMOST_01263	3.88	3.91	5.44	62nd Hour
AA2		ARMOST_01179	0.94	0.91	2.39	62nd Hour
AA2		ARMOST_01279	1.88	2.06	4.10	62nd Hour
AA3_2		ARMOST_16710	4.94	5.08	6.04	62nd Hour
AA3_2		ARMOST_20378	7.61	8.44	9.34	62nd Hour
AA3_2		ARMOST_12719	0.99	1.25	2.49	62nd Hour
AA3_2		ARMOST_16604	2.59	5.35	5.51	62nd Hour
AA3_2		ARMOST_16629	1.73	3.81	4.80	62nd Hour
AA3_2		ARMOST_11851	4.07	4.85	11.02	62nd Hour
AA3_2		ARMOST_11855	2.63	3.40	9.52	62nd Hour
AA6		ARMOST_14042	5.11	6.56	8.80	62nd Hour
AA7		ARMOST_07847	3.06	3.41	4.05	62nd Hour
AA7		ARMOST_05706	3.47	3.30	8.94	62nd Hour
AA9		ARMOST_13556	7.89	8.17	9.09	62nd Hour
AA9		ARMOST_18350	0.98	1.65	1.85	62nd Hour
AA9, CBM1		ARMOST_10843	1.73	1.88	2.60	62nd Hour
CBM1		ARMOST_13810	2.87	3.74	3.90	62nd Hour
CBM1, GH6		ARMOST_04232	1.27	1.40	3.38	62nd Hour
CBM21		ARMOST_08338	4.78	5.04	6.09	62nd Hour
CBM21		ARMOST_17055	4.25	4.87	5.87	62nd Hour
CBM48		ARMOST_05013	5.00	5.24	6.77	62nd Hour
CBM50		ARMOST_16961	5.04	5.36	6.19	62nd Hour
CBM67		ARMOST_15471	1.46	1.29	2.30	62nd Hour
CE4		ARMOST_13355	0.54	0.84	1.58	62nd Hour
CE4		ARMOST_05321	2.07	2.89	4.05	62nd Hour
CE8		ARMOST_12332	0.25	0.15	1.57	62nd Hour
EXPN		ARMOST_09015	7.75	8.41	9.07	62nd Hour
EXPN		ARMOST_15306	2.28	2.58	3.52	62nd Hour
EXPN		ARMOST_03777	9.37	9.91	11.03	62nd Hour
EXPN		ARMOST_00895	2.01	4.09	6.54	62nd Hour
EXPN		ARMOST_00438	1.57	4.77	6.46	62nd Hour
GH1		ARMOST_12473	0.71	1.65	1.38	62nd Hour
GH1		ARMOST_12474	1.60	2.93	3.15	62nd Hour
GH31		ARMOST_09619	6.37	6.65	7.71	62nd Hour
GH37		ARMOST_13182	6.33	6.95	7.47	62nd Hour
GH45		ARMOST_07341	0.89	1.51	2.18	62nd Hour
GH5_5		ARMOST_13121	2.67	3.05	3.62	62nd Hour
GH6		ARMOST_04231	1.81	2.28	3.52	62nd Hour

GH79		ARMOST_14752	2.31	4.35	4.09	62nd Hour
GT1		ARMOST_08256	3.09	3.01	4.19	62nd Hour
GT1		ARMOST_17497	2.68	3.21	4.24	62nd Hour
GT2		ARMOST_16675	6.92	6.76	8.01	62nd Hour
GT2		ARMOST_06316	7.54	7.41	8.66	62nd Hour
GT2		ARMOST_06013	7.09	7.31	8.40	62nd Hour
GT2		ARMOST_05425	7.07	7.16	8.80	62nd Hour
GT32		ARMOST_08705	5.63	6.20	6.83	62nd Hour
GT32		ARMOST_05168	6.55	7.00	8.23	62nd Hour
GT33		ARMOST_08710	4.74	5.03	5.74	62nd Hour
GT48		ARMOST_13503	7.00	7.64	8.98	62nd Hour
GT57		ARMOST_07081	4.35	4.83	5.37	62nd Hour
GT69		ARMOST_14292	4.51	5.33	5.58	62nd Hour
GT8		ARMOST_09117	5.13	5.91	7.48	62nd Hour
GT8		ARMOST_00145	0.84	0.72	2.43	62nd Hour
PL3_2		ARMOST_22631	1.40	2.27	3.59	62nd Hour
PL35		ARMOST_10965	6.36	7.16	8.16	62nd Hour
AA1_1		ARMOST_13394	2.48	1.48	1.57	0th Hour
AA1_1		ARMOST_02569	2.83	1.97	1.08	0th Hour
AA3_2		ARMOST_13932	5.87	3.98	3.68	0th Hour
AA5_1		ARMOST_16336	3.17	2.04	1.90	0th Hour
CBM20, GH13_32		ARMOST_15338	2.69	1.31	1.62	0th Hour
CBM35, GH27		ARMOST_11127	4.18	2.11	2.54	0th Hour
CBM35, GH43		ARMOST_09674	2.93	1.41	2.09	0th Hour
CBM67		ARMOST_01994	6.01	2.85	2.45	0th Hour
CBM67		ARMOST_15466	5.85	2.80	2.61	0th Hour
CBM67		ARMOST_04052	5.31	2.97	3.01	0th Hour
CE12		ARMOST_13144	5.02	1.59	1.92	0th Hour
CE12		ARMOST_13145	1.70	0.67	0.76	0th Hour
CE15		ARMOST_04676	4.90	3.89	3.93	0th Hour
CE16		ARMOST_17433	2.41	1.06	1.56	0th Hour
CE8		ARMOST_12801	2.46	1.31	1.48	0th Hour
CE8		ARMOST_00444	2.79	1.64	0.88	0th Hour
EXPN		ARMOST_08316	6.67	3.29	1.23	0th Hour
EXPN		ARMOST_11001	6.29	4.28	2.18	0th Hour
GH10		ARMOST_08096	2.07	1.31	0.64	0th Hour
GH12		ARMOST_08301	3.89	2.80	2.81	0th Hour
GH13_1		ARMOST_07729	1.63	0.89	0.71	0th Hour
GH145		ARMOST_19354	7.56	5.75	6.15	0th Hour
GH2		ARMOST_10283	5.61	4.26	3.60	0th Hour
GH28		ARMOST_13687	3.90	1.70	1.73	0th Hour
GH28		ARMOST_17334	1.58	0.82	0.55	0th Hour
GH3		ARMOST_05840	8.02	6.65	6.07	0th Hour
GH35		ARMOST_07441	2.87	1.32	1.38	0th Hour
GH39		ARMOST_01149	7.28	5.20	4.27	0th Hour
GH43		ARMOST_10670	2.63	1.45	1.36	0th Hour
GH47		ARMOST_07252	7.44	4.12	3.28	0th Hour

GH47		ARMOST_01782	9.20	6.31	5.48	0th Hour
GH5_7		ARMOST_09017	4.64	2.22	3.29	0th Hour
GH51		ARMOST_09851	3.93	1.97	2.59	0th Hour
GH51		ARMOST_19253	3.56	2.13	1.65	0th Hour
GH51		ARMOST_18073	3.84	2.79	2.18	0th Hour
GH78		ARMOST_00942	7.45	5.36	5.85	0th Hour
GH79		ARMOST_03290	8.70	6.81	6.14	0th Hour
GH79		ARMOST_01674	7.10	5.51	5.49	0th Hour
GH95		ARMOST_12635	7.40	6.24	5.94	0th Hour
GT90		ARMOST_16027	3.54	1.80	1.80	0th Hour
AA1_1		ARMOST_22340	0.73	0.53	0.06	0th Hour
AA3_2		ARMOST_16609	0.56	0.52	0.06	0th Hour
AA3_2		ARMOST_00430	1.26	0.68	0.24	0th Hour
AA3_2		ARMOST_02077	8.52	7.55	6.04	0th Hour
AA3_2		ARMOST_06799	1.03	0.76	0.39	0th Hour
AA3_2		ARMOST_16611	1.18	1.08	0.52	0th Hour
AA3_2		ARMOST_01152	5.64	4.92	4.31	0th Hour
AA3_2		ARMOST_01584	5.50	5.00	4.45	0th Hour
AA3_3		ARMOST_04818	10.26	9.81	8.78	0th Hour
AA3_3		ARMOST_13238	4.42	4.62	3.06	0th Hour
AA3_4		ARMOST_19329	1.92	1.43	1.24	0th Hour
AA9		ARMOST_01648	1.25	0.74	0.14	0th Hour
AA9		ARMOST_17862	0.69	0.42	0.14	0th Hour
CBM1, GH5_7		ARMOST_15975	1.44	1.05	0.52	0th Hour
CBM13		ARMOST_13531	7.97	7.14	6.77	0th Hour
CBM67		ARMOST_21242	2.07	1.27	1.28	0th Hour
EXPN		ARMOST_05275	2.33	2.06	1.50	0th Hour
GH13_1		ARMOST_07832	7.50	6.56	6.28	0th Hour
GH13_40		ARMOST_05929	5.26	4.37	2.72	0th Hour
GH27		ARMOST_11098	10.58	9.59	9.23	0th Hour
GH27		ARMOST_14829	6.25	6.02	5.03	0th Hour
GH27		ARMOST_00704	4.12	3.42	3.14	0th Hour
GH28		ARMOST_17320	1.81	1.46	0.98	0th Hour
GH29		ARMOST_17579	5.42	5.00	4.00	0th Hour
GH29		ARMOST_17577	4.34	4.89	3.20	0th Hour
GH3		ARMOST_21600	1.97	1.53	0.87	0th Hour
GH31		ARMOST_08458	7.29	6.41	5.69	0th Hour
GH43		ARMOST_05901	1.99	1.50	0.37	0th Hour
GH43		ARMOST_10672	1.63	1.37	0.78	0th Hour
GH43		ARMOST_09818	4.12	3.40	2.75	0th Hour
GH43		ARMOST_01936	7.49	7.59	6.50	0th Hour
GH47		ARMOST_11323	3.70	3.17	2.74	0th Hour
GH5_22		ARMOST_10261	4.25	3.34	2.33	0th Hour
GH5_50		ARMOST_03596	1.89	1.37	0.71	0th Hour
GH53		ARMOST_01831	0.38	0.20	0.00	0th Hour
GH53		ARMOST_00915	6.23	5.36	4.37	0th Hour
GH78		ARMOST_00947	5.57	4.88	3.64	0th Hour

GH78		ARMOST_18328	3.24	2.75	2.30	0th Hour
GT2		ARMOST_00685	3.93	3.10	2.98	0th Hour
PL1_7		ARMOST_13458	4.40	3.71	3.18	0th Hour
PL14_4		ARMOST_14617	6.29	5.47	5.03	0th Hour
PL3_2		ARMOST_10011	2.93	2.45	2.10	0th Hour
AA1_1		ARMOST_20610	2.51	0.95	2.81	0th Hour
AA14		ARMOST_08454	4.27	3.29	3.53	0th Hour
AA3_2		ARMOST_16331	2.42	1.64	2.35	0th Hour
AA3_3		ARMOST_11817	7.86	6.46	7.12	0th Hour
CBM20, GH15		ARMOST_11123	3.93	2.94	3.26	0th Hour
CBM50		ARMOST_12714	8.29	7.09	7.66	0th Hour
CE12		ARMOST_09510	2.32	0.84	1.54	0th Hour
CE16		ARMOST_09541	2.95	2.02	2.40	0th Hour
CE4		ARMOST_04867	6.97	5.92	6.02	0th Hour
GH28		ARMOST_10222	4.92	3.78	4.07	0th Hour
GH31		ARMOST_03486	3.16	2.19	3.04	0th Hour
GH43		ARMOST_07191	3.36	1.97	2.48	0th Hour
PL1_2		ARMOST_03823	5.87	4.78	5.01	0th Hour
PL8_4		ARMOST_09075	3.66	1.57	2.83	0th Hour

Supplementary material 8. Differentially expressed CAZymes in *T. atroviride* against *A. ostoyae* in *in-vitro* interaction assay

CAZYme	FCWDE	GeneID	0th Hour	53rd Hour	62nd Hour	Upreg_in
GH125	fcwde	XM_014093580.1	2.36	2.45	1.54	0th Hour
GH128	fcwde	XM_014085194.1	1.88	1.54	0.00	0th Hour
GH18	fcwde	XM_014085820.1	1.84	1.74	0.63	0th Hour
GH18	fcwde	XM_014082779.1	2.46	2.38	1.80	0th Hour
GH18	fcwde	XM_014090565.1	1.86	1.90	0.66	0th Hour
GH18	fcwde	XM_014083559.1	2.48	2.38	1.61	0th Hour
GH18	fcwde	XM_014083450.1	2.10	2.18	1.21	0th Hour
GH18	fcwde	XM_014086461.1	2.03	2.12	0.88	0th Hour
GH18	fcwde	XM_014085864.1	2.31	2.22	1.08	0th Hour
EXPN,GH18	fcwde	XM_014090026.1	2.47	2.50	1.54	0th Hour
GH18	fcwde	XM_014090551.1	2.65	2.50	1.38	0th Hour
GH18	fcwde	XM_014092021.1	2.87	2.87	2.04	0th Hour
GH18	fcwde	XM_014089918.1	2.71	2.73	1.72	0th Hour
GH20	fcwde	XM_014088835.1	2.61	2.63	0.66	0th Hour
GH30_5	fcwde	XM_014082886.1	2.60	2.55	1.05	0th Hour
GH55	fcwde	XM_014092200.1	2.49	2.23	1.61	0th Hour
GH55	fcwde	XM_014092865.1	2.14	2.14	1.35	0th Hour
GH55	fcwde	XM_014089026.1	2.07	2.00	0.00	0th Hour
GH55	fcwde	XM_014085316.1	2.50	2.53	1.54	0th Hour
GH71	fcwde	XM_014088990.1	2.48	2.49	1.88	0th Hour
GH71	fcwde	XM_014082837.1	2.58	2.66	1.94	0th Hour
GH71	fcwde	XM_014085671.1	2.67	2.58	1.99	0th Hour
GH75	fcwde	XM_014093431.1	1.95	1.82	0.84	0th Hour
GH76	fcwde	XM_014086105.1	2.58	2.60	1.95	0th Hour
GH92	fcwde	XM_014092898.1	2.15	2.11	1.39	0th Hour

GH92	fcwde	XM_014090973.1	2.54	2.51	1.88	0th Hour
GH92	fcwde	XM_014088328.1	2.40	2.39	1.54	0th Hour
GH92	fcwde	XM_014088291.1	1.95	2.02	0.66	0th Hour
GH92	fcwde	XM_014093062.1	2.46	2.49	1.54	0th Hour
GH92	fcwde	XM_014091992.1	2.91	3.02	2.24	0th Hour
GH18	fcwde	XM_014088518.1	2.69	2.59	3.50	62nd Hour
GH18	fcwde	XM_014093807.1	1.93	1.88	3.03	62nd Hour
GH18	fcwde	XM_014085328.1	1.00	1.37	2.33	62nd Hour
GH18	fcwde	XM_014089522.1	1.37	1.52	2.23	62nd Hour
GH71	fcwde	XM_014086187.1	1.47	1.53	2.08	62nd Hour
GH81	fcwde	XM_014086384.1	2.41	2.36	3.17	62nd Hour
GH72	fcwde	XM_014082543.1	1.30	2.25	0.61	53rd Hour
GT0		XM_014090061.1	2.14	1.77	0.00	0th Hour
CE3		XM_014090400.1	1.58	2.01	0.00	0th & 53rd Hour
AA1_2		XM_014091647.1	2.37	2.41	0.61	0th Hour
AA3_2		XM_014093769.1	2.67	2.67	1.99	0th Hour
AA3_3		XM_014090503.1	2.50	2.76	0.97	0th Hour
AA3_3		XM_014088824.1	2.99	3.01	1.65	0th Hour
AA7		XM_014084369.1	2.04	2.12	1.05	0th Hour
AA9		XM_014089472.1	1.94	1.83	0.61	0th Hour
CBM13		XM_014082202.1	3.30	3.46	2.76	0th Hour
CBM50		XM_014090024.1	1.62	1.65	0.00	0th Hour
CBM50		XM_014088736.1	2.83	2.95	2.24	0th Hour
CE16		XM_014083348.1	1.46	1.20	0.00	0th Hour
CE4		XM_014084023.1	2.87	2.81	2.12	0th Hour
CE4		XM_014090947.1	2.14	2.21	0.00	0th Hour
GH105		XM_014089571.1	1.96	2.15	0.84	0th Hour
GH115		XM_014087888.1	1.43	1.46	0.00	0th Hour
GH13_1		XM_014085248.1	1.97	1.73	0.63	0th Hour
GH154		XM_014084584.1	2.29	2.24	1.24	0th Hour
GH2		XM_014082626.1	2.27	2.27	1.39	0th Hour
GH2		XM_014084140.1	2.34	2.44	1.54	0th Hour
GH2		XM_014092198.1	2.83	2.76	2.12	0th Hour
GH2		XM_014086398.1	2.45	2.54	1.54	0th Hour
GH2		XM_014085627.1	2.41	2.61	1.56	0th Hour
GH27		XM_014092115.1	2.02	2.18	0.63	0th Hour
GH27		XM_014092539.1	2.40	2.47	1.41	0th Hour
GH28		XM_014093792.1	1.61	1.70	0.00	0th Hour
GH28		XM_014083208.1	1.83	1.90	0.00	0th Hour
GH3		XM_014088830.1	2.31	2.28	1.41	0th Hour
GH3		XM_014085109.1	2.07	2.07	0.88	0th Hour
GH3		XM_014085346.1	2.17	2.20	1.09	0th Hour
GH3		XM_014085010.1	2.63	2.69	1.99	0th Hour
GH3		XM_014089439.1	2.71	2.80	2.11	0th Hour
GH3		XM_014083670.1	2.80	2.92	2.22	0th Hour
GH3		XM_014089433.1	1.93	2.06	0.00	0th Hour
GH3		XM_014088923.1	2.23	1.88	1.34	0th Hour
GH31		XM_014088670.1	2.67	2.85	2.09	0th Hour

GH31		XM_014084935.1	1.83	1.85	0.00	0th Hour
GH31		XM_014083470.1	2.45	2.30	0.84	0th Hour
GH31		XM_014084572.1	2.92	2.94	2.16	0th Hour
GH31		XM_014087540.1	2.07	2.25	0.00	0th Hour
GH31		XM_014093498.1	2.59	2.39	0.00	0th Hour
GH31		XM_014085307.1	1.73	1.58	0.63	0th Hour
GH38		XM_014083822.1	2.98	3.02	2.32	0th Hour
GH45		XM_014093435.1	2.80	2.69	1.92	0th Hour
GH47		XM_014092611.1	2.84	2.87	2.20	0th Hour
GH47		XM_014083546.1	2.88	2.85	2.05	0th Hour
GH6		XM_014092666.1	2.65	2.38	1.51	0th Hour
GH78		XM_014088791.1	1.46	1.51	0.00	0th Hour
GT1		XM_014086629.1	2.04	2.05	0.66	0th Hour
GT2		XM_014090306.1	2.20	2.09	1.24	0th Hour
GT22		XM_014092481.1	2.18	2.07	1.05	0th Hour
GT22		XM_014088295.1	1.90	1.99	0.83	0th Hour
GT22		XM_014087940.1	2.05	2.03	0.63	0th Hour
GT24		XM_014082571.1	2.68	2.71	1.94	0th Hour
GT31		XM_014082048.1	1.45	1.56	0.00	0th Hour
GT31		XM_014090557.1	2.54	2.40	1.85	0th Hour
GT31		XM_014092920.1	2.22	2.13	1.34	0th Hour
GT31		XM_014083948.1	2.13	2.19	1.08	0th Hour
GT31		XM_014092921.1	1.73	1.87	0.00	0th Hour
GT31		XM_014093590.1	1.93	1.95	1.21	0th Hour
GT32		XM_014090048.1	1.91	2.02	0.95	0th Hour
GT32		XM_014089348.1	2.83	2.71	1.92	0th Hour
GT32		XM_014089347.1	2.72	2.62	1.39	0th Hour
GT35		XM_014086119.1	3.38	3.41	2.87	0th Hour
GT57		XM_014090334.1	2.42	2.49	1.73	0th Hour
GT58		XM_014093007.1	2.31	2.27	1.24	0th Hour
GT76		XM_014083543.1	2.07	2.11	0.00	0th Hour
GT90		XM_014090561.1	2.28	2.37	1.25	0th Hour
PL8_4		XM_014087625.1	2.02	2.02	0.95	0th Hour
AA0		XM_014090749.1	1.95	2.02	0.97	0th Hour
AA0		XM_014082135.1	3.15	3.17	2.62	0th Hour
AA3		XM_014082908.1	1.63	1.54	0.00	0th Hour
AA4		XM_014092593.1	2.78	2.78	1.89	0th Hour
AA5		XM_014083886.1	3.28	3.33	2.70	0th Hour
CBM57		XM_014085906.1	3.02	3.08	2.43	0th Hour
CBM66		XM_014085204.1	2.21	2.13	0.63	0th Hour
CE1		XM_014088043.1	1.98	1.97	1.08	0th Hour
CE3		XM_014089659.1	2.17	2.24	1.31	0th Hour
CE3		XM_014088877.1	2.25	2.32	1.24	0th Hour
CE5		XM_014084305.1	1.85	1.65	0.00	0th Hour
CE5		XM_014084747.1	2.80	2.64	1.25	0th Hour
GH16_1		XM_014090075.1	2.33	2.06	0.00	0th Hour
GH16_1		XM_014083768.1	2.12	2.09	0.66	0th Hour

GH16_23		XM_014093711.1	2.04	1.92	1.09	0th Hour
GH36		XM_014083101.1	2.90	2.96	1.92	0th Hour
GH43_11		XM_014086642.1	1.57	1.72	0.00	0th Hour
GH43_21		XM_014086927.1	2.76	2.77	1.59	0th Hour
GH54		XM_014087288.1	2.54	2.53	1.89	0th Hour
GH65		XM_014089524.1	1.47	1.64	0.00	0th Hour
GH89		XM_014083499.1	1.73	1.68	0.00	0th Hour
GT0		XM_014085932.1	2.29	2.37	1.10	0th Hour
GT13		XM_014083801.1	3.06	3.03	2.44	0th Hour
GT71		XM_014088445.1	1.92	1.69	0.00	0th Hour
PL38		XM_014093791.1	1.41	1.28	0.00	0th Hour
AA1		XM_014089632.1	0.73	2.16	1.34	53rd Hour
CBM48		XM_014088205.1	1.95	2.63	3.44	53rd Hour
AA3_2		XM_014088283.1	1.58	1.38	2.70	62nd Hour
AA7		XM_014090038.1	1.35	1.34	2.26	62nd Hour
AA7		XM_014084867.1	1.85	2.16	2.84	62nd Hour
CBM48		XM_014092097.1	1.61	1.10	2.74	62nd Hour
CE9		XM_014087002.1	2.18	2.20	3.22	62nd Hour
GH27		XM_014090559.1	2.38	2.50	3.25	62nd Hour
GT1		XM_014082689.1	2.64	2.66	3.19	62nd Hour
GT1		XM_014090549.1	1.62	1.79	2.41	62nd Hour
GT4		XM_014084952.1	1.43	1.29	2.43	62nd Hour
AA3		XM_014085064.1	1.16	1.31	1.83	62nd Hour
GH0		XM_014082072.1	0.60	0.48	1.54	62nd Hour
GT87		XM_014083243.1	1.94	1.73	2.90	62nd Hour
AA7		XM_014089795.1	1.29	0.58	0.00	0th Hour
GT2		XM_014090120.1	0.77	1.20	0.00	53rd Hour

Supplementary material 9. Differentially expressed peptidases in *A. ostoyae* against *T. atroviride* in *in-vitro* interaction assay

Peptidase Family	Peptidase ID	GeneID	0th Hour	53rd Hour	62nd Hour	Upreg_in
Serine_peptidases	S08A	ARMOST_01782	9.20	6.31	5.48	0th Hour
Serine_peptidases	S10	ARMOST_21257	8.22	4.43	3.37	0th Hour
Metallo_peptidases	M17	ARMOST_00710	5.84	4.69	3.87	0th Hour
Metallo_peptidases	M38	ARMOST_12167	6.64	5.54	4.93	0th Hour
Cysteine_peptidases	C56	ARMOST_01925	2.64	1.72	1.19	0th Hour
Cysteine_peptidases	C12	ARMOST_20586	8.35	7.34	6.75	0th Hour
Threonine_peptidases	T03	ARMOST_09017	4.64	2.22	3.29	0th Hour
Threonine_peptidases	T01A	ARMOST_15821	4.60	1.04	0.13	0th Hour
Serine_peptidases	S10	ARMOST_00444	2.79	1.64	0.88	0th Hour
Serine_peptidases	S10	ARMOST_04431	6.03	4.42	4.98	0th Hour
Serine_peptidases	S08A	ARMOST_07252	7.44	4.12	3.28	0th Hour
Serine_peptidases	S09X	ARMOST_08096	2.07	1.31	0.64	0th Hour
Serine_peptidases	S08A	ARMOST_08127	9.73	8.36	6.88	0th Hour
Serine_peptidases	S01A	ARMOST_18976	2.98	1.84	1.21	0th Hour
Serine_peptidases	S54	ARMOST_22367	6.29	5.12	3.84	0th Hour
Metallo_peptidases	M41	ARMOST_00450	6.40	5.18	4.33	0th Hour

Metallo_peptidases	M14A	ARMOST_00458	9.33	7.00	6.19	0th Hour
Metallo_peptidases	M16A	ARMOST_15461	4.65	2.38	2.92	0th Hour
Metallo_peptidases	M36	ARMOST_21485	5.13	2.20	1.68	0th Hour
Cysteine_peptidases	C110	ARMOST_02569	2.83	1.97	1.08	0th Hour
Cysteine_peptidases	C12	ARMOST_03290	8.70	6.81	6.14	0th Hour
Cysteine_peptidases	C56	ARMOST_04119	5.64	3.38	4.29	0th Hour
Aspartic_peptidases	A1A	ARMOST_03336	8.29	5.84	5.01	0th Hour
Threonine_peptidases	T03	ARMOST_15975	1.44	1.05	0.52	0th Hour
Serine_peptidases	S08A	ARMOST_04559	7.28	6.86	5.65	0th Hour
Serine_peptidases	S15	ARMOST_15160	3.13	2.83	2.32	0th Hour
Serine_peptidases	S08A	ARMOST_16075	7.61	7.53	6.47	0th Hour
Serine_peptidases	S09C	ARMOST_20634	2.34	1.95	1.38	0th Hour
Serine_peptidases	S15	ARMOST_21614	3.05	2.25	1.72	0th Hour
Metallo_peptidases	M77	ARMOST_03574	5.16	5.24	3.85	0th Hour
Metallo_peptidases	M26	ARMOST_03596	1.89	1.37	0.71	0th Hour
Metallo_peptidases	M49	ARMOST_11136	8.04	8.25	6.63	0th Hour
Metallo_peptidases	M38	ARMOST_00940	5.60	5.35	3.72	0th Hour
Metallo_peptidases	M20A	ARMOST_06864	4.64	4.21	3.58	0th Hour
Inhibitor_family	I87	ARMOST_16901	2.07	1.63	0.93	0th Hour
Inhibitor_family	I63	ARMOST_17832	4.03	3.44	2.76	0th Hour
Cysteine_peptidases	C14B	ARMOST_02366	5.21	4.86	4.06	0th Hour
Cysteine_peptidases	C56	ARMOST_04164	6.44	6.41	4.53	0th Hour
Aspartic_peptidases	A11A	ARMOST_14610	3.70	3.02	2.25	0th Hour
Serine_peptidases	S10	ARMOST_15388	3.03	2.22	1.72	0th Hour
Cysteine_peptidases	C56	ARMOST_01648	1.25	0.74	0.14	0th Hour
Threonine_peptidases	T01A	ARMOST_02436	4.82	4.23	3.48	0th Hour
Serine_peptidases	S09B	ARMOST_01936	7.49	7.59	6.50	0th Hour
Serine_peptidases	S09B	ARMOST_05901	1.99	1.50	0.37	0th Hour
Serine_peptidases	S01A	ARMOST_08458	7.29	6.41	5.69	0th Hour
Serine_peptidases	S12	ARMOST_09818	4.12	3.40	2.75	0th Hour
Serine_peptidases	S28	ARMOST_10629	5.44	5.03	4.46	0th Hour
Serine_peptidases	S09B	ARMOST_14108	2.90	2.46	1.90	0th Hour
Serine_peptidases	S10	ARMOST_14111	1.75	1.44	0.91	0th Hour
Serine_peptidases	S33	ARMOST_17579	5.42	5.00	4.00	0th Hour
Serine_peptidases	S12	ARMOST_21600	1.97	1.53	0.87	0th Hour
Metallo_peptidases	M26	ARMOST_09471	7.16	6.46	5.69	0th Hour
Metallo_peptidases	M16C	ARMOST_10995	6.48	6.01	5.41	0th Hour
Metallo_peptidases	M26	ARMOST_13007	5.62	4.82	3.96	0th Hour
Metallo_peptidases	M18	ARMOST_11029	1.56	1.03	0.43	0th Hour
Metallo_peptidases	M14A	ARMOST_11491	5.84	5.62	4.73	0th Hour
Metallo_peptidases	M16B	ARMOST_17577	4.34	4.89	3.20	0th Hour
Inhibitor_family	I02	ARMOST_16319	5.51	4.90	4.21	0th Hour
Aspartic_peptidases	A1A	ARMOST_01584	5.50	5.00	4.45	0th Hour
Aspartic_peptidases	A1A	ARMOST_16611	1.18	1.08	0.52	0th Hour
Serine_peptidases	S15	ARMOST_00213	4.90	8.18	10.03	53rd & 62nd Hour
Serine_peptidases	S01A	ARMOST_01402	7.88	9.65	10.91	53rd & 62nd Hour
Serine_peptidases	S09X	ARMOST_01950	7.00	8.22	8.77	53rd & 62nd Hour
Serine_peptidases	S33	ARMOST_06134	2.54	3.74	4.89	53rd & 62nd Hour
Serine_peptidases	S53	ARMOST_08361	0.94	3.15	3.93	53rd & 62nd Hour
Serine_peptidases	S09X	ARMOST_09883	5.47	8.57	9.43	53rd & 62nd Hour
Serine_peptidases	S33	ARMOST_10343	7.73	10.23	11.05	53rd & 62nd Hour

Serine_peptidases	S12	ARMOST_12765	2.27	4.76	5.30	53rd & 62nd Hour
Serine_peptidases	S09B	ARMOST_15582	2.11	5.05	5.95	53rd & 62nd Hour
Serine_peptidases	S33	ARMOST_19449	2.81	7.29	9.22	53rd & 62nd Hour
Serine_peptidases	S09X	ARMOST_20055	4.20	8.46	10.67	53rd & 62nd Hour
Metallo_peptidases	M16B	ARMOST_04218	1.17	3.15	4.09	53rd & 62nd Hour
Cysteine_peptidases	C12	ARMOST_01954	6.82	8.24	9.06	53rd & 62nd Hour
Cysteine_peptidases	C12	ARMOST_08320	6.08	7.75	8.84	53rd & 62nd Hour
Cysteine_peptidases	C01A	ARMOST_09493	6.29	7.42	7.93	53rd & 62nd Hour
Cysteine_peptidases	C48	ARMOST_17150	1.21	3.29	4.19	53rd & 62nd Hour
Cysteine_peptidases	C48	ARMOST_17180	5.10	6.14	6.67	53rd & 62nd Hour
Cysteine_peptidases	C12	ARMOST_18526	5.52	6.93	7.59	53rd & 62nd Hour
Aspartic_peptidases	A1A	ARMOST_15448	0.78	2.93	4.13	53rd & 62nd Hour
Metallo_peptidases	M12A	ARMOST_18251	2.61	3.73	4.77	53rd & 62nd Hour
Cysteine_peptidases	C14B	ARMOST_17503	3.38	8.84	9.35	53rd & 62nd Hour
Serine_peptidases	S09X	ARMOST_02859	2.04	3.08	3.79	53rd & 62nd Hour
Serine_peptidases	S33	ARMOST_04491	4.01	6.96	5.55	53rd & 62nd Hour
Serine_peptidases	S08A	ARMOST_05720	7.02	8.10	9.23	53rd & 62nd Hour
Serine_peptidases	S12	ARMOST_15873	2.93	4.48	5.22	53rd & 62nd Hour
Serine_peptidases	S09X	ARMOST_16041	5.60	9.05	11.31	53rd & 62nd Hour
Metallo_peptidases	M19	ARMOST_07409	5.77	7.59	8.71	53rd & 62nd Hour
Metallo_peptidases	M20D	ARMOST_07735	1.13	7.89	8.66	53rd & 62nd Hour
Metallo_peptidases	M20A	ARMOST_16640	2.04	8.11	7.15	53rd & 62nd Hour
Metallo_peptidases	M20A	ARMOST_16666	5.59	8.42	9.75	53rd & 62nd Hour
Metallo_peptidases	M36	ARMOST_18333	2.41	3.40	4.28	53rd & 62nd Hour
Inhibitor_family	I63	ARMOST_11315	4.29	6.40	6.96	53rd & 62nd Hour
Cysteine_peptidases	C12	ARMOST_04555	1.76	2.66	3.21	53rd & 62nd Hour
Cysteine_peptidases	C02A	ARMOST_11604	1.85	7.93	9.19	53rd & 62nd Hour
Cysteine_peptidases	C02A	ARMOST_11606	4.65	8.97	10.70	53rd & 62nd Hour
Cysteine_peptidases	C110	ARMOST_16700	1.89	6.45	7.44	53rd & 62nd Hour
Aspartic_peptidases	A11A	ARMOST_18298	3.38	4.84	5.83	53rd & 62nd Hour
Serine_peptidases	S12	ARMOST_10620	5.73	6.53	7.06	62nd Hour
Serine_peptidases	S33	ARMOST_17967	1.81	2.18	3.60	62nd Hour
Inhibitor_family	I29	ARMOST_07847	3.06	3.41	4.06	62nd Hour
Cysteine_peptidases	C56	ARMOST_01274	3.48	4.21	5.11	62nd Hour
Aspartic_peptidases	A11A	ARMOST_01651	3.58	3.71	5.79	62nd Hour
Cysteine_peptidases	C14B	ARMOST_13355	0.54	0.84	1.58	62nd Hour
Threonine_peptidases	T03	ARMOST_04232	1.27	1.40	3.38	62nd Hour
Serine_peptidases	S53	ARMOST_05656	5.65	5.50	8.26	62nd Hour
Serine_peptidases	S09B	ARMOST_07363	3.56	4.80	5.91	62nd Hour
Serine_peptidases	S10	ARMOST_12332	0.25	0.15	1.57	62nd Hour
Serine_peptidases	S12	ARMOST_12651	3.60	3.92	4.84	62nd Hour
Serine_peptidases	S01A	ARMOST_14725	2.01	2.33	6.40	62nd Hour
Serine_peptidases	S09B	ARMOST_15583	0.78	0.64	1.43	62nd Hour
Serine_peptidases	S12	ARMOST_15865	1.02	1.11	2.18	62nd Hour
Serine_peptidases	S12	ARMOST_15878	0.36	0.67	1.26	62nd Hour
Serine_peptidases	S12	ARMOST_17065	4.69	5.90	7.28	62nd Hour
Serine_peptidases	S28	ARMOST_20072	1.02	0.97	2.35	62nd Hour
Metallo_peptidases	M12B	ARMOST_08742	7.89	8.38	9.56	62nd Hour
Metallo_peptidases	M36	ARMOST_12239	2.41	2.86	4.06	62nd Hour
Metallo_peptidases	M16A	ARMOST_15463	4.21	4.80	6.63	62nd Hour
Metallo_peptidases	M20A	ARMOST_16664	3.78	4.47	5.93	62nd Hour

Inhibitor_family	I29	ARMOST_05706	3.47	3.30	8.94	62nd Hour
Inhibitor_family	I51	ARMOST_08004	3.64	4.04	4.75	62nd Hour
Cysteine_peptidases	C19	ARMOST_02773	4.83	5.44	6.19	62nd Hour
Cysteine_peptidases	C14B	ARMOST_05321	2.07	2.89	4.05	62nd Hour
Cysteine_peptidases	C110	ARMOST_05369	8.59	8.50	9.87	62nd Hour
Cysteine_peptidases	C02A	ARMOST_11851	4.07	4.85	11.02	62nd Hour
Cysteine_peptidases	C02A	ARMOST_11855	2.63	3.40	9.52	62nd Hour
Cysteine_peptidases	C02A	ARMOST_12719	0.99	1.25	2.49	62nd Hour
Cysteine_peptidases	C56	ARMOST_13556	7.89	8.17	9.09	62nd Hour
Cysteine_peptidases	C110	ARMOST_18249	2.98	3.51	5.90	62nd Hour
Aspartic_peptidases	A1A	ARMOST_00677	2.10	2.07	3.05	62nd Hour
Aspartic_peptidases	A1A	ARMOST_00730	6.21	6.61	7.22	62nd Hour
Aspartic_peptidases	A1A	ARMOST_03357	5.59	5.08	6.70	62nd Hour
Aspartic_peptidases	A11A	ARMOST_04477	1.67	5.15	4.39	62nd Hour
Aspartic_peptidases	A11A	ARMOST_07174	0.55	0.59	1.90	62nd Hour
Aspartic_peptidases	A1A	ARMOST_11115	4.01	4.54	5.47	62nd Hour
Aspartic_peptidases	A1A	ARMOST_16629	1.73	3.81	4.80	62nd Hour
Aspartic_peptidases	A1A	ARMOST_20378	7.61	8.44	9.34	62nd Hour

Supplementary material 10. Differentially expressed peptidases in *T. atroviride* against *A. ostoyae* in *in-vitro* interaction assay

Peptidase Family	**PeptidaseID**	**GeneID**	**0th Hour**	**53rd Hour**	**62nd Hour**	**Upreg_in**
Aspartic_peptidases	A01A	XM_014084360.1	3.31	2.14	0.76	0th Hour
Aspartic_peptidases	A01A	XM_014085126.1	5.64	3.99	2.01	0th Hour
Serine_peptidases	S12	XM_014090073.1	3.58	1.08	0.83	0th Hour
Aspartic_peptidases	A01A	XM_014087661.1	6.96	6.91	5.91	0th Hour
Aspartic_peptidases	A01A	XM_014090772.1	7.46	7.60	5.88	0th Hour
Aspartic_peptidases	A01A	XM_014091443.1	7.46	7.39	6.40	0th Hour
Aspartic_peptidases	A01A	XM_014089336.1	2.51	2.58	0.74	0th Hour
Cysteine_peptidases	C14B	XM_014091055.1	2.74	3.07	0.00	0th Hour
Inhibitor_family	I63	XM_014083930.1	7.69	8.06	4.01	0th Hour
Metallo_peptidases	M12A	XM_014083450.1	3.33	3.53	1.61	0th Hour
Metallo_peptidases	M14A	XM_014092898.1	3.46	3.34	1.98	0th Hour
Metallo_peptidases	M14A	XM_014083950.1	5.90	6.62	4.75	0th Hour
Metallo_peptidases	M14A	XM_014091992.1	6.60	7.11	4.31	0th Hour
Metallo_peptidases	M20A	XM_014085358.1	3.51	3.50	1.69	0th Hour
Metallo_peptidases	M28X	XM_014082486.1	6.92	7.22	4.59	0th Hour
Serine_peptidases	S08A	XM_014092865.1	3.42	3.41	2.01	0th Hour
Serine_peptidases	S08A	XM_014085316.1	4.65	4.78	1.94	0th Hour
Serine_peptidases	S08A	XM_014083546.1	6.38	6.19	4.16	0th Hour
Serine_peptidases	S09B	XM_014084297.1	5.25	5.11	3.81	0th Hour
Serine_peptidases	S09X	XM_014093769.1	5.36	5.37	3.04	0th Hour
Serine_peptidases	S09X	XM_014083707.1	5.11	5.16	2.72	0th Hour
Serine_peptidases	S10	XM_014088787.1	5.10	5.19	3.97	0th Hour
Serine_peptidases	S10	XM_014092018.1	2.72	2.65	0.74	0th Hour
Serine_peptidases	S15	XM_014090024.1	2.08	2.16	0.00	0th Hour
Serine_peptidases	S33	XM_014090068.1	7.29	6.66	4.44	0th Hour
Serine_peptidases	S51	XM_014092032.1	2.63	2.45	0.00	0th Hour
Cysteine_peptidases	C56	XM_014091102.1	6.19	5.10	5.97	0th Hour

Serine_peptidases	S12	XM_014087548.1	1.46	0.25	0.00	0th Hour
Cysteine_peptidases	C56	XM_014086354.1	0.95	3.10	3.17	53rd & 62nd Hour
Aspartic_peptidases	A01A	XM_014085069.1	3.20	5.50	2.57	53rd Hour
Cysteine_peptidases	C46	XM_014089632.1	0.65	3.47	2.00	53rd Hour
Metallo_peptidases	M14A	XM_014086647.1	2.03	3.04	1.65	53rd Hour
Serine_peptidases	S09X	XM_014086374.1	2.81	5.14	1.24	53rd Hour
Aspartic_peptidases	A01A	XM_014088391.1	2.01	1.76	3.13	62nd Hour
Aspartic_peptidases	A01A	XM_014088521.1	5.39	5.73	7.48	62nd Hour
Aspartic_peptidases	A01A	XM_014091935.1	7.96	7.11	9.14	62nd Hour
Aspartic_peptidases	A01A	XM_014093734.1	6.92	6.74	9.74	62nd Hour
Glutamic_peptidases	G01	XM_014088298.1	4.65	4.15	7.26	62nd Hour
Glutamic_peptidases	G01	XM_014091441.1	4.93	5.72	7.87	62nd Hour
Glutamic_peptidases	G01	XM_014093585.1	7.65	8.65	10.15	62nd Hour
Metallo_peptidases	M16B	XM_014092182.1	5.02	4.94	7.06	62nd Hour
Metallo_peptidases	M20D	XM_014084936.1	3.55	3.72	5.28	62nd Hour
Serine_peptidases	S01A	XM_014086309.1	1.85	1.05	3.32	62nd Hour
Serine_peptidases	S01A	XM_014090664.1	7.17	8.18	10.04	62nd Hour
Serine_peptidases	S08A	XM_014092016.1	3.94	3.57	5.55	62nd Hour
Serine_peptidases	S08A	XM_014085013.1	4.57	4.73	6.86	62nd Hour
Serine_peptidases	S09X	XM_014085139.1	1.11	1.08	2.77	62nd Hour
Serine_peptidases	S09X	XM_014089984.1	2.83	3.03	4.51	62nd Hour
Serine_peptidases	S12	XM_014091324.1	3.22	3.17	5.02	62nd Hour
Serine_peptidases	S54	XM_014093737.1	3.75	3.78	5.31	62nd Hour

Supplementary material 11. Diversity of Hydrophobin genes in *A. ostoyae.* The genes in yellow are upregulated specifically in wood degradation experiments, blue in *in-vitro* stem invasion and red in in-vivo interaction. Black do not show differential expression.

Supplementary material 12. Comparison of laccases between *A. ostoyae* and *Heterobasidion annosum.* The genes in red are upregulated in *A.ostoyae* during *in-vivo* interaction.